Title
The Role of Iron in Lung Pathophysiology

Author
Zhang, Vida

Publication Date
2022

Peer reviewed|Thesis/dissertation

UNIVERSITY OF CALIFORNIA

Los Angeles

The Role of Iron in Lung Pathophysiology

A dissertation submitted in partial satisfaction

of requirements for the degree Doctor of Philosophy

in Molecular and Medical Pharmacology

by

Vida Zhang

2022

ABSTRACT OF THE DISSERTATION

The Role of Iron in Lung Pathophysiology

by

Vida Zhang

Doctor of Philosophy in Molecular and Medical Pharmacology

University of California, Los Angeles, 2022

Professor Ting-Ting Wu, Co-Chair

Professor Tomas Ganz, Co-Chair

Iron is an essential trace mineral for normal biological function, and systemic iron homeostasis is tightly regulated via complex systemic mechanisms and iron transporters. While there has been much focus on systemic iron regulation and homeostasis, iron regulation in the lung has not been well characterized. In addition, little is understood about the regulation of iron transporters and their role in specific cell types and under different pathophysiological conditions in the lung. Altered iron levels have also been associated with various lung pathologies, with iron overload associated with acute lung iron injury and idiopathic pulmonary fibrosis severity and iron deficiency correlating with worse pulmonary arterial hypertension (PAH). Our goals were to elucidate the effect of iron dysregulation in multiple lung pathologies and to further explore the role of iron transporters in the lung.

For Chapters One and Two, we utilized hepcidin knockout mice (HKO) as a model of severe iron overload. In Chapter One, we induced acute lung injury (ALI) in HKO mice and wild-type (WT)

littermates via oropharyngeal aspiration (OP) of lipopolysaccharide. While we did not observe any major differences in systemic inflammatory response or airway neutrophil infiltration, we did notice a mild and transient increase in vascular leakage and increased neutrophil activity, potentially due to increased lung tissue apoptosis. In Chapter Two, we treated HKO mice and WT littermates with bleomycin OP to induce pulmonary fibrosis and did not observe any effect of iron overload on lung collagen levels nor any differences in overall disease severity. Together, these data indicate that despite increased lung iron levels in human patients with ALI or idiopathic pulmonary fibrosis, iron overload may not play a significant role in the progression of either disease.

In Chapter Three, we examined the role of ZIP8, a transmembrane divalent metal ion importer that is most highly expressed in the lung and inducible by inflammatory stimuli. We generated and characterized a novel global inducible ZIP8 knockout (KO) mouse and observed an unexpected phenotype of elevated spleen iron levels and decreased serum iron in ZIP8 KO mice. These data suggest that ZIP8 plays a role in iron recycling during homeostasis. However, we did not see any difference in response to the stress states of hemolytic anemia or iron deficiency in ZIP8 KO versus wild-type mice, suggesting that Zip8 may be redundant in this system. We also showed that ZIP8 is expressed on lung distal airspace epithelial cells and transports iron from the airway into lung tissue. ZIP8 deletion, however, had no detrimental effect on the severity of LPS-induced acute lung injury or on the outcomes of *Klebsiella pneumoniae* lung infection. Thus, ZIP8 plays a role in systemic iron homeostasis but does not modulate the severity of inflammatory lung injury or the host defense against a common bacterial cause of pneumonia.

In Chapter Four, our goal was to establish a mouse model of iron deficiency in bone morphogenetic protein (BMP) type II receptor (Bmpr2)-associated PAH, as mutations in Bmpr2 are the most common genetic cause of PAH. We placed mice heterozygous for a Bmpr2-null

allele and littermate controls on a low-iron diet to induce iron deficiency. Surprisingly, we found that iron-deficient Bmpr2 heterozygous mice may have less severe PAH than corresponding controls as evidenced by hemodynamics. We determined that while there are associations between iron deficiency and PAH potentially through Bmpr2, the Bmpr2 mutant mouse model is not the appropriate model for elucidating this relationship.

Chapter Five explored the role of erythroferrone (ERFE) in a mouse model of β-thalassemia. ERFE is an erythroid hormone that increases iron availability by functioning as a BMP trap and inhibiting the master iron regulatory hormone hepcidin. Humans with β-thalassemia and other forms of ineffective erythropoiesis produce very high levels of ERFE. To define the contribution of excessive ERFE levels on the severity of β-thalassemia, we generated a "humanized" mouse model of β-thalassemia by crossing mice overexpressing ERFE with Th3/+ mice, a β-thalassemia mouse model that does not expresses high levels of ERFE. We found that elevated ERFE levels impair pup survival in a mouse model of β-thalassemia during early life and greatly increase iron loading in the context of ineffective erythropoiesis. These findings suggest that targeting ERFE in β-thalassemia should be further studied for potential therapeutic applications.

In conclusion, we have examined the effect of iron overload and deficiency as well as the role of iron regulators and transporters on lung iron homeostasis and pathologies. Using various mouse models, we have characterized the effects of iron during ALI, pulmonary fibrosis and pulmonary vascular disease, the role of ZIP8 in iron pathophysiology, and the role of ERFE in β-thalassemia.

The dissertation of Vida Zhang is approved.

Elizabeta Nemeth

Airie Kim

Andreas Schwingshackl

Ting-Ting Wu, Committee Co-Chair

Tomas Ganz, Committee Co-Chair

University of California, Los Angeles

2022

TABLE OF CONTENTS

PREFACE

This dissertation was supported in part by the National Institute of Health grants K08 HL127293 (A.K.), R01HL159507 (A.K.), R01DK126680 (T.G.) and R01HD096863 (E.N.). All the work was performed primarily by me, and specific author contributions are indicated in each Chapter. The Chapters listed below are reprints or versions of published or submitted manuscripts, reproduced with permission:

The Overview is reprint of:

> **Zhang V**, Nemeth E, Kim A. Iron in Lung Pathology. Pharmaceuticals (Basel). 2019 Feb 15;12(1):30. doi: 10.3390/ph12010030. PMID: 30781366; PMCID: PMC6469192.

Chapter 1 is a reprint of:

> **Zhang V**, Ganz T, Nemeth E, Kim A. Iron overload causes a mild and transient increase in acute lung injury. Physiol Rep. 2020 Jun;8(12):e14470. doi: 10.14814/phy2.14470. PMID: 32596989; PMCID: PMC7322498.

Chapter 2 is a reprint of:

> **Zhang V**, Nemeth E, Kim A. Lung Iron Overload Does Not Exacerbate the Fibrotic Response to Bleomycin in a Mouse Model of Pulmonary Fibrosis. Am J Respir Cell Mol Biol. 2020 Nov;63(5):713-716. doi: 10.1165/rcmb.2020-0192LE. PMID: 33124901; PMCID: PMC7605158.

Chapter 3 is a version of:

> **Zhang V**, Jenkitkasemwong S, Liu Q, Ganz T, Nemeth E, Knutson MD, Kim A. The role of ZIP8 in iron homeostasis, inflammation and infection. In revision, Blood Advances.

Chapter 4 is a version of:

> **Zhang V**, Ganz T, Nemeth E, Umar S, Kim A. Bmpr2 mice are not a good model for studying iron deficiency in pulmonary hypertension. Submitted (Letter).

Chapter 5 is a version of:

> **Zhang V**, Olivera J, Coffey R, Nemeth E, Kim, A, Ganz T. Overexpression of erythroferrone impairs survival and increases tissue iron loading in a mouse model of β thalassemia. In preparation for publication. In preparation for submission.

VITA

EDUCATION

University of California, Berkeley 2010 - 2014

Berkelely, CA

B.A., Molecular and Cell Biology

PUBLICATIONS

Stanford SM, Collins M, Diaz MA, Holmes ZJ, Gries P, Bliss MR, Lodi A, **Zhang V**, Tiziani S, Bottini N. The low molecular weight protein tyrosine phosphatase promotes adipogenesis and subcutaneous adipocyte hypertrophy. J Cell Physiol. 2021 Sep;236(9):6630-6642. doi: 10.1002/jcp.30307. Epub 2021 Feb 21. PMID: 33615467; PMCID: PMC8222063.

Zhang V, Nemeth E, Kim A. Lung Iron Overload Does Not Exacerbate the Fibrotic Response to Bleomycin in a Mouse Model of Pulmonary Fibrosis. Am J Respir Cell Mol Biol. 2020 Nov;63(5):713-716. doi: 10.1165/rcmb.2020-0192LE. PMID: 33124901; PMCID: PMC7605158.

Zhang V, Ganz T, Nemeth E, Kim A. Iron overload causes a mild and transient increase in acute lung injury. Physiol Rep. 2020 Jun;8(12):e14470. doi: 10.14814/phy2.14470. PMID: 32596989; PMCID: PMC7322498.

Zhang V, Nemeth E, Kim A. Iron in Lung Pathology. Pharmaceuticals (Basel). 2019 Feb 15;12(1):30. doi: 10.3390/ph12010030. PMID: 30781366; PMCID: PMC6469192.

Bottini A, Wu DJ, Ai R, Le Roux M, Bartok B, Bombardieri M, Doody KM, **Zhang V**, Sacchetti C, Zoccheddu M, Lonic A, Li X, Boyle DL, Hammaker D, Meng TC, Liu L, Corr M, Stanford SM, Lewis M, Wang W, Firestein GS, Khew-Goodall Y, Pitzalis C, Bottini N. PTPN14 phosphatase and YAP promote TGFβ signalling in rheumatoid synoviocytes. Ann Rheum Dis. 2019 May;78(5):600-609. doi: 10.1136/annrheumdis-2018-213799. Epub 2019 Feb 26. PMID: 30808624; PMCID: PMC7039277.

Stanford SM, Aleshin AE, **Zhang V**, Ardecky RJ, Hedrick MP, Zou J, Ganji SR, Bliss MR, Yamamoto F, Bobkov AA, Kiselar J, Liu Y, Cadwell GW, Khare S, Yu J, Barquilla A, Chung TDY, Mustelin T, Schenk S, Bankston LA, Liddington RC, Pinkerton AB, Bottini N. Diabetes reversal by inhibition of the low molecular weight tyrosine phosphatase. Nat Chem Biol. 2017 Jun;13(6):624-632. doi: 10.1038/nchembio.2344. PMID: 28346406; PMCID: PMC5435566.

Maeshima K, Stanford SM, Hammaker D, Sacchetti C, Zeng LF, Ai R, **Zhang V**, Boyle DL, Aleman Muench GR, Feng GS, Whitaker JW, Zhang ZY, Wang W, Bottini N, Firestein GS. Abnormal PTPN11 enhancer methylation promotes rheumatoid arthritis fibroblast-like synoviocyte

aggressiveness and joint inflammation. JCI Insight. 2016; 1(7):e86580. doi: 10.1172/jci.insight.86580. PMID: 27275015; PMCID: PMC4889026.

PRESENTATIONS

Zhang V, Coffey R, Nemeth E, Kim A, Ganz T. Overexpression of erythroferrone impairs survival in β-thalassemia mouse models. UCLA Department of Molecular and Medical Pharmacology Seminar, Los Angeles, CA, 2022. Oral presentation.

Zhang V, Coffey R, Nemeth E, Kim A, Ganz T. Overexpression of erythroferrone impairs survival in β-thalassemia mouse models. UCLA Department of Molecular and Medical Pharmacology Retreat. Santa Monica, CA, 2021. Poster presentation.

Zhang V, Ganz T, Nemeth E, Kim A. The role of iron in pulmonary arterial hypertension. UCLA Department of Molecular and Medical Pharmacology Seminar, Los Angeles, CA, 2021. Oral presentation.

Zhang V, Ganz T, Nemeth E, Kim A. The role of the iron transporter Zip8 in pulmonary host defense. ATS Conference 2020, Philadelphia, PA; Abstract accepted for poster presentation.

Zhang V, Ganz T, Nemeth E, Kim A. The role of the iron transporter Zip8 in iron homeostasis. UCLA Department of Molecular and Medical Pharmacology Seminar, Los Angeles, CA, 2020. Oral presentation.

Zhang V, Ganz T, Nemeth E, Kim A. The role of the iron transporter Zip8 in pulmonary host defense. UCLA Department of Molecular and Medical Pharmacology Retreat, Huntington Beach, CA, 2019. Poster presentation.

Zhang V, Ganz T, Nemeth E, Kim A. Acute lung injury is only mildly enhanced by iron overload. 8th Congress of the International BioIron Society, Heidelberg, Germany. Poster presentation, 2019. **Travel Award**

Zhang V, Ganz T, Nemeth E, Kim A. Characterization of role of iron and iron transporter Zip8 in acute lung injury. UCLA Department of Molecular and Medical Pharmacology Retreat, Huntington Beach, CA, 2018. Poster presentation. **Best Poster Award.**

OVERVIEW

pharmaceuticals

MDPI

Review

Iron in Lung Pathology

Vida Zhang [1], Elizabeta Nemeth [2] and Airie Kim [2,*]

[1] Department of Molecular and Medical Pharmacology, David Geffen School of Medicine at the University of California, Los Angeles, CA 90095, USA; vzhang@mednet.ucla.edu

[2] Department of Medicine, David Geffen School of Medicine at the University of California, Los Angeles, CA 90095, USA; enemeth@mednet.ucla.edu

* Correspondence: airiekim@mednet.ucla.edu

Received: 14 December 2018; Accepted: 10 February 2019; Published: 15 February 2019

Abstract: The lung presents a unique challenge for iron homeostasis. The entire airway is in direct contact with the environment and its iron particulate matter and iron-utilizing microbes. However, the homeostatic and adaptive mechanisms of pulmonary iron regulation are poorly understood. This review provides an overview of systemic and local lung iron regulation, as well as the roles of iron in the development of lung infections, airway disease, and lung injury. These mechanisms provide an important foundation for the ongoing development of therapeutic applications.

Keywords: hepcidin; iron; lung; acute lung injury; COPD; lung infection; cystic fibrosis

1. Introduction

Iron is an essential trace mineral for normal biological function in almost all organisms. Most of the body's iron is contained within the heme of hemoglobin, the vital oxygen carrier in blood. Iron is also required for cell viability and proliferation as a catalytic constituent of iron-containing proteins that are involved in DNA synthesis and repair, and cellular energy metabolism [1]. As expected, iron deficiency results in the impairment of both systemic oxygen delivery and cellular function. Conversely, an excess of iron also has deleterious effects for the host, leading to cellular toxicity via iron-generated oxyradicals and peroxidation of lipid membranes [2]. Systemically, increased iron availability is also associated with the increased virulence of multiple pathogens, including *Yersinia enterocolitica* [3], *Escherichia coli* [4], and *Klebsiella pneumoniae* [5]. In order to maintain an appropriate iron balance, organisms have evolved complex systemic homeostatic and cellular iron transport mechanisms [6].

Iron homeostasis in the lung faces unique challenges. The entire lung epithelium is exposed to inhaled air containing iron particulate matter and infectious pathogens, and is also part of a delicate air–blood interface whose gas exchange function is highly susceptible to impairment by cytotoxic injury. Thus, lung iron bioavailability must be highly regulated to prevent its use by microbes during infection and to ensure sequestration of catalytically active iron to prevent cytotoxicity. The terminal respiratory unit, the alveolus, is composed of three major cell types, all of which are active in the maintenance of lung iron homeostasis: types 1 and 2 alveolar epithelial cells, and alveolar macrophages. Alveolar macrophages are a specialized subset of macrophages that defend against pulmonary infections, and mediate damage and repair of the lung parenchyma [7]. However, the specific roles of these cell types in basal iron regulation or in response to injury or infection is still poorly understood. The purpose of this review is to explore recent scientific advances in understanding the role of iron regulation in lung pathologies.

2. Iron Regulation

2.1. Systemic Iron Homeostasis

A human adult requires ~25 mg/day of iron for baseline homeostasis and the replacement of minor unregulated iron losses. The majority of this iron comes from the recycling of senescent erythrocytes, while 1–2 mg is obtained from the absorption of dietary iron in the form of heme or non-heme iron [8]. During times of stress erythropoiesis, iron utilization by the bone marrow can increase 10-fold to accommodate the increased hemoglobin synthesis [9]. Thus, rapidly acting compensatory mechanisms have evolved to increase dietary iron absorption and to allow the rapid mobilization of iron from stores.

Hepcidin, a 25 amino acid peptide hormone produced primarily by hepatocytes [10], is the key regulator of systemic iron homeostasis. Hepcidin acts by binding to the transmembrane protein ferroportin (Fpn), the only known cellular iron exporter [11], causing its internalization and degradation within lysosomes [11,12]. As Fpn is highly expressed on duodenal enterocytes, macrophages, and hepatocytes, hepcidin controls the flow of iron from dietary gut absorption, recycling of erythrocytes, and tissue iron stores. Hepcidin production is stimulated by increases in plasma iron or iron stores, and during times of inflammation [13,14].

In addition to the mechanisms controlling systemic iron availability, each cell possesses regulatory mechanisms to coordinate its iron uptake, storage, and export. Most cells acquire iron by importing transferrin bound iron from blood via the membrane transferrin receptor (TfR1), after which iron is used for basal cellular requirements or stored in the form of ferritin. Splenic and hepatic macrophages also acquire iron through the phagocytosis of damaged or senescent erythrocytes, and this iron is similarly stored as ferritin or utilized for basic cellular functions [15]. Cellular iron export occurs through Fpn, which allows cells such as duodenal enterocytes and macrophages to release iron into circulation and maintain systemic iron homeostasis. In addition, Fpn expression is increased in iron-overloaded tissues and acts as a safety valve to export excess cellular iron to prevent oxidative damage.

Coordination of cellular iron acquisition and distribution is regulated post-transcriptionally in response to changes in intracellular iron levels by the iron regulatory protein/iron responsive elements (IRP/IRE) system [16–18]. The iron regulatory proteins, IRP1 and IRP2, bind to IREs, which are untranslated regions of mRNA located at either the 5′ or 3′ end. IREs at the 5′ end are associated with genes involved in the storage or export of iron (ferritin, Fpn), while 3′ IREs are associated with genes involved in iron uptake (TfR1, DMT1). Under conditions of cellular iron depletion, IRP1/IRP2 bind to IREs, preventing translation of mRNA containing 5′ IREs and stabilizing mRNA containing 3′ IREs. This leads to the increased expression of iron uptake proteins and decreased expression of iron storage and export proteins. Conversely, in iron-loaded cells, IRP1 is converted to c-aconitase and IRP2 is degraded, resulting in decreased IRP binding to IREs. This leads to increased expression of iron storage and export proteins and decreased expression of iron uptake proteins.

2.2. Lung Iron Regulation

Iron regulation in the lung has not been well characterized, with only a few in vitro and in vivo studies attempting to identify the iron transporters in pulmonary cells (Figure 1). TfR1 has been identified as an importer of transferrin-bound iron in the alveolar epithelium and alveolar macrophages. In response to systemic iron deficiency, TfR1 protein levels increased in whole rat lung. Conversely, TfR1 protein expression in whole lung did not increase with intratracheally instilled iron oxide [19]. The DMT1 transporter, a principal importer of dietary non-heme iron and an importer of endosomal iron from the Tf-TfR1 complex into cytoplasm, has also been shown to be expressed in both alveolar epithelial cells and alveolar macrophages [20]. While respiratory DMT1 appears to be regulated by the IRP/IRE system, there is inconclusive evidence on the effects of iron deficiency and overload on the production of DMT1 mRNA and protein in the lung [19,21,22]. Multiple studies utilizing DMT1 mutated murine models have implicated this iron transporter in the pathogenesis of lung

injury. The Belgrade rat, an animal model of functional DMT1 deficiency, develops more severe lung injury in response to lipopolysaccharide (LPS) and oil fly ash [23,24]. Similarly, *mk/mk* mice, also defective in DMT1, have increased bleomycin-induced lung injury compared to wild-type controls [25]. The mechanism of DMT1 attenuating the lung's response to inflammatory stimuli is unclear, but these descriptive studies demonstrate a link between DMT1 and the lung's inflammatory response. Thus, although iron importers are present in the lung, little is understood about their regulation and role in specific cell types and under different pathophysiological conditions.

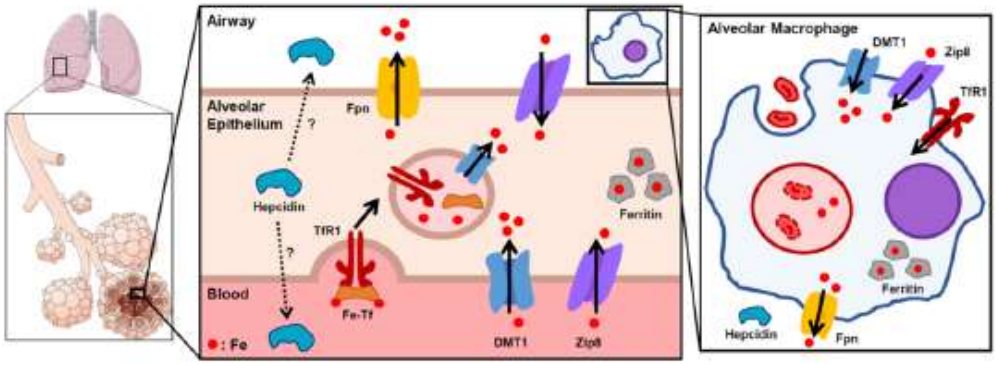

Figure 1. Proposed scheme of lung iron homeostasis. Iron is taken up into the alveolar epithelial cells through transferrin receptor (TfR1) and DMT1, and exported through ferroportin (Fpn), which was reported to be localized on the apical/airway facing layer of the epithelium. Within the cells, iron is stored in a non-reactive state in ferritin. Though hepcidin is mostly produced in the liver for systemic circulation, local production of hepcidin has also been suggested to play a role in lung iron homeostasis. Zip8 is highly expressed in the lung and facilitates iron intake, though its specific distribution remains unknown. Inset depicts an alveolar macrophage. Macrophages phagocytose airway red blood cells to recycle iron from heme. Solid arrows indicate direction of iron transport.

Fpn was reported to be localized on the apical layer of the airway epithelia of human lung [26] and also expressed in alveolar macrophages [27]. While the liver is the predominant source of circulating hepcidin, the hormone is also expressed at lower levels in human airway epithelial cells and alveolar macrophages [28], raising the possibility that hepcidin has a paracrine role in the lung. One ex vivo study showed that LPS-stimulated mouse alveolar macrophages increased the expression of hepcidin mRNA and decreased *Fpn* mRNA. Iron treatment had no effect on hepcidin mRNA expression, but did upregulate both *Dmt1* and *Fpn* [29]. Interestingly, another in vitro study showed that Fpn in airway epithelial cells did not internalize in response to hepcidin and that hepcidin itself had no significant effect on iron transport in either airway epithelial cells or alveolar macrophages [30]. However, Fpn levels do correlate with changes in iron status [27,31], suggesting that lung Fpn expression may be controlled preferentially by the IRP/IRE regulatory system, rather than a purely hepcidin-dependent mechanism. Additionally, the reported distribution pattern of Fpn on the apical layer of airway epithelial cells suggests that Fpn may play a tissue-specific role of iron detoxification in lungs [26].

Recent studies in mouse models with genetic iron overload have begun characterizing the roles of hepcidin and Fpn in lung iron homeostasis. Neves et al. investigated a murine disease model of hereditary hemochromatosis type 4, created by a global C326S amino acid substitution in Fpn that confers resistance to hepcidin binding and leads to systemic iron overload [32]. They reported that the Fpn mutant mice develop increased iron levels in airway epithelial cells and bronchoalveolar lavage (BAL) fluid [27]. Interestingly, while splenic and hepatic macrophages are predictably iron-depleted from the increased Fpn protein exporting iron, a subset of alveolar macrophages showed iron overload. The authors suggest that these differences could be partially due to the varying levels of Fpn expression in alveolar macrophages.

Deschemin et al. characterized the lungs in hepcidin knockout (HKO) mice, a mouse model of severe genetic iron overload [31]. The lack of hepcidin results in increased gut iron absorption with systemic iron overload, iron deposition in parenchymal tissues, and iron depletion of macrophages in the liver and spleen. Iron content in the lung increased, which resulted in compensatory decreases in *Tfrc* and *Dmt1* mRNA expression, and increased levels of Fpn and ferritin mRNA and protein levels. Specific examination of the alveolar macrophages also demonstrated increased levels of Fpn and ferritin. However, similar to the paper by Neves et al., these macrophages were iron-loaded, which is in stark contrast to the iron depletion of splenic macrophages. This is likely related to the much lower expression of Fpn in the alveolar macrophages of HKO mice compared to the splenic macrophages. While these genetic mouse models of iron overload clearly demonstrate some unique characteristics of lung iron homeostasis, further studies are necessary to clarify the role of the hepcidin–Fpn axis in the lung.

ZIP8, encoded by the *SLC39A8* gene, is a member of the SLC39A transmembrane metal importer family and is expressed many-fold higher in the lung than in any other organ system [33]. Initially identified as a zinc transporter, recent studies have shown that Zip8 also imports iron into the cytosolic space [33]. Early in vitro and animal studies consistently show that inflammatory stimulation with LPS greatly increases Zip8 expression, suggesting that this iron importer has a function in host defense [34,35]. As of yet, there have been no studies investigating the role of Zip8 in human lung infections or lung injury.

3. Iron in Lung Pathology

3.1. Acute Lung Injury

Acute lung injury (ALI), clinically known as acute respiratory distress syndrome (ARDS), is an acute inflammatory process with neutrophil infiltration, increased vascular permeability, and diffuse alveolar damage [36]. ARDS can occur as a result of a direct insult to the lung, including pneumonia, aspiration, and smoke inhalation, or a systemic inflammatory response, including sepsis, trauma, burns, and transfusion-related ALI. The pathophysiology of ARDS is largely mediated by the release of free radicals and reactive oxygen species and their injurious effects on endothelial integrity [37]. In the presence of iron, peroxides are converted to damaging radicals and enhance cytotoxicity by the Fenton reaction [38]. The relevance of iron in the development of ARDS has been evaluated with numerous clinical studies, showing strong correlations with iron and iron-related proteins, as well as the presence or severity of ARDS. One study found increased concentrations of BAL total iron and non-heme iron in ARDS patients, as compared to healthy controls. Iron-related proteins, including hemoglobin, transferrin, TfR1, lactoferrin, and ferritin, were also all elevated in BAL [39]. Future studies are needed to examine whether these changes in BAL iron and iron-related proteins have a causal effect on lung injury or are simply a byproduct of lung injury and increased vascular permeability. Serum ferritin has also been investigated as a predictor of ARDS, and was found to predict the development of ARDS with high sensitivity and specificity in one clinical study [40]. As ferritin is a known acute phase reactant and could simply be rising as part of the inflammatory response, a second clinical study confirmed the predictive value of serum ferritin for the progression to ARDS while also demonstrating no correlation of ferritin with the degree of hypoxia, time of invasive ventilation, or mortality [41]. These studies consistently illustrate a strong association between iron-related proteins and the development of lung injury, but further clinical and basic mechanistic studies are necessary to delineate the causative effects of iron on ARDS.

3.2. Lung Infections

Host defense of the lung organ system is particularly challenging as the entire epithelium is in constant and direct contact with environmental air containing numerous potential infectious pathogens. As the delicate single-cell-layer alveolar epithelium is responsible for vital air–blood gas exchange,

non-cytotoxic nutrient deprivation mechanisms of host defense play an important role against lung microbial pathogens. The biological relevance of iron in the pathology of infections has been established through numerous clinical and animal studies. Iron overload has been associated with increased incidence of bacteremia with hemodialysis [42], and increased virulence of multiple microbes, including *Yersinia enterocolitica* [3], *Escherichia coli* [4], and *Klebsiella pneumoniae* [5]. One clinical study found a significant correlation between high dietary iron and the development of active tuberculosis in a high-risk population [43]. Another study of 137 iron-deficient Somali patients found that iron repletion resulted in a significant increase in infection incidence, with the activation of pre-existing malaria, brucellosis, and tuberculosis [44].

Both invading pathogens and their hosts have developed multiple mechanisms to control the supply of iron necessary for microbial survival (Figure 2). One particularly effective and well-described method of iron scavenging by microbes is through the siderophore-dependent pathways, in which microbes secrete small compounds called siderophores that complex with iron for active uptake by the microbe [45]. In response, the host circumvents this pathway with neutrophil gelatinase-associated lipocalin (NGAL), otherwise known as siderocalin or lipocalin-2. Produced by neutrophil granules and epithelial cells in response to inflammation, this innate immune protein acts by binding to, and sequestering, iron-loaded bacterial siderophores [46]. One murine study showed that intratracheal *Escherichia coli* instillation resulted in a strong induction of NGAL expression in bronchial epithelium and type 2 pneumocytes [47]. An in vitro study of *Mycobacterium tuberculosis* found that recombinant NGAL restricted the growth of the organism in broth media in an iron-dependent manner [48]. Another major iron-binding protein in the airways is lactoferrin, a member of the transferrin gene family that is found in nasobronchial epithelial secretions and neutrophil granules. Lactoferrin sequesters airway iron away from microbes and is taken up by the lactoferrin receptor on lung epithelial cells and macrophages for iron reabsorption. Levels of lactoferrin correlate with the severity of infectious pneumonia, pulmonary tuberculosis, and sepsis [49]. Another iron transporter that is vital in host defense is natural resistance-associated macrophage protein 1 (NRAMP1), a divalent metal transporter expressed specifically in phagosomes. NRAMP1 reduces phagosomal iron availability and confers resistance to several intraphagosomal microbes [50,51].

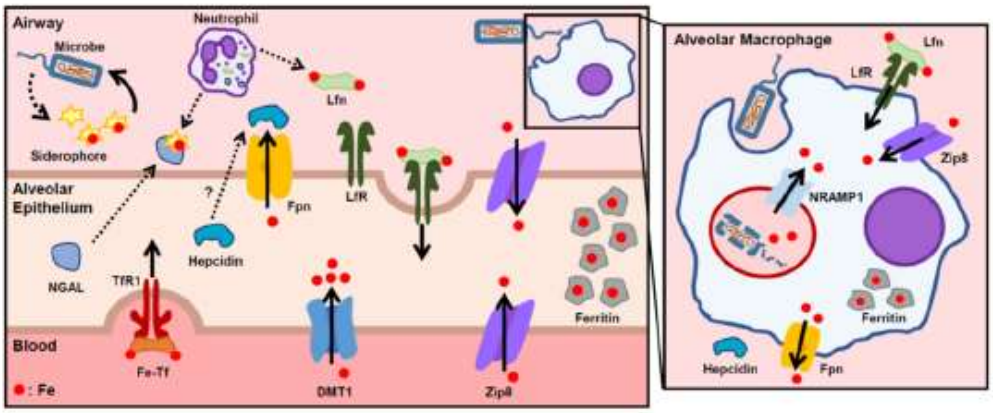

Figure 2. Proposed scheme of lung iron regulation during infection and inflammation. Bacteria secrete siderophores to capture host iron. The host combats this by increasing import of iron (lactoferrin (Lfn), DMT1), decreasing export of iron through ferroportin (Fpn), and increasing iron stores through ferritin. Secreted Lfn and NGAL bind free iron and siderophore-bound iron in the airway to prevent bacterial iron uptake. Inset shows an alveolar macrophage during infection. Alveolar macrophages phagocytose bacteria as a host defense response. NRAMP1 is expressed in macrophage phagosomes and transports iron out of the phagosome to limit iron availability to pathogens. Solid arrows indicate direction of iron transport.

The hepcidin–Fpn axis also has a principal role in innate immunity. Hepcidin plays a role in host defense by sequestering iron to hinder the growth and proliferation of invading pathogens [52]. During times of infection and inflammation, there appears to be multiple mechanisms of hepcidin expression regulation. The primary regulator of inflammation-induced hepcidin production is the inflammatory cytokine IL-6. A single infusion of IL-6 into healthy human subjects increased hepcidin production and decreased serum iron [13]. In an inflammatory state, increased IL-6 causes the activation of STAT3 (signal transducer and activator of transcription 3) and its binding to the hepcidin promoter [53]. In response to bacterial stimulation, myeloid cells have also been shown to upregulate hepcidin and decrease Fpn expression in a Toll-like receptor 4 (TLR4)-dependent manner [54].

Recently, several transgenic murine studies have established the roles of hepcidin and iron status in the morbidity and mortality of various pathogenic infections. Hepcidin knockout mice developed hyperferremia with a profound susceptibility to bacteremia from *Klebsiella pneumoniae*, *Yersinia enterocolitica*, and *E. coli*, and treatment with a hepcidin analogue restored hypoferremia, decreased bacterial burden, and improved survival in each model of infection [5,55,56]. These studies indicate that hepcidin has a protective effect against siderophilic pathogens by limiting the availability of non-transferrin bound iron, a form of iron that is readily accessed by microbes. Another study showed that cell-specific knockdown of hepcidin in airway epithelium increased lung bacterial burden and injury in mice after cecal ligation and puncture, a model of polymicrobial sepsis [57]. By contrast, hepcidin–Fpn regulation may have a deleterious effect on the host during infections with intracellular pathogens. For example, one in vitro study demonstrated that the intracellular growth of *Chlamydia psittaci*, *C. trachomatis*, and *Legionella pneumophila* in macrophages is enhanced by the addition of hepcidin. Accordingly, macrophages from flatiron mice, a mouse strain heterozygous with a loss-of-function Fpn mutation (H32R), had increased bacterial proliferation that was unchanged by the addition of exogenous hepcidin [58]. Another study used murine macrophages to show decreased virulence of intracellular *Salmonella enterica* when Fpn expression was increased, and increased virulence with hepcidin-induced Fpn downregulation [59].

3.3. Cystic Fibrosis

Cystic fibrosis (CF) is a genetic disorder caused by mutations in the cystic fibrosis transmembrane conductance regulator (CFTR) gene, and is characterized by the retention of thick airway secretions and chronic pulmonary infections. Patients with CF also have increased levels of iron and iron-related proteins in their lower respiratory tract [60], and these iron levels are strongly correlated with increases in inflammatory cytokines [61]. A clinically important area of study in CF is the microbial pathogen *Pseudomonas aeruginosa*, which is responsible for the majority of CF infectious exacerbations. This pathogen forms biofilms that are more resistant to antibiotics than the free-floating (planktonic) state and hinder the eradication of these bacteria. Construction of this biofilm is highly dependent on iron availability, and *Pseudomonas aeruginosa* has developed sophisticated mechanisms to acquire iron from the environment, including both siderophore-dependent and independent systems [62].

3.4. Chronic Obstructive Pulmonary Disease

Both cigarette smoking and chronic obstructive pulmonary disease (COPD) are associated with a disruption of iron homeostasis in the lung. Regular cigarette smoking results in a great increase in lung exposure to iron, estimated at 5.2–13.8 µg of iron daily in a subject smoking 20 cigarettes per day [63]. Compared to nonsmokers, smokers have increased total non-heme iron and ferritin levels in BAL fluid and in alveolar macrophages [64], as well as increased serum ferritin levels [65]. Smokers also have increased redox-active iron levels in exhaled breath condensate [66].

Although cigarette smoking is the largest risk factor for the development of COPD, genetic association studies have uncovered differentially expressed iron-related genes that indicate a role for iron in the susceptibility to developing COPD. The most relevant is the iron-regulatory protein IRP2 that was discovered to be a major COPD susceptibility gene in a case–control study [67]. Notably,

IRP2 is located within a cluster of genes on a chromosome that also includes several components of the nicotinic acetylcholine receptor [68]. As in smokers, levels of iron and iron-binding proteins are increased in the lung tissue, BAL fluid, and alveolar macrophages of COPD patients, and iron levels are correlated with disease severity and with worsening lung function [64]. A recent study used mouse models of COPD to investigate the mechanism of IRP2's role in the development of COPD [69]. The group showed that IRP2 increases mitochondrial iron loading and levels of cytochrome c oxidase (COX), leading to mitochondrial dysfunction and COPD development. Frataxin-deficient mice, which develop higher mitochondrial iron loading due to lack of the mitochondrial iron-sulfur regulator frataxin, were shown to develop worse airway mucociliary clearance and higher pulmonary inflammation at baseline. Conversely, mice with decreased COX synthesis were protected from cigarette smoke-induced lung inflammation and impairment in mucociliary clearance. Mice treated with the mitochondrial iron chelator deferiprone were protected from impaired mucociliary clearance, pulmonary inflammation, and the development of COPD. Together, these data indicate that IRP2 functions as a COPD susceptibility gene by increasing mitochondrial iron overload and levels of COX, leading to mitochondrial dysfunction and the development of COPD.

4. Potential Therapeutics

Due to the apparent importance of iron homeostasis in the development of many lung pathologies and infections, there has been a lot of interest in manipulating iron availability for potential therapeutic applications. Conventional means of reducing iron load in the body include dietary restriction [70], phlebotomy, and chelators, including deferoxamine, deferiprone, and deferasirox [71]. However, such systemic iron depletion can predispose patients to multiple adverse effects, including nutritional deficiency, anemia, and infection. For example, systemic iron chelators such as deferoxamine have been shown to eliminate *Pseudomonas aeruginosa* biofilms on a CF line in vitro [72], but deferoxamine also functions as a bacterial siderophore and can paradoxically act as an iron supply to specific microbes such as *Rhizopus* [73]. Newer synthetic iron chelators with fewer adverse effects are also being considered for a broad range of oxidative stress-related conditions, ranging from cardiovascular to inflammatory and malignant pathologies [74]. In addition, there has been early work examining the therapeutic potential of modulating specific iron transporters, including DMT1 and Fpn [12,75]. Studies in mice have shown that hepcidin mimetics are effective in lowering systemic iron and modulating the virulence and mortality of gram-negative pneumonia [5,76]. Another approach in the field of CF research is the use of an iron competitor. Interfering with iron uptake by *Pseudomonas aeruginosa*, with the cationic metal gallium, has been shown to have antimicrobial and antibiofilm activity [77]. Another proposed, but undeveloped, therapeutic approach would be the local or regional delivery of iron modulators, such as chelators, iron competitors, or hepcidin analogues.

While there have been substantial scientific advances in our understanding of systemic iron regulation and the pathogenesis of different iron disorders in recent years, lung iron regulation and its role in pulmonary pathology has been an understudied area. Future basic and translational studies are clearly necessary to advance this field and to enable the development of clinical therapeutic applications. On a mechanistic level, the field requires a systematic characterization of the roles and regulation of the principal iron transporters and iron-related proteins in each of the major alveolar cell types as well as the bronchial airway epithelium. Transgenic mice with lung-specific deletions of iron transporters, and further mouse models of key pulmonary pathologies, could be utilized to study the roles of specific iron-related proteins in the development of lung disease.

Funding: NIH NHLBI K08-HL127293 (AK).

Conflicts of Interest: E.N. is a stockholder of Intrinsic LifeSciences and Silarus Therapeutics. V.Z. and A.K. have no conflicts of interest.

References

1. Ganz, T.; Nemeth, E. Regulation of iron acquisition and iron distribution in mammals. *Biochim. Biophys. Acta* **2006**, *1763*, 690–699. [CrossRef] [PubMed]
2. Ramm, G.A.; Ruddell, R.G. Hepatotoxicity of iron overload: Mechanisms of iron-induced hepatic fibrogenesis. *Semin. Liver Dis.* **2005**, *25*, 433–449. [CrossRef] [PubMed]
3. Chiu, H.Y.; Flynn, D.M.; Hoffbrand, A.V.; Politis, D. Infection with Yersinia enterocolitica in patients with iron overload. *Br. Med. J. (Clin. Res. Ed.)* **1986**, *292*, 97. [CrossRef]
4. Parrow, N.L.; Fleming, R.E.; Minnick, M.F. Sequestration and scavenging of iron in infection. *Infect. Immun.* **2013**, *81*, 3503–3514. [CrossRef]
5. Michels, K.R.; Zhang, Z.; Bettina, A.M.; Cagnina, R.E.; Stefanova, D.; Burdick, M.D.; Vaulont, S.; Nemeth, E.; Ganz, T.; Mehrad, B. Hepcidin-mediated iron sequestration protects against bacterial dissemination during pneumonia. *JCI Insight* **2017**, *2*, e92002. [CrossRef] [PubMed]
6. Muckenthaler, M.U.; Rivella, S.; Hentze, M.W.; Galy, B. A Red Carpet for Iron Metabolism. *Cell* **2017**, *168*, 344–361. [CrossRef]
7. Hussell, T.; Bell, T.J. Alveolar macrophages: Plasticity in a tissue-specific context. *Nat. Rev. Immunol.* **2014**, *14*, 81–93. [CrossRef]
8. Finberg, K.E. Unraveling mechanisms regulating systemic iron homeostasis. *Hematol. Am. Soc. Hematol. Educ. Progr.* **2011**, *2011*, 532–537. [CrossRef]
9. Finch, C. Regulators of iron balance in humans. *Blood* **1994**, *84*, 1697–1702.
10. Park, C.H.; Valore, E.V.; Waring, A.J.; Ganz, T. Hepcidin, a urinary antimicrobial peptide synthesized in the liver. *J. Biol. Chem.* **2001**, *276*, 7806–7810. [CrossRef]
11. Nemeth, E.; Tuttle, M.S.; Powelson, J.; Vaughn, M.B.; Donovan, A.; Ward, D.M.; Ganz, T.; Kaplan, J. Hepcidin regulates cellular iron efflux by binding to ferroportin and inducing its internalization. *Science* **2004**, *306*, 2090–2093. [CrossRef] [PubMed]
12. Ganz, T.; Nemeth, E. The hepcidin-ferroportin system as a therapeutic target in anemias and iron overload disorders. *Hematol. Am. Soc. Hematol. Educ. Progr.* **2011**, *2011*, 538–542. [CrossRef] [PubMed]
13. Nemeth, E.; Rivera, S.; Gabayan, V.; Keller, C.; Taudorf, S.; Pedersen, B.K.; Ganz, T. IL-6 mediates hypoferremia of inflammation by inducing the synthesis of the iron regulatory hormone hepcidin. *J. Clin. Investig.* **2004**, *113*, 1271–1276. [CrossRef] [PubMed]
14. Rodriguez, R.; Jung, C.L.; Gabayan, V.; Deng, J.C.; Ganz, T.; Nemeth, E.; Bulut, Y. Hepcidin induction by pathogens and pathogen-derived molecules is strongly dependent on interleukin-6. *Infect. Immun.* **2014**, *82*, 745–752. [CrossRef] [PubMed]
15. Ganz, T.; Nemeth, E. Iron homeostasis in host defence and inflammation. *Nat. Rev. Immunol.* **2015**, *15*, 500–510. [CrossRef]
16. Rouault, T.A. The role of iron regulatory proteins in mammalian iron homeostasis and disease. *Nat. Chem. Biol.* **2006**, *2*, 406–414. [CrossRef]
17. Anderson, C.P.; Shen, M.; Eisenstein, R.S.; Leibold, E.A. Mammalian iron metabolism and its control by iron regulatory proteins. *Biochim. Biophys. Acta* **2012**, *1823*, 1468–1483. [CrossRef]
18. Wilkinson, N.; Pantopoulos, K. The IRP/IRE system in vivo: Insights from mouse models. *Front. Pharmacol.* **2014**, *5*, 176. [CrossRef]
19. Heilig, E.A.; Thompson, K.J.; Molina, R.M.; Ivanov, A.R.; Brain, J.D.; Wessling-Resnick, M. Manganese and iron transport across pulmonary epithelium. *Am. J. Physiol. Lung Cell Mol. Physiol.* **2006**, *290*, L1247–L1259. [CrossRef]
20. Ghio, A.J.; Wang, X.; Silbajoris, R.; Garrick, M.D.; Piantadosi, C.A.; Yang, F. DMT1 expression is increased in the lungs of hypotransferrinemic mice. *Am. J. Physiol. Lung Cell Mol. Physiol.* **2003**, *284*, L938–L944. [CrossRef]
21. Wang, X.; Ghio, A.J.; Yang, F.; Dolan, K.G.; Garrick, M.D.; Piantadosi, C.A. Iron uptake and Nramp2/DMT1/DCT1 in human bronchial epithelial cells. *Am. J. Physiol. Lung Cell Mol. Physiol.* **2002**, *282*, L987–L995. [CrossRef] [PubMed]
22. Giorgi, G.; D'Anna, M.C.; Roque, M.E. Iron homeostasis and its disruption in mouse lung in iron deficiency and overload. *Exp. Physiol.* **2015**, *100*, 1199–1216. [CrossRef]

23. Ghio, A.J.; Piantadosi, C.A.; Wang, X.; Dailey, L.A.; Stonehuerner, J.D.; Madden, M.C.; Yang, F.; Dolan, K.G.; Garrick, M.D.; Garrick, L.M. Divalent metal transporter-1 decreases metal-related injury in the lung. *Am. J. Physiol. Lung Cell Mol. Physiol* **2005**, *289*, L460–L467. [CrossRef] [PubMed]
24. Kim, J.; Molina, R.M.; Donaghey, T.C.; Buckett, P.D.; Brain, J.D.; Wessling-Resnick, M. Influence of DMT1 and iron status on inflammatory responses in the lung. *Am. J. Physiol. Lung Cell Mol. Physiol.* **2011**, *300*, L659–L665. [CrossRef] [PubMed]
25. Yang, F.; Stonehuerner, J.G.; Richards, J.H.; Nguyen, N.B.; Callaghan, K.D.; Haile, D.J.; Ghio, A.J. Deficiency in the divalent metal transporter 1 increases bleomycin-induced lung injury. *Biometals Int. J. Role Met. Ions Biol. Biochem. Med.* **2010**, *23*, 657–667. [CrossRef] [PubMed]
26. Yang, F.; Haile, D.J.; Wang, X.; Dailey, L.A.; Stonehuerner, J.G.; Ghiom, A.J. Apical location of ferroportin 1 in airway epithelia and its role in iron detoxification in the lung. *Am. J. Physiol. Lung Cell Mol. Physiol.* **2005**, *289*, L14–L23. [CrossRef]
27. Neves, J.; Leitz, D.; Kraut, S.; Brandenberger, C.; Agrawal, R.; Weissmann, N.; Muhlfeld, C.; Mall, M.A.; Altamura, S.; Muckenthaler, M.U. Disruption of the Hepcidin/Ferroportin Regulatory System Causes Pulmonary Iron Overload and Restrictive Lung Disease. *EBioMedicine* **2017**, *20*, 230–239. [CrossRef]
28. Chen, Q.; Wang, L.; Ma, Y.; Wu, X.; Jin, L.; Yu, F. Increased hepcidin expression in non-small cell lung cancer tissue and serum is associated with clinical stage. *Thorac. Cancer* **2014**, *5*, 14–24. [CrossRef]
29. Nguyen, N.B.; Callaghan, K.D.; Ghio, A.J.; Haile, D.J.; Yang, F. Hepcidin expression and iron transport in alveolar macrophages. *Am. J. Physiol. Lung Cell Mol. Physiol.* **2006**, *291*, L417–L425. [CrossRef]
30. Frazier, M.D.; Mamo, L.B.; Ghio, A.J.; Turi, J.L. Hepcidin expression in human airway epithelial cells is regulated by interferon-gamma. *Respir. Res.* **2011**, *12*, 100. [CrossRef]
31. Deschemin, J.C.; Mathieu, J.R.R.; Zumerle, S.; Peyssonnaux, C.; Vaulont, S. Pulmonary Iron Homeostasis in Hepcidin Knockout Mice. *Front. Physiol.* **2017**, *8*, 804. [CrossRef] [PubMed]
32. Altamura, S.; Kessler, R.; Grone, H.J.; Gretz, N.; Hentze, M.W.; Galy, B.; Muckenthaler, M.U. Resistance of ferroportin to hepcidin binding causes exocrine pancreatic failure and fatal iron overload. *Cell Metab.* **2014**, *20*, 359–367. [CrossRef] [PubMed]
33. Wang, C.Y.; Jenkitkasemwong, S.; Duarte, S.; Sparkman, B.K.; Shawki, A.; Mackenzie, B.; Knutson, M.D. ZIP8 is an iron and zinc transporter whose cell-surface expression is up-regulated by cellular iron loading. *J. Biol. Chem.* **2012**, *287*, 34032–34043. [CrossRef] [PubMed]
34. Liu, M.J.; Bao, S.; Galvez-Peralta, M.; Pyle, C.J.; Rudawsky, A.C.; Pavlovicz, R.E.; Killilea, D.W.; Li, C.; Nebert, D.W.; Wewers, M.D.; et al. ZIP8 regulates host defense through zinc-mediated inhibition of NF-kappaB. *Cell Rep.* **2013**, *3*, 386–400. [CrossRef] [PubMed]
35. Pyle, C.J.; Akhter, S.; Bao, S.; Dodd, C.E.; Schlesinger, L.S.; Knoell, D.L. Zinc Modulates Endotoxin-Induced Human Macrophage Inflammation through ZIP8 Induction and C/EBPbeta Inhibition. *PLoS ONE* **2017**, *12*, e0169531. [CrossRef] [PubMed]
36. Johnson, E.R.; Matthay, M.A. Acute lung injury: Epidemiology, pathogenesis, and treatment. *J. Aerosol Med. Pulm. Drug Deliv.* **2010**, *23*, 243–252. [CrossRef]
37. Chabot, F.; Mitchell, J.A.; Gutteridge, J.M.; Evans, T.W. Reactive oxygen species in acute lung injury. *Eur. Respir. J.* **1998**, *11*, 745–757.
38. Dixon, S.J.; Stockwell, B.R. The role of iron and reactive oxygen species in cell death. *Nat. Chem. Biol.* **2014**, *10*, 9–17. [CrossRef]
39. Ghio, A.J.; Carter, J.D.; Richards, J.H.; Richer, L.D.; Grissom, C.K.; Elstad, M.R. Iron and iron-related proteins in the lower respiratory tract of patients with acute respiratory distress syndrome. *Crit. Care Med.* **2003**, *31*, 395–400. [CrossRef]
40. Connelly, K.G.; Moss, M.; Parsons, P.E.; Moore, E.E.; Moore, F.A.; Giclas, P.C.; Seligman, P.A.; Repine, J.E. Serum ferritin as a predictor of the acute respiratory distress syndrome. *Am. J. Respir. Crit. Care Med.* **1997**, *155*, 21–25. [CrossRef]
41. Sharkey, R.A.; Donnelly, S.C.; Connelly, K.G.; Robertson, C.E.; Haslett, C.; Repine, J.E. Initial serum ferritin levels in patients with multiple trauma and the subsequent development of acute respiratory distress syndrome. *Am. J. Respir. Crit. Care Med.* **1999**, *159*, 1506–1509. [CrossRef] [PubMed]
42. Jean, G.; Charra, B.; Chazot, C.; Vanel, T.; Terrat, J.C.; Hurot, J.M.; Laurent, G. Risk factor analysis for long-term tunneled dialysis catheter-related bacteremias. *Nephron* **2002**, *91*, 399–405. [CrossRef] [PubMed]

43. Gangaidzo, I.T.; Moyo, V.M.; Mvundura, E.; Aggrey, G.; Murphree, N.L.; Khumalo, H.; Saungweme, T.; Kasvosve, I.; Gomo, Z.A.; Rouault, T.; et al. Association of pulmonary tuberculosis with increased dietary iron. *J. Infect. Dis.* **2001**, *184*, 936–939. [CrossRef] [PubMed]
44. Murray, M.J.; Murray, A.B.; Murray, M.B.; Murray, C.J. The adverse effect of iron repletion on the course of certain infections. *Br. Med. J.* **1978**, *2*, 1113–1115. [CrossRef] [PubMed]
45. Weinberg, E.D. Iron and susceptibility to infectious disease. *Science* **1974**, *184*, 952–956. [CrossRef] [PubMed]
46. Bao, G.H.; Barasch, J.; Xu, J.; Wang, W.; Hu, F.L.; Deng, S.X. Purification and Structural Characterization of "Simple Catechol", the NGAL-Siderocalin Siderophore in Human Urine. *RSC Adv.* **2015**, *5*, 28527–28535. [CrossRef] [PubMed]
47. Wu, H.; Santoni-Rugiu, E.; Ralfkiaer, E.; Porse, B.T.; Moser, C.; Hoiby, N.; Borregaard, N.; Cowland, J.B. Lipocalin 2 is protective against E. coli pneumonia. *Respir. Res.* **2010**, *11*, 96. [CrossRef]
48. Martineau, A.R.; Newton, S.M.; Wilkinson, K.A.; Kampmann, B.; Hall, B.M.; Nawroly, N.; Packe, G.E.; Davidson, R.N.; Griffiths, C.J.; Wilkinson, R.J. Neutrophil-mediated innate immune resistance to mycobacteria. *J. Clin. Investig.* **2007**, *117*, 1988–1994. [CrossRef]
49. Baynes, R.; Bezwoda, W.; Bothwell, T.; Khan, Q.; Mansoor, N. The non-immune inflammatory response: Serial changes in plasma iron, iron-binding capacity, lactoferrin, ferritin and C-reactive protein. *Scand. J. Clin. Lab. Investig.* **1986**, *46*, 695–704. [CrossRef]
50. Cellier, M.F.; Courville, P.; Campion, C. Nramp1 phagocyte intracellular metal withdrawal defense. *Microbes Infect. Inst. Pasteur* **2007**, *9*, 1662–1670. [CrossRef]
51. Wessling-Resnick, M. Nramp1 and Other Transporters Involved in Metal Withholding during Infection. *J. Biol. Chem.* **2015**, *290*, 18984–18990. [CrossRef] [PubMed]
52. Michels, K.; Nemeth, E.; Ganz, T.; Mehrad, B. Hepcidin and Host Defense against Infectious Diseases. *PLoS Pathog.* **2015**, *11*, e1004998. [CrossRef] [PubMed]
53. Wrighting, D.M.; Andrews, N.C. Interleukin-6 induces hepcidin expression through STAT3. *Blood* **2006**, *108*, 3204–3209. [CrossRef] [PubMed]
54. Peyssonnaux, C.; Zinkernagel, A.S.; Datta, V.; Lauth, X.; Johnson, R.S.; Nizet, V. TLR4-dependent hepcidin expression by myeloid cells in response to bacterial pathogens. *Blood* **2006**, *107*, 3727–3732. [CrossRef] [PubMed]
55. Stefanova, D.; Raychev, A.; Deville, J.; Humphries, R.; Campeau, S.; Ruchala, P.; Nemeth, E.; Ganz, T.; Bulut, Y. Hepcidin Protects against Lethal Escherichia coli Sepsis in Mice Inoculated with Isolates from Septic Patients. *Infect. Immun.* **2018**, *86*. [CrossRef] [PubMed]
56. Stefanova, D.; Raychev, A.; Arezes, J.; Ruchala, P.; Gabayan, V.; Skurnik, M.; Dillon, B.J.; Horwitz, M.A.; Ganz, T.; Bulut, Y.; et al. Endogenous hepcidin and its agonist mediate resistance to selected infections by clearing non-transferrin-bound iron. *Blood* **2017**, *130*, 245–257. [CrossRef] [PubMed]
57. Chen, Q.X.; Song, S.W.; Chen, Q.H.; Zeng, C.L.; Zheng, X.; Wang, J.L.; Fang, X.M. Silencing airway epithelial cell-derived hepcidin exacerbates sepsis induced acute lung injury. *Crit. Care* **2014**, *18*, 470. [CrossRef]
58. Paradkar, P.N.; De Domenico, I.; Durchfort, N.; Zohn, I.; Kaplan, J.; Ward, D.M. Iron depletion limits intracellular bacterial growth in macrophages. *Blood* **2008**, *112*, 866–874. [CrossRef]
59. Chlosta, S.; Fishman, D.S.; Harrington, L.; Johnson, E.E.; Knutson, M.D.; Wessling-Resnick, M.; Cherayil, B.J. The iron efflux protein ferroportin regulates the intracellular growth of Salmonella enterica. *Infect. Immun.* **2006**, *74*, 3065–3067. [CrossRef]
60. Stites, S.W.; Plautz, M.W.; Bailey, K.; O'Brien-Ladner, A.R.; Wesselius, L.J. Increased concentrations of iron and isoferritins in the lower respiratory tract of patients with stable cystic fibrosis. *Am. J. Respir. Crit. Care Med.* **1999**, *160*, 796–801. [CrossRef]
61. Reid, D.W.; Lam, Q.T.; Schneider, H.; Walters, E.H. Airway iron and iron-regulatory cytokines in cystic fibrosis. *Eur. Respir. J.* **2004**, *24*, 286–291. [CrossRef] [PubMed]
62. Reid, D.W.; Anderson, G.J.; Lamont, I.L. Role of lung iron in determining the bacterial and host struggle in cystic fibrosis. *Am. J. Physiol. Lung Cell Mol. Physiol.* **2009**, *297*, L795–L802. [CrossRef] [PubMed]
63. Mussalo-Rauhamaa, H.; Leppanen, A.; Salmela, S.S.; Pyysalo, H. Cigarettes as a source of some trace and heavy metals and pesticides in man. *Arch. Environ. Health* **1986**, *41*, 49–55. [CrossRef] [PubMed]
64. Cloonan, S.M.; Mumby, S.; Adcock, I.M.; Choi, A.M.K.; Chung, K.F.; Quinlan, G.J. The "Iron"-y of Iron Overload and Iron Deficiency in Chronic Obstructive Pulmonary Disease. *Am. J. Respir. Crit. Care Med.* **2017**, *196*, 1103–1112. [CrossRef] [PubMed]

65. Ghio, A.J.; Hilborn, E.D.; Stonehuerner, J.G.; Dailey, L.A.; Carter, J.D.; Richards, J.H.; Crissman, K.M.; Foronjy, R.F.; Uyeminami, D.L.; Pinkerton, K.E. Particulate matter in cigarette smoke alters iron homeostasis to produce a biological effect. *Am. J. Respir. Crit. Care Med.* **2008**, *178*, 1130–1138. [CrossRef] [PubMed]
66. Mumby, S.; Saito, J.; Adcock, I.M.; Chung, K.F.; Quinlan, G.J. Decreased breath excretion of redox active iron in COPD: A protective failure? *Eur. Respir. J.* **2016**, *47*, 1267–1270. [CrossRef] [PubMed]
67. DeMeo, D.L.; Mariani, T.; Bhattacharya, S.; Srisuma, S.; Lange, C.; Litonjua, A.; Bueno, R.; Pillai, S.G.; Lomas, D.A.; Sparrow, D.; et al. Integration of genomic and genetic approaches implicates IREB2 as a COPD susceptibility gene. *Am. J. Hum. Genet.* **2009**, *85*, 493–502. [CrossRef]
68. Kim, W.J.; Wood, A.M.; Barker, A.F.; Brantly, M.L.; Campbell, E.J.; Eden, E.; McElvaney, G.; Rennard, S.I.; Sandhaus, R.A.; Stocks, J.M.; et al. Association of IREB2 and CHRNA3 polymorphisms with airflow obstruction in severe alpha-1 antitrypsin deficiency. *Respir Res.* **2012**, *13*, 16. [CrossRef]
69. Cloonan, S.M.; Glass, K.; Laucho-Contreras, M.E.; Bhashyam, A.R.; Cervo, M.; Pabon, M.A.; Konrad, C.; Polverino, F.; Perez, E.; Mizumura, K.; et al. Mitochondrial iron chelation ameliorates cigarette smoke-induced bronchitis and emphysema in mice. *Nat. Med.* **2016**, *22*, 163–174. [CrossRef]
70. Ghio, A.J.; Jaskot, R.H.; Hatch, G.E. Lung injury after silica instillation is associated with an accumulation of iron in rats. *Am. J. Physiol.* **1994**, *267*, L686–L692. [CrossRef]
71. Kim, J.; Wessling-Resnick, M. The Role of Iron Metabolism in Lung Inflammation and Injury. *J. Allergy* **2012**, *3*. [CrossRef] [PubMed]
72. Moreau-Marquis, S.; O'Toole, G.A.; Stanton, B.A. Tobramycin and FDA-approved iron chelators eliminate Pseudomonas aeruginosa biofilms on cystic fibrosis cells. *Am. J. Respir. Cell Mol. Biol.* **2009**, *41*, 305–313. [CrossRef] [PubMed]
73. Andrianaki, A.M.; Kyrmizi, I.; Thanopoulou, K.; Baldin, C.; Drakos, E.; Soliman, S.S.M.; Shetty, A.C.; McCracken, C.; Akoumianaki, T.; Stylianou, K.; et al. Iron restriction inside macrophages regulates pulmonary host defense against Rhizopus species. *Nat. Commun.* **2018**, *9*, 3333. [CrossRef] [PubMed]
74. Hatcher, H.C.; Singh, R.N.; Torti, F.M.; Torti, S.V. Synthetic and natural iron chelators: Therapeutic potential and clinical use. *Future Med. Chem.* **2009**, *1*, 1643–1670. [CrossRef] [PubMed]
75. Wetli, H.A.; Buckett, P.D.; Wessling-Resnick, M. Small-molecule screening identifies the selanazal drug ebselen as a potent inhibitor of DMT1-mediated iron uptake. *Chem. Biol.* **2006**, *13*, 965–972. [CrossRef] [PubMed]
76. Preza, G.C.; Ruchala, P.; Pinon, R.; Ramos, E.; Qiao, B.; Peralta, M.A.; Sharma, S.; Waring, A.; Ganz, T.; Nemeth, E. Minihepcidins are rationally designed small peptides that mimic hepcidin activity in mice and may be useful for the treatment of iron overload. *J. Clin. Investig.* **2011**, *121*, 4880–4888. [CrossRef] [PubMed]
77. Kaneko, Y.; Thoendel, M.; Olakanmi, O.; Britigan, B.E.; Singh, P.K. The transition metal gallium disrupts Pseudomonas aeruginosa iron metabolism and has antimicrobial and antibiofilm activity. *J. Clin. Investig.* **2007**, *117*, 877–888. [CrossRef] [PubMed]

CHAPTER 1: IRON OVERLOAD CAUSES A MILD AND TRANSIENT INCREASE IN ACUTE LUNG INJURY

DOI: 10.14814/phy2.14470

ORIGINAL RESEARCH

Physiological Reports

Iron overload causes a mild and transient increase in acute lung injury

Vida Zhang[1,2] | **Tomas Ganz**[1] | **Elizabeta Nemeth**[1] | **Airie Kim**[1]

[1]Department of Medicine, David Geffen School of Medicine, UCLA, Los Angeles, CA, USA

[2]Department of Molecular and Medical Pharmacology, UCLA, Los Angeles, CA, USA

Correspondence
Airie Kim, Department of Medicine, David Geffen School of Medicine, UCLA, 10833 LeConte Ave 43-229 CHS, Los Angeles, CA 90024, USA.
Email: airiekim@mednet.ucla.edu

Funding information
National Heart, Lung, and Blood Institute, Grant/Award Number: K08 HL127293

Abstract

Recent studies have demonstrated a strong link between acute respiratory distress syndrome (ARDS) and the levels of iron and iron-related proteins in the lungs. However, the role of iron overload in ARDS development has yet to be characterized. In this study, we compared the highly iron-overloaded hepcidin knockout mice (HKO) to their iron-sufficient wild-type (WT) littermates in a model of sterile acute lung injury (ALI) induced by treatment with oropharyngeal (OP) LPS. There were no major differences in systemic inflammatory response or airway neutrophil infiltration between the two groups at the time of maximal injury (days 2 and 3) or during the recovery phase (day 7). Hepcidin knockout mice had transiently increased bronchoalveolar lavage fluid (BALF) protein and MPO activity in the lung and BALF on day 3, indicating worse vascular leakage and increased neutrophil activity, respectively. The increased ALI severity in iron-overloaded mice may be a result of increased apoptosis of lung tissue, as evidenced by an increase in cleaved capsase-3 protein in lung homogenates from HKO mice versus WT mice on day 3. Altogether, our data suggest that even severe iron overload has a relatively minor and transient effect in LPS-induced ALI.

KEYWORDS
acute lung injury, ARDS, inflammation, iron overload

1 | INTRODUCTION

Acute respiratory distress syndrome (ARDS) is a highly prevalent pathology with considerable associated morbidities and mortality. The etiologies of ARDS are varied, and include infectious pneumonia, sepsis, aspiration of gastric or oral contents, and major trauma (Matthay et al., 2019). Aside from treating the underlying pathologies, current therapies are primarily focused on supportive care and minimizing long-term damage from the destructive effects of ARDS and mechanical ventilation. Despite advances in ARDS therapeutics, including low tidal volume ventilation (Brower et al., 2000), neuromuscular agents (Papazian et al., 2010), and prone positioning (Sud et al., 2010), patient outcomes remain unacceptably poor. The recent LUNG SAFE (Large Observational Study to Understand the Global Impact of Severe Acute Respiratory Failure) was a multicenter international prospective study of ARDS patients in Intensive Care Units (ICUs) in 2014 (Bellani et al., (2016)). Of the 29,144 patients admitted to participating ICUs, >10% fulfilled ARDS criteria, and in-hospital mortality ranged from 35% to 46% depending on disease severity. Among those patients that survive ARDS, multiple studies have documented

the long-term detrimental effects on health-related quality of life, with a high incidence of posttraumatic stress disorder (PTSD) symptoms (Davidson, Caldwell, Curtis, Hudson, & Steinberg, 1999; Schelling et al., 1998). Coupled with the staggering costs associated with an episode of ARDS, estimated at $170,000 for the hospitalization alone (Bice, Cox, & Carson, 2013), this disease process is a large public health concern that warrants persistent investigation into its pathophysiologic mechanisms.

One recent area of ARDS research is the role of iron in the development of ARDS (Zhang, Nemeth, and Kim (2019)). While iron is an essential trace mineral that is required for oxygen carrying capacity, DNA synthesis and repair, and cellular energy metabolism (Ganz & Nemeth, 2006), an excess of iron has deleterious effects for the host by leading to cellular toxicity via iron-generated oxyradicals and peroxidation of lipid membranes (Ramm & Ruddell, 2005). Because of their direct exposure to the environment's particulate matter and high oxygen levels, the lungs are uniquely vulnerable to iron-induced oxidative damage via Fenton's reaction (Dixon & Stockwell, 2014). The pathophysiology of ARDS is known to be mediated by the release of free radicals and reactive oxygen species and their injurious effects on endothelial integrity (Chabot, Mitchell, Gutteridge, & Evans, 1998).

While the clinical literature indicates a strong relationship between ARDS severity and alterations in the levels of iron and iron-related proteins (Connelly et al., 1997; Ghio et al., 2003; Sharkey et al., 1999), there has been no systematic experimental investigation of the effects of iron overload on the development of ARDS in a mouse model. We examined the effect of severe iron overload on LPS-induced acute inflammatory lung injury in a mouse model. Extreme iron overload was induced by the combination of a high-iron diet and the deficiency of the iron-regulatory hormone hepcidin (the whole-body *Hamp1* knockout mouse) (Lesbordes-Brion et al., 2006). Hepcidin deficiency causes unregulated intestinal iron absorption, making mice highly susceptible to extreme tissue iron overload from high-iron diet and increased levels of circulating iron. Hepcidin knockout (HKO) mice were previously shown to develop pulmonary iron overload (Deschemin, Mathieu, Zumerle, Peyssonnaux, & Vaulont, 2017; Neves et al., 2017). This study aimed to detect the potentially detrimental effects of iron overload on the development of ARDS, by comparing HKO mice fed with high-iron diet to their WT littermates on normal iron diet after both groups were challenged with LPS aspiration.

2 | METHODS

2.1 | Animal models

All animal studies were approved by the University of California Los Angeles (UCLA) Office of Animal Research Oversight. Hepcidin knockout mice were originally provided to our laboratory by Dr. Sophie Vaulont (Lesbordes-Brion et al., 2006) and were backcrossed onto the C57BL/6J background (Ramos et al., 2012). Under specific pathogen-free conditions, *Hamp1* ± mice were bred to produce *Hamp1*-/- (HKO) mice and wild-type (WT) *Hamp1*+/+ mice for littermate controls. Seven- to twelve-week-old age- and sex-matched male and female mice were used in experiments. Hepcidin knockout mice were placed on a high-iron diet (5,000 ppm iron; Teklad diet TD.140464, Envigo) at 3 weeks of age for 3–4 weeks to augment iron loading, then placed on standard chow diet. WT mice were maintained on standard chow.

To induce acute lung injury ALI, mice were treated with 15 mg/kg LPS in saline through oropharyngeal (OP) aspiration, which was modified from De Vooght, et al. (De Vooght et al., 2009) In brief, mice are anesthetized with an intraperitoneal injection of ketamine/xylazine (Sigma-Aldrich), then suspended on a wire by the front incisors. After placement of a nose clip, the tongue is gently pulled out of the mouth and to the side using forceps. The LPS solution is then pipetted into the posterior oropharyngeal space, and the nose and tongue released 5 s after the solution is aspirated into the lungs. The dose of 15 mg/kg LPS was used after a titration study for the lowest dose necessary to consistently yield evaluable ALI parameters. Control mice were not administered any saline by OP route because our goal was for the control group to not be exposed to any inflammation. We used LPS-injected mice as a model of generalized inflammation, rather than to investigate the specific effects of LPS or the TLR4 pathway on lung injury.

Mice were euthanized 2, 3, and 7 days after LPS treatment, and bronchoalveolar lavage fluid (BALF) was obtained by lavaging the lungs three times with 0.8 ml of cold phosphate-buffered saline (PBS). Lungs were perfused with 5 ml of cold PBS via the right ventricle, then lungs and liver were harvested and snap frozen in liquid nitrogen for analysis. Bronchoalveolar lavage fluid cell number was counted using a hemacytometer, and a cytocentrifuge (CytoSpin3 Cytocentrifuge; Shandon) was used to make slides. Cell differential staining was performed using the Hema 3™ Fixative and Solutions (Fisher), and the percentages of different immune cell populations were counted manually. Bronchoalveolar lavage fluid protein was measured using the Pierce BCA Protein Assay Kit (Thermo Fisher).

2.2 | Quantitative PCR

Tissue RNA was extracted via TRIzol (Thermo Fisher), and cDNA was synthesized using the iScript cDNA Synthesis Kit (BioRad). Gene transcript levels were quantified in duplicate by SsoAdvanced Universal SYBR Green Supermix

(BioRad) using a CFX Connect or CFX96 Touch Real-Time PCR Detection System (BioRad). mRNA expression was calculated using the ΔCT method normalized to hypoxanthine guanine phosphoribosyl transferase (Hprt) expression levels. Primers are listed in Table 1.

2.3 | Iron measurements

After lung and liver tissues were ground up in liquid nitrogen in order to homogenize the samples, lung and liver non-heme iron concentrations were determined by a colorimetric assay for iron quantification (Sekisui Diagnostics). ~40 mg tissue was weighed and digested in a fixed volume of acid (3M HCl, 10% trichloroacetic acid) for 1 hr at 95°C. Samples were centrifuged to clear the insoluble material, then iron levels in the supernatant were quantified according to manufacturer instructions.

2.4 | MPO assay

A quantity of ~10 mg of ground lung tissue was weighed and homogenized in 50 mM potassium phosphate solution, pH 6.0. The solution was centrifuged, then the pellet resuspended in 0.5% CETAB in Cell-Based Assay Buffer (Cayman #10009322). After sonication and incubation, MPO activity in the supernatant was measured using the colorimetric neutrophil myeloperoxidase activity assay kit (Cayman #600620). BALF MPO activity was measured directly with the assay kit. MPO activity was measured as the rate of change of absorbance over time.

TABLE 1 Primers for RT-PCR

	ForwardPrimer (5′ –> 3′)	Reverse Primer(5′ –> 3′)
Mouse Hprt	CTG GTT AAG CAG TAC AGC CCC	CGA GAG GTC CTT TTC ACC AGC
Mouse Saa-1	TGA CCA GGA AGC CAA CAG	GTA GGA AGA CCA GAC C
Mouse Il6	CTC TGC AA GAGA CTT CCA TCC	CGT GGT TGT CAC CAG CAT CA
Mouse Tnf	AAT GGC CTC CCT CTC ATC AG	GCT ACG ACGTGG GCT ACA GG
Mouse Nqo1	CAC GGG GAC ATG AAC GTC AT	GGA GTG TGG CCA ATG CTG TA
Mouse Il1b	CCT TCC AGG ATG AGG ACA TGA	TGA GTC ACA GAG GAT GGG CTC
Mouse Hamp	CCT ATC TCC ATC AAC AGA TG	AAC AGA TAC CAC ACT GGG AA

2.5 | Western blot

Ground lung tissue was homogenized in RIPA buffer containing protease and phosphatase inhibitors. Protein concentration in lung lysates was determined by a BCA assay (ThermoFisher Pierce, 23225), and then lysates were denatured by SDS and boiling. The following antibodies were used for western blot: anti-mouse cleaved caspase 1 (Cell Signaling #89332), anti-mouse cleaved caspase 3 (Cell Signaling #9661), HRP-conjugated anti-beta actin (Sigma A3854), HRP-conjugated anti-rabbit IgG (ThermoFisher #31462).

2.6 | Statistics

SigmaPlot (Systat Software) was used for all statistical analyses. Normally distributed data were analyzed using Student's *t* test, and not normally distributed data were analyzed using the nonparametric Mann–Whitney rank sum test. Multivariate analyses of the effects of genotype and time point on outcome were performed using a two-way ANOVA. $p < .05$ was considered statistically significant.

3 | RESULTS

3.1 | Systemic inflammatory response to LPS-induced ALI is not affected by iron overload

In order to uncover any potential phenotypic difference in iron-sufficient (regular chow) versus severely iron-overloaded mice, we further iron-loaded our HKO mice with a high-iron (5,000 ppm Fe) diet starting at weaning for 3–4 weeks before returning them to regular chow. WT littermates were maintained on standard chow throughout the study as iron-sufficient controls. After LPS administration on day 0, mice were euthanized and analyzed on days 2, 3, and 7, which represent the time points of maximum lung injury (days 2 and 3) as well as recovery (day 7). By analyzing mice during significant injury and during recovery, we aimed to test the hypothesis that iron overload could affect either the development of lung injury or the subsequent recovery.

Hepcidin deletion was confirmed by qRT-PCR (Figure 1), and the two mouse groups were characterized by liver and lung non-heme iron measurements (Figure 2a). As expected, HKO mice on high-iron diet developed severe iron overload, with liver and lung iron levels 40-fold and 10-fold higher than those of iron-sufficient mice, respectively, providing a stringent test of the hypothesis.

Systemic inflammatory response was assessed by monitoring weight loss and measuring levels of SAA-1, which

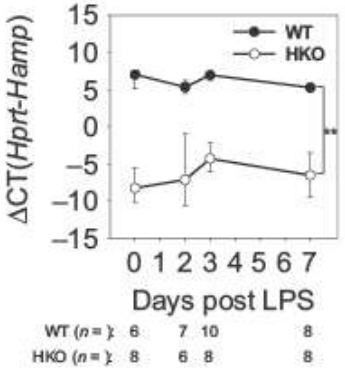

FIGURE 1 Hepcidin mRNA levels confirm knockout of hepcidin. WT and HKO mice were treated LPS OP, then analyzed on days 2, 3, and 7. Untreated WT and HKO mice were used as day 0 samples. Liver *Hamp* mRNA levels confirm knockout of hepcidin. Graph depicts mean ± *SD*; $^{**}p < .001$ by a two-way ANOVA for comparison of genotypes

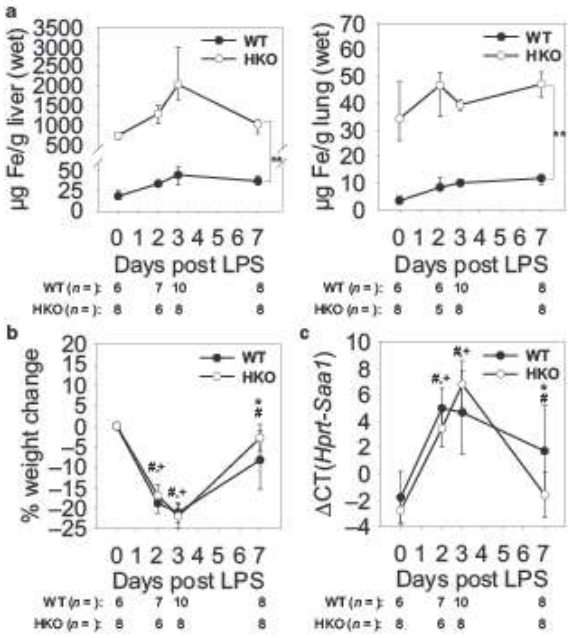

FIGURE 2 Systemic response to LPS aspiration is unaffected by iron overload. WT and HKO mice were treated with LPS OP, then analyzed on days 2, 3, and 7. Untreated WT and HKO mice were used as day 0 samples. (a) Non-heme iron levels in *(left)* liver and *(right)* lung tissues confirm iron overload in HKO mice on high-iron diet. (b and c) There was no significant difference in whole-body response to LPS between WT and HKO mice as seen by (b) weight loss or (c) liver *Saa1* mRNA levels during peak inflammation. Graphs depict (a) median ± 25th/75th percentile or (b,c) mean ± *SD*; $p < .05$ by a two-way ANOVA for comparison of WT (#) and HKO (+) mice versus day 0, $^{*}p < .05$ and $^{**}p < .001$ by a two-way ANOVA for comparison of genotypes

is induced by proinflammatory cytokines and is an accepted marker of IL-6 activity (Hagihara et al., 2004). Mice in both groups showed evidence of systemic inflammation with significant weight loss of >20% from baseline by day 3 (Figure 2b). As expected, mice that were analyzed on day 7 had recovered more than half of their lost weight, with <10% weight loss from baseline. There was no significant difference in weight loss between the two groups at any time point, and there were no incidences of mortality in either mouse group throughout the course of the experiment (data not shown). *Saa1* mRNA levels similarly had peaked by days 2 and 3, with 32- and 128-fold increases compared to baseline for WT and HKO mice, respectively (Figure 2c). Similar to the weight loss pattern, *Saa1* levels had largely recovered by day 7, and there was no significant difference between the two mouse groups during peak inflammation, days 2 and 3. Although there was a statistically significant difference in the *Saa1* mRNA levels on day 7, the difference is of questionable physiologic significance during this time of mostly resolved inflammation. Thus, we were able to establish that despite severe iron overloading, the systemic inflammatory response to OP LPS was similar in the iron-sufficient and iron-overloaded groups during both active inflammation and recovery.

3.2 | Inflammatory cell infiltration of the airway is similar in iron-sufficient and iron-overloaded mice in the LPS model of ALI

The characteristics of BALF leukocyte populations at each time point were evaluated to determine the degree of acute airway inflammation for each mouse group. BALF was centrifuged immediately after harvesting, and the respective cell pellets were characterized by cell counting and microscopic analysis via differential staining of cytospin slides (Figure 3a). The total number of BALF leukocytes per mouse peaked by day 2 at 3.4×10^6 and 2.6×10^6 for WT and HKO mice, respectively, after which they began a gradual return to baseline levels (Figure 3b). As expected, baseline uninflamed mouse airway immune cells were essentially all macrophages with very few neutrophils, but acutely inflamed airway immune cell populations were made up of > 90% neutrophils on days 2 and 3 (Figure 3c,d). During the recovery phase of the inflammation, mouse BALF leukocyte subpopulations began to return to their baseline composition (Alber, Howie, Wallace, & Hirani, 2012). Of note, the differences in total leukocyte numbers were primarily driven by neutrophil recruitment into the lungs. While macrophage percentages varied widely depending on the influx of neutrophils, absolute macrophage numbers remained relatively stable through the course of the inflammation (Figure 3d). In comparing the evolution of the leukocyte profile of iron-sufficient versus iron-overloaded mice, aside from a minor increase in %

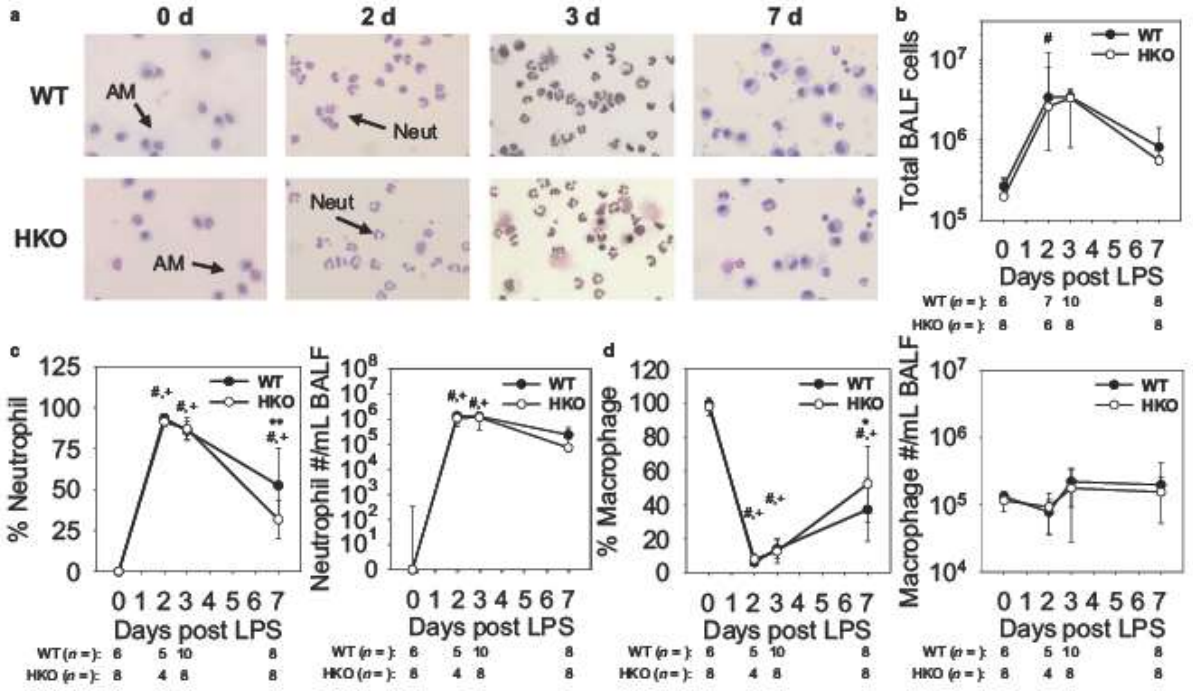

FIGURE 3 LPS induces airway neutrophil infiltration similarly in WT and HKO mice. (a) Representative images of BALF cell cytospins show an evolving leukocyte population. Neut: neutrophil; AM: alveolar macrophages. (b) Increased cell count and (c) % neutrophil and neutrophil count in BALF reflect neutrophil infiltration during the early and recovery phases of inflammation. (d) Though % macrophage in BALF decreases due to influx of neutrophils, absolute macrophage count in BALF remains similar throughout the course of inflammation. Graphs depict (b,c) median ± 25th/75th percentile or (c,d) mean ± *SD*; $p < .05$ by a two-way ANOVA for comparison of WT (#) and HKO (+) mice versus day 0, $^{*}p < .05$ and $^{**}p < .001$ by a two-way ANOVA for comparison of genotypes

neutrophils and decrease in % macrophages in BALF from WT mice compared to HKO mice on day 7, we found that there was no significant difference in any of the parameters at any time point. However, one potential caveat is that the neutrophil population at peak inflammation already made up >90% of the total leukocyte population in iron-sufficient WT mice, which may have masked any additional increase in neutrophil percentage in iron-overloaded HKO mice.

3.3 | Iron-overloaded mice develop a mild and transient increase in ALI severity compared to iron-sufficient mice

We measured BALF protein and MPO activity of the lung and BALF in order to assess and quantify the development of ALI. BALF protein levels indicated that vascular fluid leakage and pulmonary edema were most severe for both mouse groups at day 3, but with significantly increased BALF protein levels in iron-overloaded mice (WT 0.6 mg/ml vs. HKO 1.1 mg/ml; $p < .001$) (Figure 4a). Similarly, MPO activity levels showed that neutrophil activity was highest at day 3 for both groups, and iron-overloaded mice had significantly higher activity levels in both lung tissue (Figure 4b) and BALF (Figure 4c) at the same time point (WT lung MPO 104 vs. HKO lung MPO 138; $p < .001$) (WT BALF MPO 0.5 vs. HKO BALF MPO 0.9; $p < .001$). Interestingly, MPO activity in BALF was higher in HKO compared to WT mice despite comparable number of neutrophils in the two groups. This may reflect increased secretion of MPO from neutrophils in the HKO group. ALI parameters by day 7 indicated substantial recovery for both groups, with no difference between iron-sufficient and iron-overloaded mice. Thus, severely iron-overloaded mice developed worse vascular leakage and lung injury after LPS aspiration, but the effect was transient and did not affect recovery.

3.4 | The transiently more severe ALI phenotype in iron-overloaded mice may be caused by increased apoptosis, and not by changes in local cytokine production, ROS generation, or pyroptosis

In order to identify potential causes of the worse ALI that occurs with iron overload, we investigated established

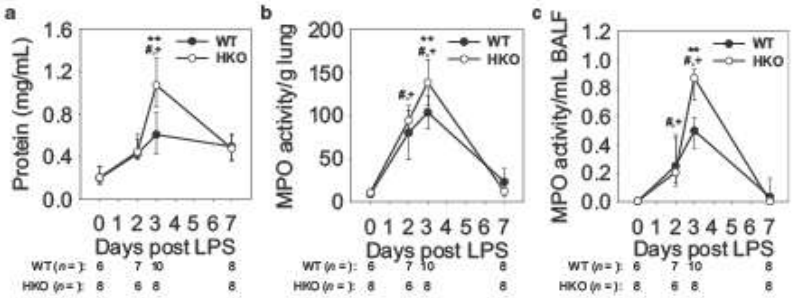

FIGURE 4 Iron-overloaded mice develop a mild and transient increase in ALI severity. (a) BALF protein concentration is increased in HKO mice compared to WT mice at 3 d. MPO activity in (b) lung tissue and (c) BALF indicate increased ALI in HKO mice compared to WT mice at 3 d. Graphs depict (a,c) median ± 25th/75thpercentile or (b) mean ± *SD*; $p < .05$ by a two-way ANOVA for comparison of WT (#) and HKO (+) mice versus day 0, ** $p < .001$ by a two-way ANOVA for comparison of genotypes

mechanisms that contribute to the development of ALI: lung inflammatory cytokines (Cross & Matthay, 2011), ROS generation (Kellner et al., 2017), pyroptosis (Li, Ren, Jiang, & Zhu, 2018), and apoptosis (Lu, Harrington, & Rounds, 2005). As expected, lung levels of *Il6* and *Tnf* mRNA peaked near days 2 and 3 and showed partial recovery by day 7 (Figure 5a,b). However, there was no difference in the levels of these proinflammatory cytokines between the two groups of mice on days 2 and 3. Similarly, lung *Nqo1* mRNA indicated that ROS generation was highest on day 2, with a significant decrease in ROS by day 7 (Figure 5c), but there were no significant differences between the mouse groups at any time point. Lung *Il1b* mRNA and cleaved caspase-1 protein were measured as markers of pyroptosis, and showed no significant difference with iron overload on days 2 and 3, and day 3, respectively (Figure 5d,e). Of note, there were subtle differences between WT and HKO mice in the levels of *Tnf* and *Il1b* mRNA on day 7, but these were not associated with any differences in ALI parameters. However, cleaved caspase-3 protein was increased in whole lung of HKO mice

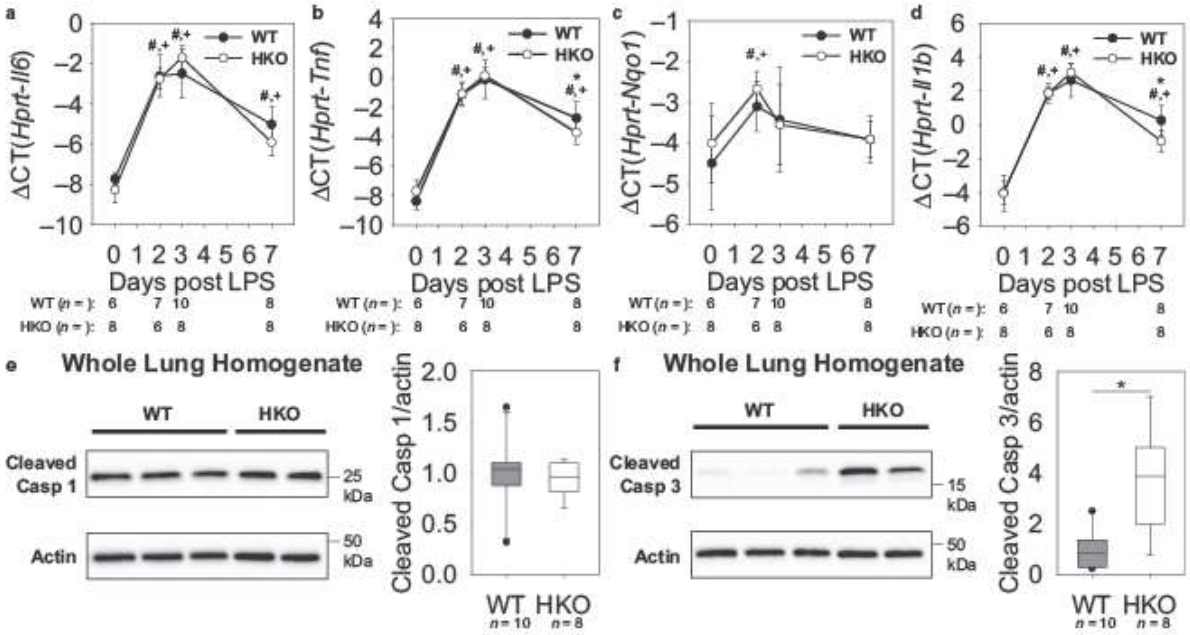

FIGURE 5 More severe ALI in iron-overloaded mice may be caused by increased apoptotic cell death. Lung (a) *Il6* mRNA and (b) *Tnf* mRNA show similar induction of lung inflammation between WT and HKO mice. (c) *Nqo1* mRNA levels indicate similar ROS generation between WT and HKO mice. Similar lung (d) *Il1b* mRNA levels and (e) cleaved caspase-1 levels at 3d between the genotypes indicate that there is no difference in pyroptosis. (f) Cleaved caspase-3 is increased in HKO mice compared to WT mice at 3 d, suggesting increased apoptosis. Graphs depict (a-d) mean ± *SD* or (e, f) median ± 25th/75th percentile; $p < .05$ by a two way ANOVA for comparison of WT (#) and HKO (+) mice versus day 0, * $p < .05$ by (b, d) a two-way ANOVA for comparison of genotypes or (f) Mann Whitney rank-sum test for comparison of genotypes

versus WT mice on day 3, indicating that iron-overloaded mice had increased apoptosis as compared to iron-sufficient mice (Figure 5f). Thus, our data suggest increased apoptosis in iron-overloaded mice that could exacerbate ALI but these effects are transient.

4 | DISCUSSION

ALI, clinically known as ARDS, is an acute inflammatory process characterized by neutrophil infiltration, increased vascular permeability, and diffuse alveolar damage (Johnson & Matthay, 2010). Despite its high incidence, conservatively estimated at 150,000 new cases/year in the United States (Reynolds et al., 1998), and high cost to the patient and to society, therapeutic options are limited and there are large gaps in our understanding of this disease process. One underexplored but promising area of research is the role of iron in the pathophysiology of ARDS. Because of the strong link between iron and oxidative stress with endothelial injury, the mechanistic study of iron in lung injury has received early attention in recent literature. In addition, iron status is of particular importance in the ICU, where approximately one-third of patients receive a blood transfusion and effectively a large iron load (Lelubre & Vincent, 2011). In this study, we have performed a systematic examination of ALI after OP LPS administration, comparing iron-sufficient versus severely iron-overloaded mice.

Multiple clinical studies have demonstrated the relevance of iron in the development of ARDS, showing strong correlations with iron and iron-related proteins and the presence or severity of ARDS. Ghio, et al. showed that ARDS patients had increased concentrations of BALF total iron and non-heme iron as compared to healthy controls (Ghio et al., 2003). Other iron-related proteins, including hemoglobin, transferrin, transferrin receptor, lactoferrin, and ferritin were also all elevated in the BALF. Whether these changes in BALF iron and iron-related proteins have a causal effect on lung injury or are simply a byproduct of increased vascular permeability is pending further study. Serum ferritin has also been investigated as a predictor of ARDS, with the caveat that ferritin is not only a marker of body iron stores, but also a known acute phase reactant. One clinical study reported serum ferritin to predict the development of ARDS with high sensitivity and specificity (Connelly et al., 1997). A second clinical study confirmed the predictive value of ferritin for ARDS in a more homogeneous group of patients who were at risk for trauma-related ARDS, (Sharkey et al., 1999) and found no correlation of ferritin with other clinical outcomes, including the severity of hypoxia, time of invasive ventilation, and mortality.

Another clinically important question in iron management during ARDS is whether there is an infectious component. Increased iron status has been associated with multiple infectious complications, including increased incidence of bacteremia with hemodialysis (Jean et al., 2002), the development of active tuberculosis in a high-risk population (Gangaidzo et al., 2001), and activation of preexisting malaria (Murray, Murray, Murray, & Murray, 1978). As pneumonia and other infectious processes often occur concurrently with ARDS, either as the primary cause or a secondary complication, the role of iron in infection virulence is clinically relevant for ARDS patients. Several animal studies have specifically examined the contribution of iron to disease severity. Michels, et al. found that hepcidin-mediated iron sequestration was protective in a mouse model of *Klebsiella pneumoniae* pneumonia, with hepcidin agonist treatment leading to decreased bacterial burden and improved survival (Michels et al., 2017). Another animal study infused commercial human haptoglobin into dog models of *Staphylococcus aureus* pneumonia, and found that treated dogs had increased clearance of cell-free hemoglobin with lower circulating iron, less injury, and increased survival (Remy et al., 2018). The authors concluded that the reduced iron levels limited nutrient availability to microbes, as well as decreased the ability for iron to cause extravascular oxidative tissue injury. Another group used cecal ligation and puncture (CLP) surgery as a model of polymicrobial sepsis induced pneumonia and ALI. The knockdown of airway epithelial cell hepcidin using adenovirus-mediated short hairpin RNA increased the severity of sepsis-induced lung injury, bacterial burden, and mortality (Chen et al., 2014).

In contrast to the abundance of animal studies examining the interplay of iron and infections, there has been a paucity of similar investigation into the role of iron in sterile ALI. One study compared WT to *Hfe-/-* mice, a model of moderate iron loading, after an intratracheal administration of LPS (Benesovaet al., 2012). The study found attenuated neutrophil recruitment to bronchoalveolar space in *Hfe-/-* mice with no difference in circulating neutrophil numbers. *Hfe-/-* mice also had altered expression of a subset of cytokines, suggesting that iron loading could worsen inflammatory injury. Another study (Deschemin et al., 2017) compared the response of WT and HKO mice to an acute LPS stimulus (6 hr), but did not find differences in lung chemokine expression or MPO activity at this early time point. To elucidate the mechanism of iron involvement in the development of ARDS, we must be careful to separate the direct contributions of iron to lung injury by ROS generation versus bacterial virulence with metal nutrient availability. In order to examine this question, we used an LPS mouse model to mimic the lung injury from a gram-negative rod pathogen, independently of any effects of microbial proliferation. To our knowledge, our current study is the first animal study to systematically investigate the contribution of iron overload to the pathophysiology of sterile ALI.

In designing this study to test the effects of iron loading in the development of ALI, we chose to compare mouse groups with extreme differences in iron loading, that is, WT mice fed normal chow versus HKO mice fed high-iron diet. The extensive literature using HKO mice does not document an iron-independent effect of hepcidin deletion, thus allowing us to use these mice as a pure model of iron overload (Khorramian et al., 2017; Kim et al., 2014; Lesbordes-Brion et al., 2006; Ramos et al., 2012). However, a potential limitation of this study is that it excluded groups of animals with intermediate iron loading, that is, WT mice fed high-iron diet or HKO mice fed regular chow. While the inclusion of these intermediate groups may have provided more subtle differences in phenotypes, the lack of a major difference in the mouse groups with extreme differences in iron status did not allow justification for the addition of more intermediate iron loaded groups.

Although we used a mouse model of extreme iron overload in order to magnify any phenotype, we saw only a mild and transient increase in ALI severity with no impact on recovery. This suggests that even severe systemic iron overload may not appreciably affect the clinical course and outcome of acute lung injury. To examine the mechanism of the mild increase in ALI in our iron-overloaded mice, we considered the potential involvement of known contributors to ARDS development: inflammatory cytokines (Matthay et al., 2019), ROS generation (Tasaka, Amaya, Hashimoto, & Ishizaka, 2008), apoptosis (Matute-Bello & Martin, 2003), and pyroptosis (Cheng et al., 2017). Interestingly, we found a difference only in the degree of apoptosis between iron-sufficient and iron-overloaded mice, with no major differences in our measurements of local cytokines, ROS generation, or pyroptosis. Thus, our study suggests that apoptosis could be the pathway of the minor iron effects in ALI. Although previous literature has shown that apoptosis in ARDS is most relevant in epithelial cells (Galani et al., 2010), further investigation is necessary to confirm the cell type that is the site of increased apoptosis in the context of iron overload.

Our mouse model of iron overload showed that even severe iron excess plays a modest role in lung injury severity in the absence of infection. Further study is necessary to examine the effects of iron status in patients with ARDS, as well as to elucidate potential contributory mechanisms.

ACKNOWLEDGMENTS

The authors acknowledge financial support from the National Institute of Health, National Heart, Lung and Blood Institute K08 HL127293 (A. K.).

CONFLICT OF INTEREST

T.G. and E.N. are shareholders and scientific advisors of Intrinsic LifeSciences and Silarus Therapeutics, and consultants for Ionis Pharmaceuticals, Protagonist, Keryx Pharmaceuticals, La Jolla Pharma, Vifor, Akebia (T.G.), and Gilead (T.G.). Neither A.K. nor V.Z. have any conflicts of interest, financial, or otherwise, to disclose.

AUTHOR CONTRIBUTIONS

T.G., E.N., and A.K. conceived and designed the experiments; V.Z. and A.K. performed experiments and prepared figures and manuscript; V.Z., T.G., E.N., and A.K. analyzed the data and approved final version of manuscript.

ORCID

Tomas Ganz https://orcid.org/0000-0002-2830-5469
Airie Kim https://orcid.org/0000-0002-8454-4472

REFERENCES

Alber, A., Howie, S. E., Wallace, W. A., & Hirani, N. (2012). The role of macrophages in healing the wounded lung. *International Journal of Experimental Pathology*, *93*, 243–251. https://doi.org/10.1111/j.1365-2613.2012.00833.x

Bellani, G., Laffey, J. G., Pham, T., Fan, E., Brochard, L., Esteban, A., … Pesenti, A.; Investigators LS and Group ET. (2016). Epidemiology, patterns of care, and mortality for patients with acute respiratory distress syndrome in intensive care units in 50 countries. *JAMA*, *315*, 788–800. https://doi.org/10.1001/jama.2016.0291

Benesova, K., Vujic Spasic, M., Schaefer, S. M., Stolte, J., Baehr-Ivacevic, T., Waldow, K., … Muckenthaler, M. U. (2012). Hfe deficiency impairs pulmonary neutrophil recruitment in response to inflammation. *PLoS One*, *7*, e39363. https://doi.org/10.1371/journal.pone.0039363

Bice, T., Cox, C. E., & Carson, S. S. (2013). Cost and health care utilization in ARDS–different from other critical illness? *Seminars in Respiratory and Critical Care Medicine*, *34*, 529–536. https://doi.org/10.1055/s-0033-1351125

Brower, R. G., Matthay, M. A., Morris, A., Schoenfeld, D., Thompson, B. T., & Wheeler, A.; Acute Respiratory Distress Syndrome Network Investigators. (2000). Ventilation with lower tidal volumes as compared with traditional tidal volumes for acute lung injury and the acute respiratory distress syndrome. *New England Journal of Medicine*, *342*, 1301–1308.

Chabot, F., Mitchell, J. A., Gutteridge, J. M., & Evans, T. W. (1998). Reactive oxygen species in acute lung injury. *The European Respiratory Journal*, *11*, 745–757.

Chen, Q. X., Song, S. W., Chen, Q. H., Zeng, C. L., Zheng, X., Wang, J. L., & Fang, X. M. (2014). Silencing airway epithelial cell-derived hepcidin exacerbates sepsis induced acute lung injury. *Critical Care*, *18*, 470. https://doi.org/10.1186/s13054-014-0470-8

Cheng, K. T., Xiong, S., Ye, Z., Hong, Z., Di, A., Tsang, K. M., … Malik, A. B. (2017). Caspase-11-mediated endothelial pyroptosis underlies endotoxemia-induced lung injury. *Journal of Clinical Investigation*, *127*, 4124–4135. https://doi.org/10.1172/JCI94495

Connelly, K. G., Moss, M., Parsons, P. E., Moore, E. E., Moore, F. A., Giclas, P. C., … Repine, J. E. (1997). Serum ferritin as a predictor of the acute respiratory distress syndrome. *American Journal of Respiratory and Critical Care Medicine*, *155*, 21–25. https://doi.org/10.1164/ajrccm.155.1.9001283

Cross, L. J., & Matthay, M. A. (2011). Biomarkers in acute lung injury: Insights into the pathogenesis of acute lung injury. *Critical Care Clinics*, *27*, 355–377. https://doi.org/10.1016/j.ccc.2010.12.005

Davidson, T. A., Caldwell, E. S., Curtis, J. R., Hudson, L. D., & Steinberg, K. P. (1999). Reduced quality of life in survivors of acute respiratory distress syndrome compared with critically ill control patients. *JAMA*, *281*, 354–360. https://doi.org/10.1001/jama.281.4.354

De Vooght, V., Vanoirbeek, J. A., Haenen, S., Verbeken, E., Nemery, B., & Hoet, P. H. (2009). Oropharyngeal aspiration: An alternative route for challenging in a mouse model of chemical-induced asthma. *Toxicology*, *259*, 84–89. https://doi.org/10.1016/j.tox.2009.02.007

Deschemin, J. C., Mathieu, J. R. R., Zumerle, S., Peyssonnaux, C., & Vaulont, S. (2017). Pulmonary iron homeostasis in hepcidin knockout mice. *Frontiers in Physiology*, *8*, 804. https://doi.org/10.3389/fphys.2017.00804

Dixon, S. J., & Stockwell, B. R. (2014). The role of iron and reactive oxygen species in cell death. *Nature Chemical Biology*, *10*, 9–17. https://doi.org/10.1038/nchembio.1416

Galani, V., Tatsaki, E., Bai, M., Kitsoulis, P., Lekka, M., Nakos, G., & Kanavaros, P. (2010). The role of apoptosis in the pathophysiology of Acute Respiratory Distress Syndrome (ARDS): An up-to-date cell-specific review. *Pathology, Research and Practice*, *206*, 145–150. https://doi.org/10.1016/j.prp.2009.12.002

Gangaidzo, I. T., Moyo, V. M., Mvundura, E., Aggrey, G., Murphree, N. L., Khumalo, H., … Gordeuk, V. R. (2001). Association of pulmonary tuberculosis with increased dietary iron. *The Journal of Infectious Diseases*, *184*, 936–939. https://doi.org/10.1086/323203

Ganz, T., & Nemeth, E. (2006). Regulation of iron acquisition and iron distribution in mammals. *Biochimica et Biophysica Acta*, *1763*, 690–699. https://doi.org/10.1016/j.bbamcr.2006.03.014

Ghio, A. J., Carter, J. D., Richards, J. H., Richer, L. D., Grissom, C. K., & Elstad, M. R. (2003). Iron and iron-related proteins in the lower respiratory tract of patients with acute respiratory distress syndrome. *Critical Care Medicine*, *31*, 395–400. https://doi.org/10.1097/01.CCM.0000050284.35609.97

Hagihara, K., Nishikawa, T., Isobe, T., Song, J., Sugamata, Y., & Yoshizaki, K. (2004). IL-6 plays a critical role in the synergistic induction of human serum amyloid A (SAA) gene when stimulated with proinflammatory cytokines as analyzed with an SAA isoform real-time quantitative RT-PCR assay system. *Biochemical and Biophysical Research Communications*, *314*, 363–369. https://doi.org/10.1016/j.bbrc.2003.12.096

Jean, G., Charra, B., Chazot, C., Vanel, T., Terrat, J. C., Hurot, J. M., & Laurent, G. (2002). Risk factor analysis for long-term tunneled dialysis catheter-related bacteremias. *Nephron*, *91*, 399–405. https://doi.org/10.1159/000064279

Johnson, E. R., & Matthay, M. A. (2010). Acute lung injury: Epidemiology, pathogenesis, and treatment. *Journal of Aerosol Medicine and Pulmonary Drug Delivery*, *23*, 243–252. https://doi.org/10.1089/jamp.2009.0775

Kellner, M., Noonepalle, S., Lu, Q., Srivastava, A., Zemskov, E., & Black, S. M. (2017). ROS Signaling in the pathogenesis of acute lung injury (ALI) and acute respiratory distress syndrome (ARDS). *Advances in Experimental Medicine and Biology*, *967*, 105–137.

Khorramian, E., Fung, E., Chua, K., Gabayan, V., Ganz, T., Nemeth, E., & Kim, A. (2017). In a mouse model of sepsis, hepcidin ablation ameliorates anemia more effectively than iron and erythropoietin treatment. *Shock*, *48*, 490–497. https://doi.org/10.1097/SHK.0000000000000886

Kim, A., Fung, E., Parikh, S. G., Valore, E. V., Gabayan, V., Nemeth, E., & Ganz, T. (2014). A mouse model of anemia of inflammation: Complex pathogenesis with partial dependence on hepcidin. *Blood*, *123*, 1129–1136. https://doi.org/10.1182/blood-2013-08-521419

Lelubre, C., & Vincent, J. L. (2011). Red blood cell transfusion in the critically ill patient. *Ann Intensive Care*, *1*, 43. https://doi.org/10.1186/2110-5820-1-43

Lesbordes-Brion, J. C., Viatte, L., Bennoun, M., Lou, D. Q., Ramey, G., Houbron, C., … Vaulont, S. (2006). Targeted disruption of the hepcidin 1 gene results in severe hemochromatosis. *Blood*, *108*, 1402–1405. https://doi.org/10.1182/blood-2006-02-003376

Li, D., Ren, W., Jiang, Z., & Zhu, L. (2018). Regulation of the NLRP3 inflammasome and macrophage pyroptosis by the p38 MAPK signaling pathway in a mouse model of acute lung injury. *Molecular Medicine Reports*, *18*, 4399–4409. https://doi.org/10.3892/mmr.2018.9427

Lu, Q., Harrington, E. O., & Rounds, S. (2005). Apoptosis and lung injury. *Keio Journal of Medicine*, *54*, 184–189. https://doi.org/10.2302/kjm.54.184

Matthay, M. A., Zemans, R. L., Zimmerman, G. A., Arabi, Y. M., Beitler, J. R., Mercat, A., … Calfee, C. S. (2019). Acute respiratory distress syndrome. *Nature Reviews Disease Primers*, *5*(1), https://doi.org/10.1038/s41572-019-0069-0

Matute-Bello, G., & Martin, T. R. (2003). Science review: Apoptosis in acute lung injury. *Critical Care*, *7*, 355–358.

Michels, K. R., Zhang, Z., Bettina, A. M., Cagnina, R. E., Stefanova, D., Burdick, M. D., … Mehrad, B. (2017). Hepcidin-mediated iron sequestration protects against bacterial dissemination during pneumonia. *JCI Insight*, *2*, e92002. https://doi.org/10.1172/jci.insight.92002

Murray, M. J., Murray, A. B., Murray, M. B., & Murray, C. J. (1978). The adverse effect of iron repletion on the course of certain infections. *British Medical Journal*, *2*, 1113–1115. https://doi.org/10.1136/bmj.2.6145.1113

Neves, J., Leitz, D., Kraut, S., Brandenberger, C., Agrawal, R., Weissmann, N., … Muckenthaler, M. U. (2017). Disruption of the hepcidin/ferroportin regulatory system causes pulmonary iron overload and restrictive lung disease. *EBioMedicine*, *20*, 230–239. https://doi.org/10.1016/j.ebiom.2017.04.036

Papazian, L., Forel, J. M., Gacouin, A., Penot-Ragon, C., Perrin, G., Loundou, A., … Roch, A.; ACURASYS Study Investigators. (2010). Neuromuscular blockers in early acute respiratory distress syndrome. *New England Journal of Medicine*, *363*, 1107–1116. https://doi.org/10.1056/NEJMoa1005372

Ramm, G. A., & Ruddell, R. G. (2005). Hepatotoxicity of iron overload: Mechanisms of iron-induced hepatic fibrogenesis. *Seminars in Liver Disease*, *25*, 433–449.

Ramos, E., Ruchala, P., Goodnough, J. B., Kautz, L., Preza, G. C., Nemeth, E., & Ganz, T. (2012). Minihepcidins prevent iron overload in a hepcidin-deficient mouse model of severe hemochromatosis. *Blood*, *120*, 3829–3836. https://doi.org/10.1182/blood-2012-07-440743

Remy, K. E., Cortés-Puch, I., Solomon, S. B., Sun, J., Pockros, B. M., Feng, J., … Natanson, C. (2018). Haptoglobin improves shock, lung injury, and survival in canine pneumonia. *JCI Insight*, *3*(18), https://doi.org/10.1172/jci.insight.123013

Reynolds, H. N., McCunn, M., Borg, U., Habashi, N., Cottingham, C., & Bar-Lavi, Y. (1998). Acute respiratory distress syndrome: Estimated incidence and mortality rate in a 5 million-person population base. *Critical Care*, *2*, 29–34.

Schelling, G., Stoll, C., Haller, M., Briegel, J., Manert, W., Hummel, T., … Peter, K. (1998). Health-related quality of life and posttraumatic stress disorder in survivors of the acute respiratory distress syndrome. *Critical Care Medicine*, *26*, 651–659. https://doi.org/10.1097/00003246-199804000-00011

Sharkey, R. A., Donnelly, S. C., Connelly, K. G., Robertson, C. E., Haslett, C., & Repine, J. E. (1999). Initial serum ferritin levels in patients with multiple trauma and the subsequent development of acute respiratory distress syndrome. *American Journal of Respiratory and Critical Care Medicine*, *159*, 1506–1509. https://doi.org/10.1164/ajrccm.159.5.9809027

Sud, S., Friedrich, J. O., Taccone, P., Polli, F., Adhikari, N. K., Latini, R., … Gattinoni, L. (2010). Prone ventilation reduces mortality in patients with acute respiratory failure and severe hypoxemia: Systematic review and meta-analysis. *Intensive Care Medicine*, *36*, 585–599. https://doi.org/10.1007/s00134-009-1748-1

Tasaka, S., Amaya, F., Hashimoto, S., & Ishizaka, A. (2008). Roles of oxidants and redox signaling in the pathogenesis of acute respiratory distress syndrome. *Antioxidants and Redox Signaling*, *10*, 739–753. https://doi.org/10.1089/ars.2007.1940

Zhang, V., Nemeth, E., & Kim, A. (2019). Iron in lung pathology. *Pharmaceuticals*, *12*(1), 30. https://doi.org/10.3390/ph12010030

How to cite this article: ZhangV, Ganz T, Nemeth E, Kim A. Iron overload causes a mild and transient increase in acute lung injury. *Physiol Rep*. 2020;8:e14470. https://doi.org/10.14814/phy2.14470

CHAPTER 2: LUNG IRON OVERLOAD DOES NOT EXACERBATE THE FIBROTIC RESPONSE TO BLEOMYCIN IN A MOUSE MODEL OF PULMONARY FIBROSIS

Vida Zhang, Elizabeta Nemeth, Airie Kim. 2020. Lung Iron Overload Does Not Exacerbate the Fibrotic Response to Bleomycin in a Mouse Model of Pulmonary Fibrosis. Am J Respir Cell Mol Biol. 63(5):713-716.

The American Journal of Respiratory Cell and Molecular Biology is an official journal of the American Thoracic Society.

Manuel Castellà, M.D., Ph.D.
Hospital Clínic-Institut d'Investigacions Biomèdiques August Pi i Sunyer (IDIBAPS)
Barcelona, Spain

Joan Albert Barberà, M.D., Ph.D.
Hospital Clínic-Institut d'Investigacions Biomèdiques August Pi i Sunyer (IDIBAPS)
Barcelona, Spain
and
Biomedical Research Networking Center on Respiratory Diseases (CIBERES)
Madrid, Spain

Marta Cascante, Ph.D.*
Hospital Clínic-Institut d'Investigacions Biomèdiques August Pi i Sunyer (IDIBAPS)
Barcelona, Spain
University of Barcelona
Barcelona, Spain
and
Biomedical Research Networking Center on Hepatic and Digestive Diseases (CIBEREHD)-ISCIII
Madrid, Spain

Olga Tura-Ceide, Ph.D.*‡
Hospital Clínic-Institut d'Investigacions Biomèdiques August Pi i Sunyer (IDIBAPS)
Barcelona, Spain
Girona Biomedical Research Institut (IDIBGI)
Girona, Catalonia, Spain
and
Biomedical Research Networking Center on Respiratory Diseases (CIBERES)
Madrid, Spain

ORCID IDs: 0000-0002-9863-7581 (V.F.E.D.S.); 0000-0003-0614-6214 (C.R.); 0000-0001-6848-7407 (C.M.); 0000-0001-9452-3432 (I.B.); 0000-0003-3808-808X (J.O.); 0000-0002-2241-7523 (L.P.); 0000-0002-6853-5760 (P.H.A.Q.); 0000-0001-9793-9433 (V.I.P.); 0000-0001-9274-2121 (M. Castellà); 0000-0003-1469-4990 (J.A.B.); 0000-0002-2062-4633 (M. Cascante); 0000-0003-4334-9790 (O.T.-C.).

*Shared last author.
‡Corresponding author (e-mail: olgaturac@gmail.com).

References

1. Sharma S, Lang IM. Current understanding of the pathophysiology of chronic thromboembolic pulmonary hypertension. *Thromb Res* 2018; 164:136–144.
2. Mercier O, Arthur Ataam J, Langer NB, Dorfmüller P, Lamrani L, Lecerf F, *et al*. Abnormal pulmonary endothelial cells may underlie the enigmatic pathogenesis of chronic thromboembolic pulmonary hypertension. *J Heart Lung Transplant* 2017;36:305–314.
3. Huang H, Vandekeere S, Kalucka J, Bierhansl L, Zecchin A, Brüning U, *et al*. Role of glutamine and interlinked asparagine metabolism in vessel formation. *EMBO J* 2017;36:2334–2352.
4. Schoors S, Bruning U, Missiaen R, Queiroz KCS, Borgers G, Elia I, *et al*. Fatty acid carbon is essential for dNTP synthesis in endothelial cells. *Nature* 2015;520:192–197.
5. Draoui N, de Zeeuw P, Carmeliet P. Angiogenesis revisited from a metabolic perspective: role and therapeutic implications of endothelial cell metabolism. *Open Biol* 2017;7:170219.
6. Tanner LB, Goglia AG, Wei MH, Sehgal T, Parsons LR, Park JO, *et al*. Four key steps control glycolytic flux in mammalian cells. *Cell Syst* 2018;7:49–62.e8.
7. Sutendra G, Bonnet S, Rochefort G, Haromy A, Folmes KD, Lopaschuk GD, *et al*. Fatty acid oxidation and malonyl-CoA decarboxylase in the vascular remodeling of pulmonary hypertension. *Sci Transl Med* 2010; 2:44ra58.
8. Archer SL, Fang Y-H, Ryan JJ, Piao L. Metabolism and bioenergetics in the right ventricle and pulmonary vasculature in pulmonary hypertension. *Pulm Circ* 2013;3:144–152.
9. Michelakis ED, Gurtu V, Webster L, Barnes G, Watson G, Howard L, *et al*. Inhibition of pyruvate dehydrogenase kinase improves pulmonary arterial hypertension in genetically susceptible patients. *Sci Transl Med* 2017;9:eaao4583.
10. Bazan IS, Fares WH. Pulmonary hypertension: diagnostic and therapeutic challenges. *Ther Clin Risk Manag* 2015;11:1221–1233.
11. Yu Q, Chan SY. Mitochondrial and metabolic drivers of pulmonary vascular endothelial dysfunction in pulmonary hypertension. *Adv Exp Med Biol* 2017;967:373–383.
12. Chen F, Wang H, Lai J, Cai S, Yuan L. 3-Bromopyruvate reverses hypoxia-induced pulmonary arterial hypertension through inhibiting glycolysis: *in vitro* and *in vivo* studies. *Int J Cardiol* 2018;266: 236–241.
13. Rafikova O, Srivastava A, Desai AA, Rafikov R, Tofovic SP. Recurrent inhibition of mitochondrial complex III induces chronic pulmonary vasoconstriction and glycolytic switch in the rat lung. *Respir Res* 2018;19:69.
14. Alias S, Redwan B, Panzenboeck A, Winter MP, Schubert U, Voswinckel R, *et al*. Defective angiogenesis delays thrombus resolution: a potential pathogenetic mechanism underlying chronic thromboembolic pulmonary hypertension. *Arterioscler Thromb Vasc Biol* 2014;34:810–819.
15. Schoors S, De Bock K, Cantelmo AR, Georgiadou M, Ghesquière B, Cauwenberghs S, *et al*. Partial and transient reduction of glycolysis by PFKFB3 blockade reduces pathological angiogenesis. *Cell Metab* 2014;19:37–48.

Check for updates

Lung Iron Overload Does Not Exacerbate the Fibrotic Response to Bleomycin in a Mouse Model of Pulmonary Fibrosis

To the Editor:

Idiopathic pulmonary fibrosis (IPF) is the most common of the idiopathic interstitial pneumonias, with a prevalence of 10–60 cases per 100,000 in North America and Europe (1). With a dismal prognosis of 2–4 years median survival from diagnosis and its associated hospitalizations and healthcare costs, IPF carries a heavy cost for both the individual patient and for society (2).

One promising area of IPF research is the role of iron in the pathogenesis of pulmonary fibrosis. Multiple translational studies have shown increased amounts of iron in IPF lung, including in BAL fluid (3) and alveolar macrophages (4), and the association of iron concentrations with severity of disease and the development of associated pulmonary vascular disease (5). One study of patients with IPF found a significantly increased incidence of *HFE* (homeostatic iron regulator) allelic variants compared with normal control subjects, with increased amounts of iron-dependent reactive

Supported by U.S. National Institutes of Health National Heart, Lung, and Blood Institute (5K08-HL127293) (A.K.).

Author Contributions: Experimental conception and design: V.Z. and A.K. Data acquisition: V.Z. and A.K. Data analysis and interpretation: V.Z., E.N., and A.K. Manuscript preparation and editing: V.Z., E.N., and A.K.

This letter has a data supplement, which is accessible from this issue's table of contents at www.atsjournals.org.

oxygen species (ROS) in patients with *HFE* allelic variants as compared with patients with wild-type alleles and IPF (4). These findings suggest that these patients have a genetic predisposition to IPF from iron dysregulation, possibly driven by increased generation of ROS by Fenton's reaction (6, 7). Another group recently proposed that a decreased proportion of transferrin receptor 1 (CD71)-expressing alveolar macrophages in patients with IPF may lead to impaired iron sequestration and ultimately worse survival (8). Building on preexisting clinical and translational data, we used mouse models of iron overload and pulmonary fibrosis to examine the causal relationship between iron and pulmonary fibrosis.

Hepcidin-knockout (HKO) mice (9) were backcrossed onto the C57BL/6J background, then bred to produce HKO and wild-type (WT) mice as age-matched and sex-matched littermates. Hepcidin deficiency causes unregulated intestinal iron absorption and systemic iron overload, with secondary lung iron loading (10). Male and female HKO mice were further placed on a high-iron diet (5,000 parts/million iron; Teklad diet TD.14064; Envigo) at weaning for 2.5–4.5 weeks to augment iron loading and then placed on standard chow for the remainder of the protocol. WT mice were maintained on standard chow throughout. At 7–9.5 weeks of age, mice were treated with bleomycin 1–1.5 U/kg (Fresenius Kabi) in sterile saline through oropharyngeal aspiration and then analyzed at 2 or 3 weeks after bleomycin administration. A subset of HKO and WT mice was harvested at 7.5–10 weeks of age and served as untreated control animals.

Blood hemoglobin (Hgb) and mean corpuscular volume (MCV) were measured using a HemaVet blood analyzer (Drew Scientific). Lung and liver tissue nonheme iron concentrations were determined with a colorimetric assay (Sekisui Diagnostics). For iron localization, formalin-fixed and paraffin-embedded lung tissues underwent enhanced Perls' stain using potassium ferrocyanide 2% and HCl 4% and the Vector SG Peroxidase Substrate kit (SK-4700; Vector Laboratories) and were then counterstained with 0.5% neutral red solution. Lung tissue sections were also treated with Masson's trichrome staining at the University of California Los Angeles Translational Pathology Core Laboratory, then scanned for digital analysis. Lung collagen quantification was performed using the Sircol Soluble Collagen Assay (Biocolor) according to the manufacturer's protocol. Lung tissue *Nqo1* was measured by qRT-PCR, as previously described (11). For a listing of primer sequences, *see* Table E1 in the data supplement.

SigmaPlot (Systat Software) was used for all statistical analyses. Normally and nonnormally distributed data were analyzed using the *t* test or Mann-Whitney rank-sum test, respectively. Multivariate analyses were performed using two-way ANOVA.

Immediately before bleomycin treatment, HKO mice and WT mice underwent hematologic measurements. As expected, iron-overloaded HKO mice had a trend toward increased Hgb (Figure 1A; median HKO Hgb, 12.9 g/dl vs. WT Hgb, 14.5 g/dl; $P = 0.20$) as well as increased MCV values (Figure 1B; mean HKO MCV, 61.8 fl vs. WT MCV, 54.5 fl; $P < 0.05$) as compared with their WT littermates. Tissue iron was measured to confirm a differential in the iron status of the WT and HKO groups. Both liver and lung iron were dramatically increased in the treated HKO mice compared with their genotype control animals, at more than 33-fold and 6-fold the concentrations of WT mice (Figures 1C and 1D; $P < 0.001$ and $P < 0.001$), reflecting effective iron loading of both tissue stores and the lung. Interestingly, liver and lung iron concentrations increased in HKO mice after bleomycin treatment, with a trend toward concurrent increase in WT mice after treatment. Although the etiology is unclear, this observation suggests that the iron loading phenotype in IPF lung may be partially secondary to the inflammatory or fibrotic process. A representative image of Perls' staining of bleomycin-treated HKO mouse lung illustrates the architectural distortion, septal thickening, and inflammatory cell infiltration that is characteristic of the model (Figure 1E). The distribution of iron staining is diffuse, including the airway epithelium and areas of intense punctate staining that are potentially sequelae of microhemorrhages.

To quantify the degree of fibrosis, lung collagen was measured in both untreated and treated mice at 2 and 3 weeks after bleomycin administration (Figure 1F). As expected, collagen concentrations for all treated groups were increased compared with untreated groups, confirming the development of fibrosis with our model. However, there were no significant differences in collagen concentrations between the genotypes at either time point. Of note, lung *Nqo1* measurements showed that iron-mediated ROS levels increased after bleomycin treatment (Figure 1G; mean WT untreated ΔCT [Δ cycle threshold], -4.3 vs. WT 3-wk ΔCT, -2.8; mean HKO untreated ΔCT, -3.9 vs. HKO 3-wk ΔCT, -1.6; $P < 0.05$ and $P < 0.001$, respectively) but without a significant difference between genotypes at each time point, indicating that iron overload alone is not sufficient to increase ROS generation and subsequent fibrotic damage in response to bleomycin. Representative digital images of Masson's trichrome–stained bleomycin-treated mouse lungs demonstrate the characteristic patchy collagen deposition of pulmonary fibrosis in both WT and HKO mice (Figure 1H). Weight loss was also tracked as a systemic marker of disease severity (Figure 1I). Although there was significant weight loss in the treated mice as compared with their own baselines (data not shown), there was no difference in the weight loss among any of the treated groups.

A recent study reported increased pulmonary fibrosis in transferrin receptor 2 mutant mice after bleomycin treatment (12). Of note, the study used collagen deposition around small airways as the primary biochemical parameter of fibrosis severity. Despite a much more severe iron overload phenotype in our HKO mice, we did not observe a significant difference between WT and transgenic mice in response to the bleomycin model, using conventional measurements of whole-lung collagen. The potential reasons for the divergent conclusions include the different outcome measures and inherent differences in the various genetic and dietary models of iron overload. The strengths of our study include the severity of the iron overload in our model, the use of a robust global measure of pulmonary fibrosis, and the inclusion of body weight as a measure of general health. ■

Author disclosures are available with the text of this letter at www.atsjournals.org.

Vida Zhang, B.A.
Elizabeta Nemeth, Ph.D.
Airie Kim, M.D., Ph.D.*
University of California–Los Angeles
Los Angeles, California

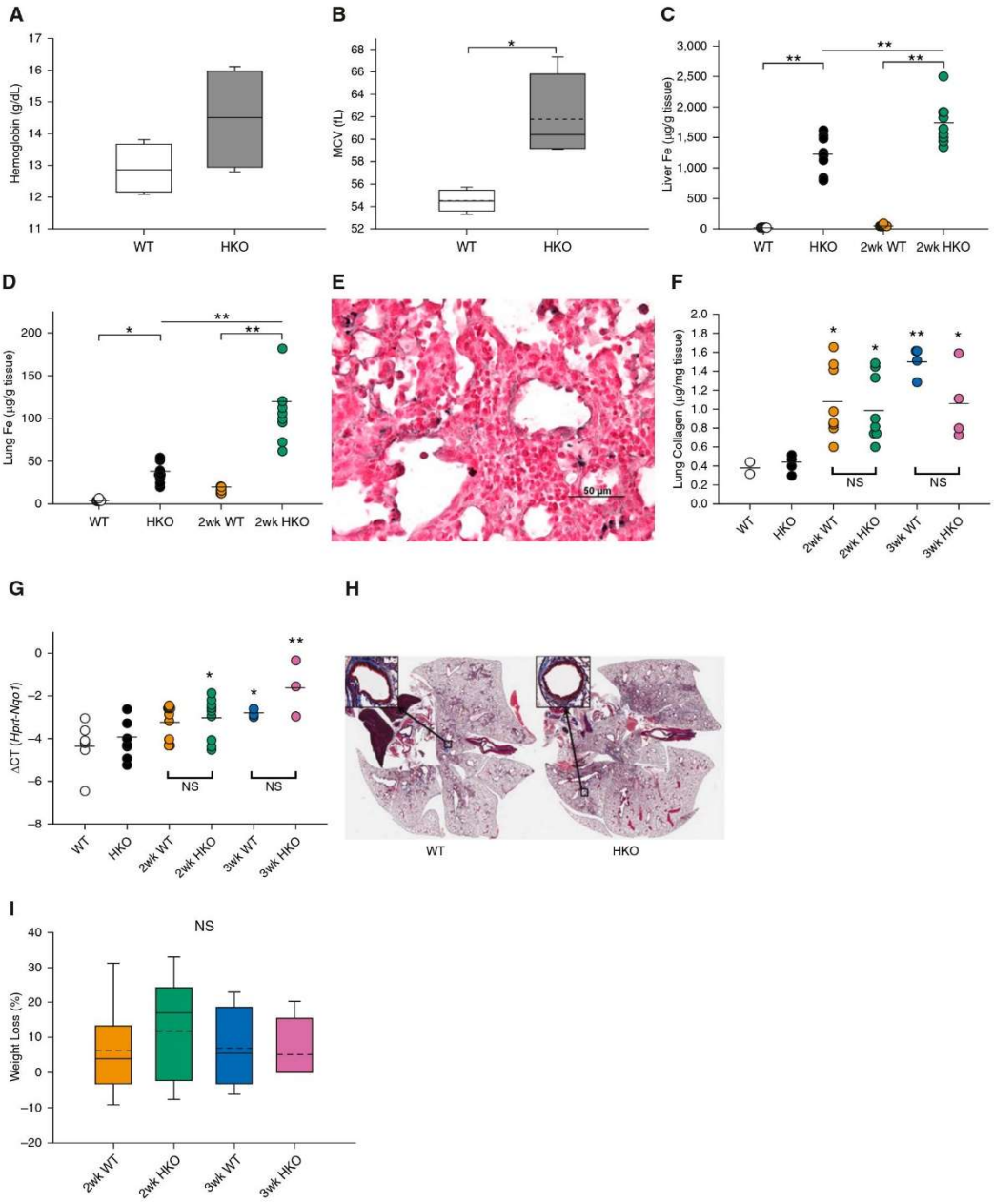

Figure 1. Severe iron (Fe) overload does not augment the response to bleomycin in a mouse model of pulmonary fibrosis. Hematologic measurements prior to bleomycin treatment show (*A*) a trend toward increased hemoglobin and (*B*) increased mean corpuscular volume (MCV) in hepcidin-knockout (HKO) mice ($n = 4$/genotype). (*C*) Liver Fe and (*D*) lung Fe measurements at 2 weeks after bleomycin treatment confirm severe Fe overload in HKO mice ($n = 6$–9/group). (*E*) Representative enhanced Perls' stain of bleomycin-treated HKO mouse lung demonstrates Fe deposition. (*F*) Collagen quantification of whole-lung tissue shows no difference between the genotypes at either 2 weeks or 3 weeks ($n = 2$–5 for untreated groups; $n = 4$–9 for treated groups). (*G*) Lung *Nqo1* increases in both genotypes after bleomycin treatment but without showing a difference between genotypes at each time point ($n = 4$–10/group). (*H*) Representative digital image of whole-lung Masson's trichrome stain of WT and HKO mice. (*I*) Mouse weights show no difference in weight loss among any of the treated groups ($n = 4$–9/group). Box-plot graphs depict the median (solid line) ± 25th/75th percentile and/or the mean (dashed line); dot density plots depict the mean (solid line). $^*P < 0.05$ and $^{**}P < 0.001$ by (*B*) *t* test or (*C* and *D*) two-way ANOVA as indicated or (*F* and *G*) two-way ANOVA for comparison of each treated group with its untreated genotype control group. CT = cycle threshold; NS = not significant; WT = wild type. Scale bar, 50 μm.

ORCID IDs: 0000-0002-3477-2397 (E.N.); 0000-0002-8454-4472 (A.K.).

*Corresponding author (e-mail: airiekim@mednet.ucla.edu).

References

1. Lederer DJ, Martinez FJ. Idiopathic pulmonary fibrosis. *N Engl J Med* 2018;379:797–798.
2. Richeldi L, Collard HR, Jones MG. Idiopathic pulmonary fibrosis. *Lancet* 2017;389:1941–1952.
3. Puxeddu E, Comandini A, Cavalli F, Pezzuto G, D'Ambrosio C, Senis L, *et al*. Iron laden macrophages in idiopathic pulmonary fibrosis: the telltale of occult alveolar hemorrhage? *Pulm Pharmacol Ther* 2014;28:35–40.
4. Sangiuolo F, Puxeddu E, Pezzuto G, Cavalli F, Longo G, Comandini A, *et al*. HFE gene variants and iron-induced oxygen radical generation in idiopathic pulmonary fibrosis. *Eur Respir J* 2015;45:483–490.
5. Kim KH, Maldonado F, Ryu JH, Eiken PW, Hartman TE, Bartholmai BJ, *et al*. Iron deposition and increased alveolar septal capillary density in nonfibrotic lung tissue are associated with pulmonary hypertension in idiopathic pulmonary fibrosis. *Respir Res* 2010;11:37.
6. Dixon SJ, Stockwell BR. The role of iron and reactive oxygen species in cell death. *Nat Chem Biol* 2014;10:9–17.
7. Zhang V, Nemeth E, Kim A. Iron in lung pathology. *Pharmaceuticals (Basel)* 2019;12:30.
8. Allden SJ, Ogger PP, Ghai P, McErlean P, Hewitt R, Toshner R, *et al*. The transferrin receptor CD71 delineates functionally distinct airway macrophage subsets during idiopathic pulmonary fibrosis. *Am J Respir Crit Care Med* 2019;200:209–219.
9. Lesbordes-Brion JC, Viatte L, Bennoun M, Lou DQ, Ramey G, Houbron C, *et al*. Targeted disruption of the hepcidin 1 gene results in severe hemochromatosis. *Blood* 2006;108:1402–1405.
10. Neves J, Haider T, Gassmann M, Muckenthaler MU. Iron homeostasis in the lungs: a balance between health and disease. *Pharmaceuticals (Basel)* 2019;12:5.
11. Fisher AL, Sangkhae V, Presicce P, Chougnet CA, Jobe AH, Kallapur SG, *et al*. Fetal and amniotic fluid iron homeostasis in healthy and complicated murine, macaque, and human pregnancy. *JCI Insight* 2020;5:e135321.
12. Ali MK, Kim RY, Brown AC, Donovan C, Vanka KS, Mayall JR, *et al*. Critical role for iron accumulation in the pathogenesis of fibrotic lung disease. *J Pathol* 2020;251:49–62.

Retraction: Obesity-induced Endoplasmic Reticulum Stress Causes Lung Endothelial Dysfunction and Promotes Acute Lung Injury

This article (1) has been retracted by the authors. It was discovered that the same immunoblot images were used to represent two different experimental conditions. This includes Figure 1D in which a blot of GRP78 is identical to a blot labeled as β-catenin in another paper (2), and Figure 2F in which a blot of GADPH is identical to a portion of a GAPDH image used in that paper (2). In addition, anomalies were identified in the Western blot images in Figures 1D, 2B, 2F, 2H, 3A, 3E, 3F, and 5B. Given that the scientific integrity of this study has been compromised, the authors believe that retraction of this paper is the best course of action. All the authors have agreed to this decision.

The authors apologize to the *Journal* and its readers. ■

Reference

1. Shah D, Romero F, Guo Z, Sun J, Li J, Kallen CB, Naik UP, Summer R. Obesity-induced endoplasmic reticulum stress causes lung endothelial dysfunction and promotes acute lung injury. *Am J Respir Cell Mol Biol* 2017;57:204–215.
2. Shah D, Romero F, Duong M, Wang N, Paudyal B, Suratt BT, Kallen CB, Sun J, Zhu Y, Walsh K, Summer R. Obesity-induced adipokine imbalance impairs mouse pulmonary vascular endothelial function and primes the lung for injury. *Sci Rep* 2015;5:11362.

Retraction: Chronic Alcohol Ingestion In Rats Alters Lung Metabolism, Promotes Lipid Accumulation, and Impairs Alveolar Macrophage Functions

An article published in the December 2014 issue of the *Journal* (1) has been retracted by the authors. It was discovered that the GAPDH band in Figure 4C is incorrect and is identical to that used in Figure 4D. Moreover, the images used to represent acetyl-CoA synthase in Figure 4D and pAMPK in Figure 4C are the same. In addition, anomalies were identified in the Western blot images for AMPK (Figure 4C) and FASN (Figure 4D). Based on these findings, although the authors continue to stand behind the conclusions reached, the scientific integrity of the manuscript has been compromised. All the authors have agreed to this decision, and they apologize to the *Journal* and its readers. ■

Reference

1. Romero F, Shah D, Duong M, Stafstrom W, Hoek JB, Kallen CB, Lang CH, Summer R. Chronic alcohol ingestion in rats alters lung metabolism, promotes lipid accumulation, and impairs alveolar macrophage functions. *Am J Respir Cell Mol Biol* 2014;51:840–849.

This article is open access and distributed under the terms of the Creative Commons Attribution Non-Commercial No Derivatives License 4.0 (http://creativecommons.org/licenses/by-nc-nd/4.0/). For commercial usage and reprints, please contact Diane Gern (dgern@ thoracic.org).

CHAPTER 3: THE ROLE OF ZIP8 IN IRON HOMEOSTASIS, INFLAMMATION, AND INFECTION

Manuscript submitted:

THE ROLE OF ZIP8 IN IRON HOMEOSTASIS, INFLAMMATION, AND INFECTION

Vida Zhang[1,2], Supak Jenkitkasemwong[3], Qingli Liu[3], Tomas Ganz[1], Elizabeta Nemeth[1], Mitchell D Knutson [3]*, Airie Kim [1*#]

[1]Department of Medicine, David Geffen School of Medicine, UCLA, Los Angeles, CA, USA

[2]Department of Molecular and Medical Pharmacology, UCLA, Los Angeles, CA, USA

[3]Food Science and Human Nutrition Department, University of Florida, Gainesville, FL, USA.

*equal contribution

[#]Airie Kim; David Geffen School of Medicine, 10833 LeConte Ave 43-229 CHS, Box 951690, Los Angeles, CA 90095; (310) 825-7499

CONFLICT OF INTEREST

T.G. and E.N. are shareholders and scientific advisors of Intrinsic LifeSciences and Silarus Therapeutics, and consultants for Ionis Pharmaceuticals, Protagonist, Keryx Pharmaceuticals, La Jolla Pharma, Vifor, Akebia (T.G.), and Gilead (T.G.). M.K. has consulted for Pharmavite. A.K. has served on an advisory board for Pharmacosmos. V.Z., S.J, and Q.L. do not have any conflicts of interest, financial or otherwise, to disclose.

ABSTRACT

ZIP8 (SLC39A8) is a transmembrane divalent metal ion importer that is most highly expressed in the lung and is inducible by inflammatory stimuli. In addition to zinc and manganese, ZIP8 can transport iron but its specific roles in iron regulation during homeostatic and pathologic processes remain poorly understood. Using a novel global inducible ZIP8 knockout (KO) mouse, we analyzed the role of ZIP8 in steady-state iron homeostasis and during inflammation and infection. We observed an unexpected phenotype of elevated spleen iron levels and decreased serum iron in ZIP8 KO mice, suggesting that ZIP8 plays a role in iron recycling. We also showed that ZIP8 is expressed on lung distal airspace epithelial cells and transports iron from the airway into lung tissue. LPS-induced inflammation induced ZIP8 expression in the lung, but ZIP8 deletion had no detrimental effect on the severity of LPS-induced acute lung injury or on the outcomes of *Klebsiella pneumoniae* lung infection. Thus, ZIP8 plays a role in systemic iron homeostasis but does not modulate the severity of inflammatory lung injury or the host defense against a common bacterial cause of pneumonia.

INTRODUCTION

Iron is an essential trace mineral for normal cellular function in all living organisms, including DNA replication, cellular metabolism and ATP generation. The largest fraction of iron in humans and other mammals is used for hemoglobin synthesis and erythrocyte production. Low iron levels most commonly lead to insufficient red blood cell production, causing anemia and impaired oxygen delivery to tissues. Excessive iron is also detrimental, leading to tissue damage as a result of excessive reactive oxygen species (ROS) generation by the Fenton reaction. Thus, iron homeostasis has evolved for tight iron regulation of iron levels.

In humans, iron is primarily obtained from the diet, particularly from foods rich in heme. Iron is taken up in the duodenum and released on the basolateral side of enterocytes into blood through ferroportin, the only known cellular iron exporter (1). As free iron is dangerous because it generates ROS through the Fenton reaction, it is quickly taken up by the iron transporter transferrin in the blood so that it can be safely transported to tissues. Iron-laden transferrin binds to transferrin receptor 1 (TFR1) on cell surfaces and is internalized, allowing iron to be utilized by the cell (2). Unused intracellular iron is stored in the iron storage protein ferritin until needed. Most of the body's iron is used by erythroid precursor cells in the bone marrow to make red blood cells (RBCs) (3). As the RBCs age or are damaged, they are phagocytosed by macrophages residing in the red pulp. The macrophages extract iron from hemoglobin and release it into circulation through ferroportin (4). Excess body iron is stored in the liver, the main iron storage organ, and is mobilized when iron demand is high. Hepcidin, a peptide hormone produced in the liver, is the master regulator of systemic iron homeostasis and functions by binding to ferroportin and causing its internalization and degradation (1).

Regulation of extracellular iron concentration plays an important role in host defense. Numerous studies have defined the detrimental effect of iron overload in infections by multiple pathogens, including *Yersinia enterocolitica*, *Escherichia coli*, and *Klebsiella pneumoniae* (5-8). Multiple host defense pathways function to sequester iron away from pathogens. Hepcidin-mediated hypoferremia during infections is an important form of nutritional immunity (1, 8). Neutrophil gelatinase-associated lipocalin (NGAL) prevents bacterial iron uptake by sequestering siderophores, bacterial compounds that bind to iron for active uptake by the microbe (9). Lactoferrin is present in mucosa and functions similarly to transferrin by binding to iron for re-uptake through lactoferrin receptors (10). Intracellularly, natural resistance-associated macrophage protein 1 (NRAMP1) is expressed in macrophage phagosomes and reduces iron availability for various intraphagosomal pathogens (11).

In addition to systemic iron regulation, cells and tissues also regulated iron in an autocrine/paracrine manner, although these mechanisms are less well understood. In the lung, iron regulation has multiple unique challenges. The lung epithelium is exposed to external air as part of its role in air-blood gas exchange, which also exposes it to iron particles and infectious pathogens that can potentially cause injury (12, 13). In addition, altered iron levels have been associated with lung pathologies, such as acute lung injury, COPD, and pulmonary hypertension (12). However, how iron uptake and distribution is regulated in the lung is still unclear.

ZIP8 (SLC39A8) is a transmembrane divalent metal transporter that was initially identified as a zinc importer, but has since been shown to transport manganese as well as iron with high affinity (14-16). In humans, ZIP8 mutations are associated with schizophrenia, Crohn's disease and manganese deficiency (17-19). However, its roles in iron homeostasis and related pathology have yet to be determined. Interestingly, ZIP8 is most highly expressed in the lung compared to other

tissues, and is also more highly expressed in the lung than known iron transporters such as ZIP14, DMT1 and TFR1 (15). In addition, ZIP8 is induced by inflammation, including that caused by LPS and tobacco smoke, which suggests that ZIP8 may play a role in lung host defense through iron regulation (20-22). Our goal was to determine the physiological functions of ZIP8 in iron homeostasis and investigate the role of ZIP8 in pulmonary host defense.

Here we report the characterization of a novel global ZIP8 KO mouse during homeostasis and pathologic conditions. The iron characterization studies were performed in parallel in two separate laboratories, the Kim lab at the University of California, Los Angeles (UCLA) and the Knutson lab at the University of Florida (UF), using the same genetic mouse model. While minor variations in phenotype were observed between laboratories, the effects of ZIP8 deletion were substantially similar between both groups, strengthening the conclusions of our findings.

RESULTS

Metal analysis of baseline ZIP8 knockout mice

As whole-body deletion of ZIP8 is embryonic lethal, and ZIP8 hypomorphic mice do not survive beyond postnatal day two (23, 24), we generated an inducible whole-body ZIP8 KO mouse to characterize the role of ZIP8 *in vivo* **(Supplemental Figure 1a)**. Loss of ZIP8 was confirmed at the DNA, RNA, and protein levels **(Supp. Fig. 1b-d)**. Mice appeared phenotypically normal up to at least 1 year of age. In addition, we used a custom-made in-house antibody targeting mouse ZIP8 that outperformed multiple commercial antibodies in our verification assays.

We performed ICP-MS on various tissues from 16-week-old ZIP8 KO and littermate controls to quantify any baseline differences in the levels of iron (heme + nonheme), zinc, and manganese (Mn). In the liver, there were no significant differences in iron or zinc concentrations, but ZIP8 KO mice did have significantly less Mn as compared to their controls **(Figure 1a-b)**, as has been previously reported (25). In the spleens, no difference in zinc levels was observed, though there was a noticeable but not statistically significant decrease in manganese levels in the ZIP8 KO spleens. Unexpectedly, ZIP8 KO spleens also had significantly more iron (both concentration and total) than their littermate controls **(Figure 1c-d)**.

ZIP8 knockout mice have impaired iron recycling

To determine the cause of this increased iron in ZIP8 KO spleens, we analyzed steady-state iron and hematologic parameters of 16-week-old ZIP8 KO mice at UCLA and 16- and 12-wk-old mice at UF. Tissue non-heme iron measurements by colorimetry confirmed no significant difference in liver iron levels between the two groups, and significantly higher spleen iron levels in ZIP8 KO mice at both institutions (UCLA: fl/fl 298 μg Fe/g tissue vs KO 516 μg Fe/g tissue, $p<0.0001$) **(Figure 2a, Supp. Fig. 2a,c)**. Accordingly, the KO mice at both institutions had lower

serum/plasma iron levels, suggesting that decreased circulating iron results from increased splenic iron sequestration. At UCLA, despite the apparent reduced iron availability for erythropoiesis, there was no significant difference in baseline hemoglobin (Hb), hematocrit (HCT) or MCV between ZIP8 KO and control littermates **(Figure 2b)**. At UF, ZIP8 KO mice at 16 wks of age had a mildly decreased Hb (fl/fl 13.47 g/dl vs KO 12.13 g/dl, $p<0.005$) and increased reticulocyte count (fl/fl 1.36% vs KO 4.51%, $p<0.001$), indicating impaired erythropoiesis secondary to splenic iron sequestration and reduced iron availability **(Supp. Fig. 2b)**. A similar decrease in Hb concentrations was also observed in a larger cohort of mice at 12 wks of age **(Supp. Fig. 2d)**. The manifestation of the mild erythropoietic impairment could potentially be a result of institutional differences in the vivarium environment, such as different diets, use of metal cages, etc. Nonetheless, splenic iron sequestration and hypoferremia were consistently observed in the ZIP8 KO mice in both laboratories. Analysis of the systemic regulators of iron homeostasis showed that liver hepcidin and bone marrow erythroferrone (ERFE, hepcidin regulator) mRNA levels were unchanged in KOs compared with control mice **(Figure 2c)**, consistent with the lack of difference in liver iron concentrations or CBCs between the two genotypes (at UCLA). Perls' staining of the spleen showed that the increased iron was in the red pulp of the spleen **(Figure 2d)**, the site of erythrocyte turnover (26). Using magnetic cell sorting, we confirmed that spleen ZIP8 is primarily expressed in red pulp macrophages, the specific cells responsible for iron recycling from senescent and damaged red blood cells (26) **(Figure 2e)**. Taken together, these data suggest that ZIP8 is involved in erythrocyte turnover and iron recycling.

Interestingly, despite higher non-heme iron concentrations in the KO spleen, there were no changes in the *Tfr1* mRNA expression, or ferroportin and ferritin protein levels. In addition, there was no difference in the mRNA levels of *Hmox*, the enzyme responsible for the first step of heme degradation **(Supp. Fig. 3a-b)**. There was also no evidence of downstream oxidative damage in

KO mice, as shown by unchanged spleen malondialdyhyde (MDA) levels and *Nqo1* expression **(Supp. Fig. 3c)**.

ZIP8 deletion does not modify hemolytic anemia

In order to evaluate whether ZIP8 has a role during conditions of accelerated erythrophagocytosis and iron recycling, we utilized mouse models of parenteral iron administration, erythrophagocytosis of aged RBCs, and phenylhydrazine (PHZ)-induced hemolytic anemia. 8 wk old C57BL/6 (B6) mice were injected IP with 10 mg iron dextran, 300 µl packed aged red blood cells, or 60 mg/kg PHZ daily for two days, then spleens were harvested 3 days after treatment. Splenic ZIP8 protein levels were induced in response to iron dextran as well as to PHZ (at both institutions) **(Figure 3a, Supp. Fig. 4a)** but not in response to aged RBCs. ZIP8 protein across different conditions positively correlated to the amount of iron present in the spleen **(Figure 3b)**. However, the inflammatory marker Saa1 was also induced in response to iron dextran and PHZ (3 days after treatment, **Figure 3c**), suggesting that the increase in ZIP8 expression could be secondary to increased inflammation rather than iron status or accelerated erythrocyte turnover. PHZ-treated mice had CBCs measured on day 4, the peak of hemolytic anemia severity, and on day 7, post recovery. We found no significant differences in RBC, Hb, HCT or MCV levels between ZIP8 KO mice and their controls on day 4 or day 7 **(Figure 3d)**. There was also no change in inflammation and oxidative stress at day 7 as measured by liver *Saa1* and spleen *Nqo1* mRNA respectively **(Figure 3e)**. After PHZ treatment, ZIP8 KO mice had more splenic iron as compared to their controls in both laboratories **(Figure 3f, Suppl Fig. 4c)**, despite an unchanged number of splenic macrophages as assessed by the expression of *Adgre,* gene encoding F4/80 **(Supp. Fig. 5b)**, and without a difference in serum iron levels **(Figure 3f)**. We observed a small but statistically significant increase in spleen ferroportin protein levels in ZIP8 KO mice at UCLA but not at UF **(Supp. Fig. 5a,c)**. Taken together, these data suggest that while ZIP8 does increase in response

to iron loading and hemolytic anemia, it does not appear to play a crucial role in recovery from hemolytic anemia.

Iron deficiency and ZIP8

We used a mouse model of iron deficiency to assess the role of ZIP8 in mobilization of recycled iron. At UCLA, 8-week-old ZIP8 KO mice and littermate controls were placed on a 4 ppm iron diet for 24 weeks, and underwent regular blood draws for CBC measurements until harvest. As expected, RBC, Hb, Hct, and MCV levels all decreased in both groups as a result of prolonged iron deficiency and repeated blood draws. However, there was no significant difference in CBC parameters between ZIP8 KO mice and littermate controls at any time point measured **(Figure 4a)**. There was also no significant difference in ZPP, a marker of iron deficiency **(Figure 4b)**, and iron measurements in serum, spleen, and liver showed no significant difference with ZIP8 deletion **(Figure 4c)**. There was also no difference in the iron transporters ferroportin or TFR1, the iron storage protein ferritin, nor in liver *Hamp* **(Figure 4d-e)**.

In a parallel experiment at UF, ZIP8 KO mice and littermates were fed iron-deficient diet for 8 weeks. Although the short-term iron-deficient diet regimen did not decrease Hb levels in either control or KO mice **(Supp. Fig. 2b,6a)**, liver non-heme iron concentrations were low in both groups, consistent with iron deficiency **(Supp. Fig. 6b)**. Splenic iron concentrations, however, were higher in ZIP8 KO mice than in control mice. The higher splenic iron levels in ZIP8 KO were associated with elevated ferritin levels in the spleen with no change in ferroportin protein levels **(Supp. Fig. 6c)**. Interestingly, although splenic non-heme iron was higher in ZIP8 KOs, TFR1 levels were paradoxically increased compared to the controls **(Supp. Fig. 6c-d)**. It is possible that the increased ferritin levels reflect macrophage iron status, whereas increased TfR1 levels reflect an increase in extramedullary hematopoiesis resulting from impaired iron availability. Indeed,

expression of several erythropoietic markers increased in ZIP8 KO compared to WT spleens (*Alas2, Erfe, Mfrn1*, **Supp. Fig. 6d**).

Taken together, our data suggest that after a short exposure to iron deficiency, ZIP8 KO mice still retained iron in the spleen, but also displayed mild compensatory extramedullary erythropoiesis. However, after prolonged iron deficiency, together with repeated blood draws, iron was effectively mobilized and no difference in CBCs was observed, suggesting that ZIP8 does not play a major role in the increased iron mobilization and handling that occurs during the stress state of iron deficiency.

ZIP8 is expressed in alveolar epithelial cells and is induced by inflammation

ZIP8 is most highly expressed in the lung compared to other tissues in the body but no studies have systematically examined the role of ZIP8 in lung iron regulation. Using IHC on normal human lung tissue sections, we found that ZIP8 is expressed on the apical side of lung epithelial cells facing the air-filled compartment **(Figure 5a)**.

There have been reports in the literature that ZIP8 is inducible with various inflammatory stimuli (20-22), and we confirmed this with in human cells *in vitro*. We treated A549 (a human alveolar epithelial cell line) with various cytokines and growth factors. ZIP8 mRNA and protein were induced after treatment with IL-1a, IL-1b and TNFα **(Figure 5b-c)**. The specificity of ZIP8 detection was confirmed through siRNA knockdown of ZIP8 **(Figure 5d)**. ZIP8 induction with inflammatory stimuli appears to be specific to alveolar epithelial cells, as there was no ZIP8 increase in HBECs (a human bronchiolar epithelial cell line) with the identical stimuli **(Figure 5e)**.

ZIP8 transports iron from the airspace to the lung

As there was no existing literature describing the *in vivo* function of ZIP8 in lung iron homeostasis, we used ZIP8 KO mice to investigate the location and directionality of ZIP8-mediated iron transport. Using magnetic sorting of mouse lung cells, we found that *Slc39a8* mRNA is primarily expressed in epithelial cells at baseline **(Figure 6a)**. Of note, although our IHC data in human lung showed no detectable ZIP8 staining on endothelial cells, the sorted mouse lung endothelial cells expressed relatively high levels of ZIP8 mRNA, potentially as a result of contamination of the endothelial cell fraction with epithelial cells. We also found that sorted mouse alveolar macrophages express very low levels of *Slc39a8* mRNA **(Figure 6a)**, in contrast to the splenic red pulp macrophages **(Figure 2e)**.

As ZIP8 expression is very high on lung epithelial cells, we determined the directionality of iron transport by ZIP8, by treating ZIP8 KO and littermate controls with ^{58}Fe via retro-orbital injection to the bloodstream or oropharyngeal aspiration into the airspace. After 4 hours, BAL fluid and lung tissue were harvested for ICP-MS analysis for ^{58}Fe. With RO ^{58}Fe, there was no difference in ^{58}Fe levels between ZIP8 KO mice and littermate controls in either BAL fluid or lung tissue. However, when ^{58}Fe was given OP, ZIP8 KO mice had more ^{58}Fe in the BAL fluid (fl/fl 54.97 ng vs KO 87.30 ng, p=0.097) and less ^{58}Fe in the lung tissue (fl/fl 3160.13 ng vs KO 1823.77 ng, p=0.013) as compared to their controls **(Figure 6b)**. These data indicate that ZIP8 functions to transport iron from the airspace into the lung. However, as we found no difference in steady-state lung iron levels between ZIP8 KO and littermate controls **(Figure 6c)**, the import of iron from the air compartment likely does not play a large role in steady-state homeostasis. In addition, there was no difference in oxidative stress as measured by lung *Nqo1* mRNA and lung MDA **(Figure 6d)**.

ZIP8 does not play a role in LPS-induced acute lung injury

Because ZIP8 expression is induced by inflammation, we investigated whether ZIP8 plays a role in the response to inflammatory acute lung injury. We treated 16-week-old ZIP8 KO mice and littermate controls with OP LPS 15 mg/kg or no treatment. Mice were harvested after 3 days for analysis of BAL fluid and tissue. LPS inflammation did induce ZIP8 expression in the lung of wild-type mice **(Figure 7a)**, but no difference was noted in lung non-heme iron levels between the ZIP8 KO mice and their controls **(Figure 7b)**. Measurement of the ALI parameters of BAL protein and BAL/lung tissue myeloperoxidase (MPO) confirmed that LPS treatment resulted in significant lung injury, but ZIP8 deletion had no effect on the severity of acute lung injury **(Figure 7c-d)**. In addition, there was no change in oxidative stress as measured by mitochondrial superoxide dismutase (SOD; **Figure 7e**). These data indicate that while lung ZIP8 is induced with inflammation, ZIP8 deletion does not modify the severity of LPS-induced acute lung injury.

Loss of ZIP8 is protective against K. pneumoniae infection

Because ZIP8 is induced by inflammation, we hypothesized that ZIP8 may play a protective role in host defense by importing iron into the epithelium, thus lowering iron availability in the airspace. To test this, we administered OP 300 CFU of *Klebsiella pneumoniae* in ZIP8 KO mice and controls then analyzed mice at 3 days post infection. Interestingly, ZIP8 KO mice experienced less weight loss than floxed littermate controls (fl/fl 15.53% vs KO 7.96%, p=0.0446) and trended towards less bacterial burden in their lungs, livers, spleens and blood as measured by CFUs **(Figure 8a-b)**. There was no significant difference in lung injury as assessed by BAL protein and BAL protein and lung MPO levels **(Figure 8c-d)**, and there was also no difference in oxidative stress, as measured by lung mitochondrial and cytosolic SOD **(Figure 8e)**. Taken together, these data suggest that ZIP8 does not play a protective role in host defense, and instead may worsen the outcomes in *K. pneumoniae* infection through an as yet unknown mechanism.

In summary, in our extensive characterization of global ZIP8 knockout mice, we have shown that ZIP8 is highly expressed in the lung and can import iron into the epithelium from the air compartment. However, our data demonstrate that ZIP8 is not critical for lung iron homeostasis, as evidenced by the analysis of baseline iron levels or the inflammatory response to lung injury. Furthermore, ZIP8 did not play a protective host defense role against *K. pneumoniae* lung infection. We have also demonstrated that ZIP8 is involved in splenic iron recycling, however, ZIP8 deletion alone is not sufficient to cause major hematological impairment at baseline or under stress conditions.

DISCUSSION

In our examinations of the role of the role of ZIP8 in iron regulation, both systemically and in the lung, we generated a number of tools. As whole body deletion of ZIP8 is embryonic lethal (23, 24), we generated an inducible ZIP8 KO mouse to allow for the study of the role of ZIP8 in an adult mouse model. In addition, we generated and validated a new anti-mouse ZIP8 antibody. These tools will serve to enable future studies of ZIP8 function *in vivo*.

Most of our findings regarding the role of ZIP8 in systemic iron regulation were replicated in two separate institutions with the same genetic mouse models, strengthening the validity of our findings. We did observe, however, some small differences between the two sets of mice. Increased splenic iron and decreased serum iron in ZIP8 KO mice at baseline were present in the findings of both labs, however lower baseline Hgb in ZIP8 KO mice compared to littermate controls was observed at UF but not UCLA. Some changes of iron-handling proteins, such as ferroportin, TFR1 and ferritin, were also observed in one set of mice but not the other. A possible explanation could be the differences in vivarium environment, such as different diets or use of metal cages, which could have altered iron bioavailability or their microbiome.

The increase in splenic iron in ZIP8 KO mice was primarily in the red pulp macrophages as determined by Perls' staining for iron, which suggests that ZIP8 is involved in iron recycling from red blood cells. Erythrophagocytosis occurs when aged or damaged RBCs are hemolyzed and phagocytosed by red pulp macrophages in the spleen. The heme is released into the erythrophagosome and transported into the cytosol through HRG1 (27). HO-1 then breaks down heme and releases iron, which is then bound and stored in ferritin (26). When the iron is needed, NCOA4 binds to and shuttles iron-laden ferritin to autophagosomes, which then fuse with lysosomes to break down ferritin and release the iron, which can then be exported from the cell

through ferroportin (28). We speculate that ZIP8 may be localized to an intracellular compartment and transport iron from within phagosomes (the erythrophagosome and/or autophagosome) to the cytosol, as indicated by the increase in iron in red pulp macrophages from ZIP8 KO mouse spleens. Despite this significant increase in splenic iron, however, we see minor or no effect on hematological parameters even after stressing the iron recycling system through hemolytic anemia or iron deficiency. In addition, we did not see any significant differences in splenic ferroportin, transferrin receptor or ferritin levels under baseline conditions. This lack of effect of ZIP8 in iron recycling, despite the increased iron, may indicate redundancy with other intracellular transporters that could compensate for the loss of ZIP8. DMT1 is also expressed intracellularly and Nramp1, closely related to DMT1, is another intracellular iron transporter present in macrophages (29, 30). In addition, ZIP14, a metal transporter with a very similar structure to ZIP8, is also present in macrophages and is upregulated in activated macrophages (14, 31). It is possible that any of these could be upregulated and blunt the effects of ZIP8 deletion and iron sequestration on the body. The observation that splenic ZIP8 levels were markedly increased in response to hemolysis or iron dextran, both of which increase iron loading in red pulp macrophages (32, 33), suggests that splenic ZIP8 levels are regulated by iron. Furthermore, the increase in splenic ZIP8 levels was positively associated with spleen iron content, suggesting a dose-response effect of iron loading on ZIP8 abundance, similar to what was found in cultured rat hepatoma cells (15).

Regarding the role of ZIP8 in the lung, we have established that ZIP8 is expressed on the apical side of lung alveolar epithelial cells and confirmed that the direction of transport is from the airspace into the lung epithelium. Furthermore, we confirmed that ZIP8 is induced by inflammation, specifically IL-1a, IL-1b and TNFα in human alveolar epithelial cells and by LPS in mice *in vivo*. As inflammation-induced ZIP8 could sequester iron away from potential pathogens

in the airspace, our initial hypothesis was that loss of ZIP8 would be detrimental during bacterial infections. However, loss of ZIP8 had no effect on response to ALI and we observed that loss of ZIP8 was actually beneficial in the case of *K. pneumoniae* infection. This is in contrast to a recent publication by the Knoell group examining the role of ZIP8 in macrophages (34). Their study demonstrated that loss of ZIP8 specifically in macrophages and dendritic cells worsened pulmonary *Streptococcus pneumoniae* infection by hindering the immune response in a zinc-dependent manner through altered NFκB signaling. One potential difference between our studies could simply be due to the differing pathogens used, as *K. pneumoniae* is a gram-negative bacterium while *S. pneumoniae* is gram-positive. Another difference could be the type of tissues where ZIP8 was deleted in the mouse models. Our mouse model was a whole-body postnatally-induced knockout of ZIP8, which leads to loss of ZIP8 in the alveolar epithelium, as well as macrophages and other cells. The mouse model used by the Knoell group specifically and constitutively knocks out ZIP8 in myeloid cells, which means that ZIP8 in the lung epithelium is still expressed. In addition, we found that ZIP8 is not expressed at baseline in alveolar macrophages, suggesting that the phenotype in the Knoell study may be related to the role of ZIP8 in monocyte-derived macrophages rather than specifically alveolar macrophages. Altogether, our study indicates that ZIP8 does not appear to play a significant role in lung iron regulation, nor a protective role in pulmonary host defense against *K pneumoniae* infection.

While ZIP8 is highly expressed in the lung, our data on the lack of any major ZIP8 role in the lung are consistent with the reports of the human diseases where ZIP8 mutations were associated with non-pulmonary manifestations. In addition, although ZIP8 may not be critical for lung iron homeostasis or iron recycling, it may play a more important role in the transport of other divalent metals. ZIP8 has already been shown to be necessary for manganese uptake and recycling from the bile, and we have observed in our own mice that ZIP8 KO mice have significantly decreased

manganese levels ((25), **Fig 1**). Furthermore, the human phenotype of ZIP8 loss has also been shown to mostly be related to manganese, as abnormal manganese homeostasis has been observed in human diseases such as schizophrenia, obesity and Crohn's disease (17-19). In addition, studies examining the role of ZIP8 in host defense characterized its effect as zinc-related and affecting the NFκB pathway (34-36).

Our study has shown that while ZIP8 may play a role in systemic iron recycling, as indicated by increased splenic iron in ZIP8 KO mice, it does not appear to have a significant role in pulmonary iron regulation or host defense. However, more remains to be learned about ZIP8 and iron regulation. One potential reason for the lack of significant iron-related differences in our ZIP8 KO mice is that ZIP8 may be most important during development, as complete loss of ZIP8 is embryonic lethal (23, 24) and the placenta is the organ with the highest expression of ZIP8 after the lung (15). As iron is critical for embryonic development (37, 38), ZIP8 may potentially play a greater role in iron regulation during development rather than in adulthood. The tools generated in our study could be helpful in exploring the role of ZIP8 during embryonic development.

METHODS

See Supplemental Figure legends for UF materials and methods.

Animal models

C57BL/6 (B6) mice were purchased from Jackson Laboratories (JAX # 000664). Conditional-ready, ZIP8 floxed allele (ZIP8$^{fl/fl}$) mice were generated from mice harboring a targeted recombinant allele (*r*) of *Slc39a8* (C57BL/6NTac-Slc39a8$^{tm1a(EUCOMM)Wtsi/Cnrm}$; European Mouse Mutant Archive (EMMA)). Briefly, the *r* allele harbors *LoxP* recombination sites flanking exon 3 of the *Slc39a8* gene and *FRT* sites flanking a neomycin resistance gene (*neo*) adjacent to the upstream *LoxP* site. To delete the neo cassette and generate ZIP8$^{fl/fl}$ mice, *Slc39a8*$^{+/r}$ mice were bred with ROSA26:FLPe knock-in mice with ubiquitous expression of FLP1 recombinase (B6.129S4-Gt(ROSA)26Sor$^{tm1(FLP1)Dym}$/RainJ; The Jackson Laboratory, JAX# 009086). PCR and DNA sequencing of ZIP8$^{fl/fl}$ mice verified deletion of the *FRT*-flanked sequence and confirmed the *LoxP* sites flanking exon 3. To generate ZIP8 KO mice, *Slc39a8*$^{fl/fl}$ mice were bred with mice expressing tamoxifen-inducible Cre under the Gt(ROSA)26Sor promoter (iRosaCre$^{+/-}$; Jackson Laboratory, JAX #008463) to generate iRosaCre$^{+/-}$;ZIP8$^{fl/fl}$ and iRosaCre$^{-/-}$;ZIP8$^{fl/fl}$ littermates. At 4 weeks of age, iRosaCre$^{+/-}$;ZIP8$^{fl/fl}$ mice were placed on a 500 mg tamoxifen/kg diet (Teklad; 80 mg/kg body weight/day) for 2 weeks to induce Cre-mediated recombination and ZIP8 gene excision, then placed back on regular chow to regain weight. These mice are referred to as ZIP8 KO mice (deletion of ZIP8 confirmed in **Supp. Fig 1**). iRosaCre$^{-/-}$;ZIP8$^{fl/fl}$ littermates were placed on the same diet regimen as controls. Fourteen- to eighteen-week-old age- and sex-matched male and female mice were used in experiments. Mice of both sexes were used for experiments.

To assess the response of splenic ZIP8 induction to iron, 8 week old B6 mice were injected with 300 µl aged red blood cells (RBCs), a single i.p. injection of 10 mg iron dextran (MilliporeSigma, D8517) or two consecutive daily doses of 60 mg/kg phenylhydrazine hydrochloride (PHZ, Sigma

114715). To obtain aged red blood cells, mouse blood was collected into heparin-containing tubes, then diluted in sterile PBS and centrifuged to remove the plasma and buffy coat. The cells were washed again in PBS, counted, then re-suspended in HEPES buffer (10 mM Hepes, 140 mM NaCl, BSA 0.1%, pH 7.4) to 10^8 RBC/ml. RBCs were aged by adding calcium and Ca2+ ionophore A23187 to a final concentration of 2.5 mM and 0.5 μM respectively, then incubating at 30°C for 16 hours. Aged RBCs were washed with PBS and counted before use.

To induce hemolytic anemia, ZIP8 KO mice and littermate controls were injected IP with 60 mg/kg PHZ (dissolved in PBS) on day 0 and day 1. CBCs were measured on day 4 via cheek bleed, the peak of hemolytic anemia severity, and on day 7, post recovery. On day 7, mice were euthanized and tissues were harvested for analysis. During the PHZ course, mice were placed on 4 ppm Fe diet to minimize uptake of dietary iron.

For iron deficiency studies, ZIP8 KO mice and littermate controls were placed on a low-iron diet (4 ppm iron; TD 80396, Envigo) at 8 weeks of age for up to 24 weeks to induce iron deficiency. Blood was collected via cheek bleeds and CBCs were assessed every 4 weeks.

To induce acute lung injury (ALI), mice were treated with 15 mg/kg LPS (Sigma, E. coli O55:B5, L2880) in saline through oropharyngeal (OP) aspiration, which was modified from (39). In brief, mice are anesthetized with an intraperitoneal injection of ketamine/xylazine (Sigma-Aldrich), then suspended on a wire by the front incisors. After placement of a nose clip, the tongue is gently pulled out of the mouth and to the side using forceps. The LPS solution is then pipetted into the posterior oropharyngeal space, and the nose and tongue released 5 s after the solution is aspirated into the lungs. The dose of 15 mg/kg LPS was used after a titration study for the lowest dose necessary to consistently yield evaluable ALI parameters. Mice were euthanized 3 days

after LPS treatment, and bronchoalveolar lavage (BAL) fluid was obtained by lavaging the lungs three times with 0.8 ml of cold phosphate-buffered saline (PBS). Lungs were perfused with 5 ml of cold PBS via the right ventricle, then lungs and liver were harvested and snap frozen in liquid nitrogen for analysis. Bronchoalveolar lavage fluid protein was measured using the Pierce BCA Protein Assay Kit (Thermo Fisher).

For *Klebsiella pneumoniae* infection experiments, bacteria was purchased from ATCC (BAA-1705). Prior to the experiment, an aliquot of the stock was thawed and cultured in Tryptic Soy Broth (TSB) overnight at 37°C, then reinoculated into fresh media and allowed to reach linear growth phase. The bacteria were then spun down and resuspended in PBS, then diluted to the desired concentration as determined by a OD600 vs colony forming units (CFU) curve for the specific strain. Mice were infected with 300 CFU of K. pneumoniae via oropharyngeal aspiration and weighed daily until euthanasia 3 days later. Blood was collected via cardiac puncture and tissues and BAL fluid were harvested for analysis. Bacterial burden was measured by homogenizing tissue in sterile water or diluting blood with sterile water and plating serial 5-fold dilutions on blood agar plates (Fisher, R01200). The plates were incubated at 37°C for 15 to 16 h, and the number of colonies was counted.

Complete blood counts (CBCs) were measured from whole blood (mixed with 1 µl of heparin to prevent clotting) using a HemaVet blood analyzer (Drew Scientific).

Iron Assay

Nonheme iron concentrations were determined by a colorimetric assay for iron quantification (Sekisui Diagnostics). For mouse tissues samples, tissues were flash frozen and ground up in liquid nitrogen in order to homogenize the samples. ~40 mg tissue was weighed and digested in

a fixed volume of acid (3M HCl, 10% trichloroacetic acid) for 1 hr at 95°C. Samples were centrifuged to clear the insoluble material, then iron levels in the supernatant were quantified according to manufacturer instructions. For mouse serum samples, blood was collected via cardiac puncture and placed in serum separator tubes (BD, 365967), then centrifuged to separate serum from RBCs according to manufacturer instructions. 10 µl of serum were used to determine concentration of iron in the serum using the same assay.

Histology/IHC

Mouse spleens were harvested and fixed in 10% neutral buffered formalin for 24 hr at room temperature, then stored in 70% ethanol until processing. The tissues were paraffin-embedded and sectioned at 4 µm thickness by the UCLA Translational Pathology Core Laboratory. Normal human lung tissue was obtained from Dr. Borna Mehrad (University of Florida) and processed at UCLA. Prior to staining, sections were heated for 45 min at 50 °C and deparaffinized through serial changes of xylenes and ethanol and rehydrated to distilled water. Light microscopy images were captured by a digital camera (Spot Imaging).

For iron localization, mouse spleen tissues underwent enhanced Perls' stain using potassium ferrocyanide 2% and HCl 4% and the Vector SG Peroxidase Substrate kit (Vector Laboratories; SK-4700) and were then counterstained with 0.5% neutral red solution.

For immunohistochemistry for ZIP8 in human lung tissue, antigen retrieval was performed by boiling in Tris-EDTA (10 mM Tris base 1 mM disodium EDTA dihydrate, pH 9.0) for 10 min. IHC was performed using ImmPRESS® HRP Goat Anti-Rabbit IgG Polymer Detection Kit, Peroxidase (Vector Laboratories, MP-7451) according to manufacturer's instructions, with anti-ZIP8 rabbit antibody (Sigma HPA038833) used as the primary antibody at 200 ng/ml. Negative control

sections were incubated with normal rabbit IgG. HRP was developed using ImmPACT® DAB Substrate, Peroxidase (HRP) (Vector Laboratories, SK-4105) according to manufacturer's instructions. Sections were counterstained with Gill's hematoxylin.

Magnetic Cell Sort

Unless otherwise stated, all reagents for the magnetic bead separation were purchased from Miltenyi. Mouse spleens were minced using the frosted side of microscope slides, rinsed with PEB buffer and filtered through a 40 μm filter to obtain single cell suspensions. Cells were incubated with F4/80 MicroBeads (magnetic beads bound to anti-CD45 antibodies), then flowed through an LS column placed in QuadroMACS magnet according to manufacturer's instructions to obtain F4/80+ and F4/80- cell populations.

Mouse lungs were lavaged with PEB buffer (PBS pH 7.2, 2mM EDTA, 0.5% BSA) to obtain BAL fluid. Lungs were perfused via right cardiac ventricle with 10 ml of cold PBS, then digested using the Lung Dissociation Kit and gentleMACS Dissociator per manufacturer's protocol, and a single-cell suspension will be obtained by filtering cells through a 40 μm filter. Airway alveolar macrophages were obtained by isolating CD45+ cells from BAL fluid. From the lungs, a sequential negative selection was performed to obtain a CD45+ population (immune cells), CD45-CD31+ population (endothelial cells), and CD45-CD31-Epcam+ population (epithelial cells). In brief, cells were incubated with CD45 MicroBeads, then flowed through an LS column placed in QuadroMACS magnet. CD45+ cells were bound to the column, while CD45- cells were in the flow through. The CD45+ cell population was obtained by flushing the column with PEB buffer after it was removed from the magnet. This process was repeated to obtain CD31+ cells from the CD45- population and Epcam+ cells from the CD45-CD31- population using MicroBeads bound to the respective antibodies.

qPCR

Tissue RNA was extracted via TRIzol (Thermo Fisher), and cDNA was synthesized using the iScript cDNA Synthesis Kit (BioRad). Gene transcript levels were quantified in duplicate by SsoAdvanced Universal SYBR Green Supermix(BioRad) using a CFX Connect or CFX96 Touch Real-Time PCR Detection System (BioRad). mRNA expression was calculated using the ΔCT method normalized to hypoxanthine guanine phosphoribosyl transferase (Hprt) expression levels. Primers are listed in Supplemental Table 1.

Western Blot

Frozen ground tissue or cells were homogenized in RIPA buffer containing protease and phosphatase inhibitors. Protein concentration in tissue lysates was determined by a BCA assay (ThermoFisher Pierce, 23225), and then lysates were denatured by SDS and boiling. For ferroportin, lysates were not denatured by SDS and not boiled. ~15 mg of protein were loaded per lane and were separated by SDS-PAGE and transferred to nitrocellulose membranes. Membranes were blocked for 1 h in 5% w/v dried nonfat milk and incubated with primary antibodies in primary antibody dilution buffer (20 mM Tris pH 8, 200 mM NaCl, 0.25% Tween 20, 2% BSA, 0.1% NaN_3) overnight at 4 °C The secondary reaction was performed using HRP-conjugated anti-rabbit or anti-mouse IgG diluted in blocking buffer. Protein blots were visualized by chemiluminescence using the ChemiDoc XRS+ imaging system and quantified using Image Lab software (Bio-RAD).

Commercial antibodies used are listed in Supplemental Table 2. Monoclonal mouse anti-ZIP8 antibody (9D4A9) was generated and purified by Genscript using the antigen protein sequence:

MHPSEGPELAFSEDVLSVFGANRSLSAAQLGRLLERLGAASQQGALDLGQLHFNQCLSAEDIF SLHGFSNVTQITSSNFSAICPAILQQLNFHPCEDLRKHNAKPSHHHHHH.

Cell lines

A549 cells (ATCC, CCL-185) and 16HBE cells (Sigma, SCC150) were cultured in RPMI 1640 medium with GlutaMAX^{TM} supplement (Thermofisher, 61870036), supplemented with 10% FBS and 1x Pen/Strep, at 37 °C in a 5% CO_2 95% air atmosphere. For experiments, cells were seeded at 2×10^5/well in 12 well plates and allowed to adhere overnight. Cells were serum starved (complete media with 0.1% FBS) for 24 hr, then treated with 50 ng/mL recombinant human IL6 (R&D Systems #206-IL), IFNγ (PeproTech #300-02), IL1α (PeproTech #200-01 A), IL1β (PeproTech #200-01B), TNFα (Biolegend #570102) or EGF (Gibco #10450). 16 hrs post treatment, cells were harvested for analysis. ZIP8 knockdown was performed using Lipofectamine RNAiMAX Reagent (Invitrogen, 13778150) and Opti-MEM according to manufacturer's instructions. OnTarget Smart Pool siRNAs targeting human ZIP8 (L-007573-01-0005) or nontargeting control siRNA (D-001810-10-05) were purchased from Horizon Discovery.

^{58}Fe isotope preparation and sample analysis

^{58}Fe (93% enrichment) was purchased from Trace Sciences International, dissolved in 12N HCl to form H_2 plus $^{58}FeCl_2$, and H_2O_2 was added to oxidize the H_2 plus $^{58}FeCl_2$ to H_2O plus $^{58}FeCl_3$. 100 mM of $^{58}FeCl_3$ in 12N HCl was diluted 1:400 in 10 mM of sodium ascorbate to obtain ferrous $^{58}Fe^{2+}$. ZIP8 KO mice and littermate controls were treated with 5 µg of $^{58}Fe^{2+}$ via retroorbital injection or oropharyngeal aspiration. 4 hours later, mice were euthanized and lung tissue and BAL fluid was collected for analysis. Acid extraction to extract non-heme iron was performed on lung tissues as listed above, and supernatant and BAL fluid were submitted to the UCLA ICP-MS Core Facility for ICP-MS analysis of ^{56}Fe and ^{58}Fe.

Tissue concentrations of other metals were also determined at the UCLA ICP-MS facility within the UC Center for Environmental Implications of Nanotechnology.

Myeloperoxidase Assay

A quantity of ~10 mg of ground lung tissue was weighed and homogenized in 50 mM potassium phosphate solution, pH 6.0. The solution was centrifuged, then the pellet resuspended in 0.5% CETAB in Cell-Based Assay Buffer (Cayman #10009322). After sonication and incubation, myeloperoxidase (MPO) activity in the supernatant was measured using the colorimetric neutrophil myeloperoxidase activity assay kit (Cayman #600620). BALF MPO activity was measured directly with the assay kit. MPO activity was measured as the rate of change of absorbance over time.

Superoxide Dismutase Assay

Superoxide dismutase activity (SOD) was assessed in tissues using the Superoxide Dismutase Assay Kit (Cayman Chemicals, #706002) following manufacturer's instructions.

Malondialdehyde Assay

Malondialdehyde was quantified in mouse tissues as a measure of lipid peroxidation using the Thiobarbituric Acid Reactive Substances (TCA Method) Assay Kit (Cayman Chemicals #700870) following the manufacturer's instructions.

Statistics

Graphpad Prism (version 9.0 for Windows, GraphPad Software) was used for all statistical analyses. Normally and non-normally distributed data were analyzed using the t test or Mann-

Whitney rank-sum test, respectively. Multivariate analyses were performed using two-way ANOVA.

Study Approval

All animal experiments were approved by the University of California, Los Angeles (UCLA) Institutional Animal Care and Use Committee and were carried out in accordance with the Guide for Care and Use of Laboratory Animals (National Institutes of Health, Bethesda, MD). All mice were maintained on a 12-h light–dark schedule in a temperature- (22–25 °C) and humidity-controlled environment. Unless specified, mice received a standard diet (PicoLab Rodent Diet 20, 5053 Irradiated, 185 ppm iron). At the end of experiments, mice were humanely euthanized using CO_2 inhalation.

AUTHOR CONTRIBUTIONS

T.G., E.N., A.K., and M.K. conceived and designed the experiments; V.Z., S.J., A.K., Q.L., and M.K. performed experiments and prepared figures and manuscript; V.Z., T.G., E.N., A.K., Q.L., and M.K. analyzed the data and approved final version of manuscript.

ACKNOWLEDGEMENTS

The authors acknowledge financial support from the National Institute of Health, National Heart, Lung and Blood Institute K08 HL127293 (A.K.) and the National Institute of Diabetes and Digestive and Kidney Diseases R01 DK080706 (M.K.). The authors would like to thank Dr. Borna Mehrad for generously providing formalin-fixed, de-identified normal human lung samples for this study. In addition, the authors would like to thank the UC CEIN Inductively Coupled Plasma Mass Spectrometry Analysis Core and the UCLA Translational Pathology Core Laboratory for the services provided for this study.

FIGURES

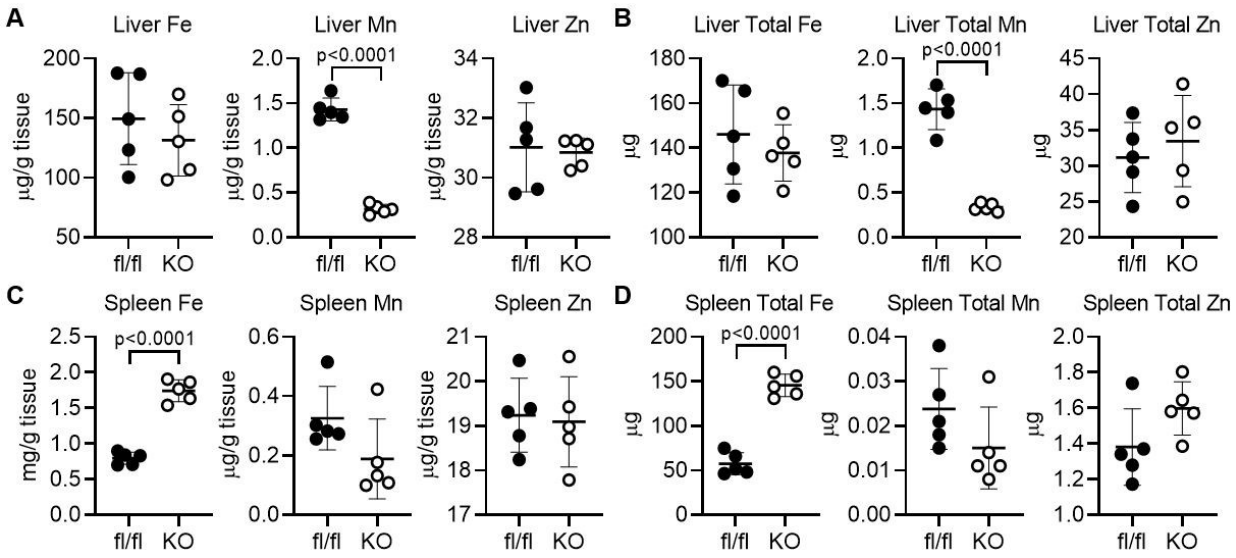

Figure 1: ZIP8 KO mice have decreased liver manganese and increased splenic iron levels. ICP-MS was performed on liver and spleens from 16-week-old ZIP8 KO mice and littermate controls (fl/fl). **(a,c)** Concentrations and **(b,d)** total levels of **(a-b)** liver and **(c-d)** splenic iron, manganese and zinc were measured. p-values determined by two-tailed t-test.

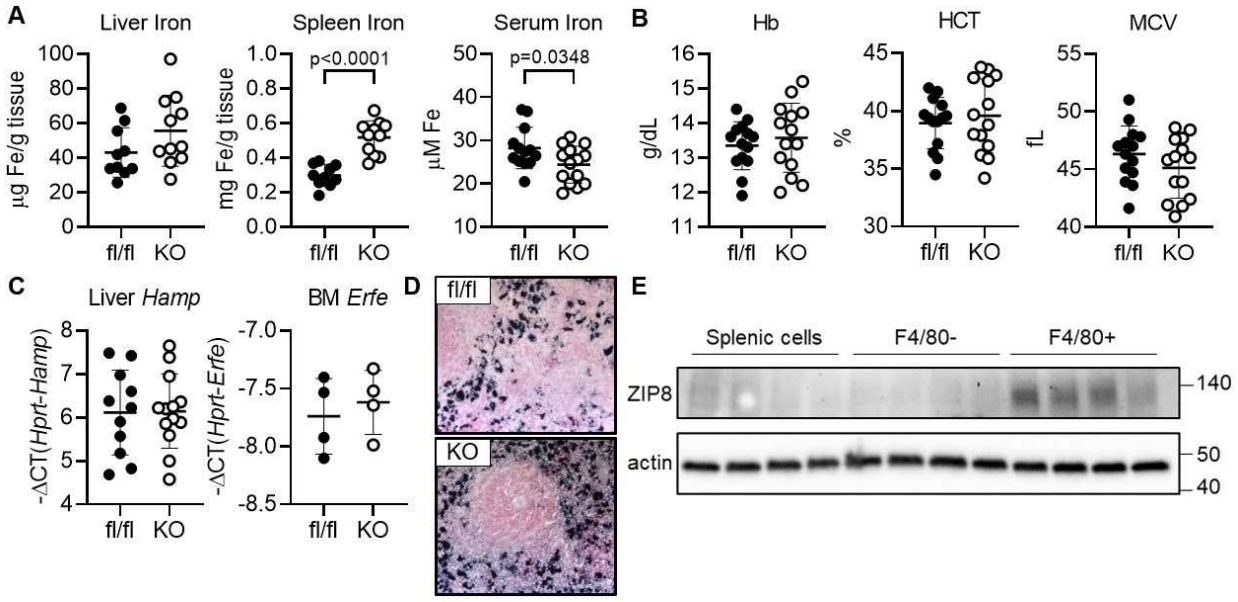

Figure 2: Baseline ZIP8 KO mice have impaired iron recycling. (a) Liver, spleen and serum non-heme iron levels from 16-week-old ZIP8 KO and littermate controls (fl/fl). **(b)** Complete blood counts. Hb: hemoglobin, HCT: hematocrit, MCV: mean corpuscular volume. **(c)** Liver *Hamp* mRNA and bone marrow (BM) *Erfe* mRNA levels. **(d)** Representative images of Perls' staining for iron in ZIP8 KO and fl/fl FFPE spleen tissue. 40x magnification. **(e)** Splenic red pulp macrophages from C57BL/6 mice were isolated via magnetic bead separation for F4/80+ cells for ZIP8 measurement by Western blot. ZIP8 protein levels are enriched in the splenic F4/80+ population as determined by Western blot. p-values determined by two-tailed t-test.

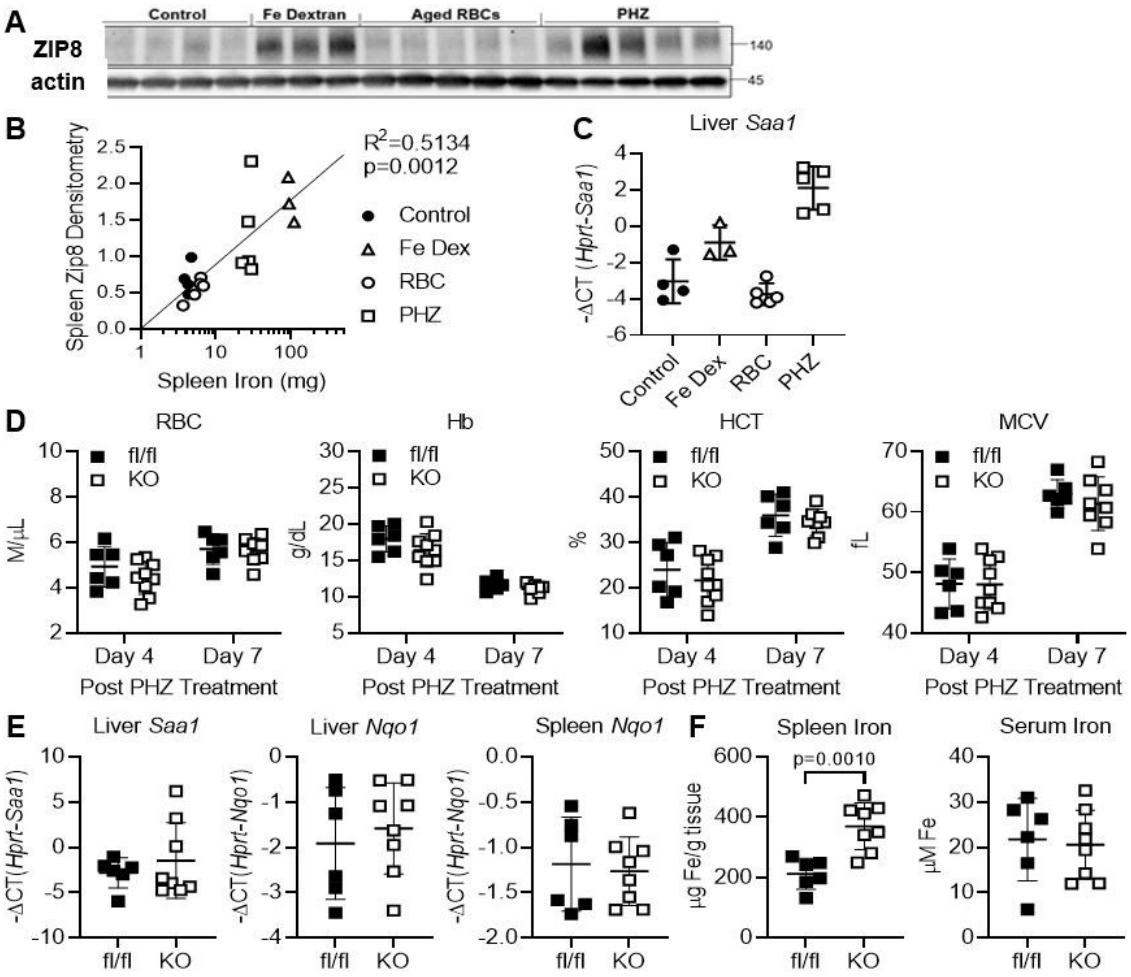

Figure 3: ZIP8 KO and WT mice have similar responses to phenylhydrazine. (a-c) C57BL/6 mice were treated with 300 µl of aged RBCs, a single i.p. injection of 10 mg iron dextran or two consecutive daily doses of 60 mg/kg phenylhydrazine hydrochloride (PHZ) to induce hemolytic anemia. n=3-5 mice for each treatment group. Tissues were harvested 3 days after treatment. **(a)** Western blot of splenic ZIP8. **(b)** Correlation between splenic ZIP8 protein levels as quantified by densitometry and splenic non-heme iron levels. **(c)** Liver *Saa1* mRNA levels. **(d-f)** ZIP8 KO and littermate controls (fl/fl) were treated with PHZ as described above. **(d)** Complete blood counts were performed on day 4 and day 7 on heparinized blood from ZIP8 KO and fl/fl mice. Hb: hemoglobin, HCT: hematocrit, MCV: mean corpuscular volume. **(e)** Day 7 liver *Saa1*, liver *Nqo1*, and spleen *Nqo1* mRNA levels and **(f)** spleen and serum non-heme iron. p-values determined by two-tailed t-test.

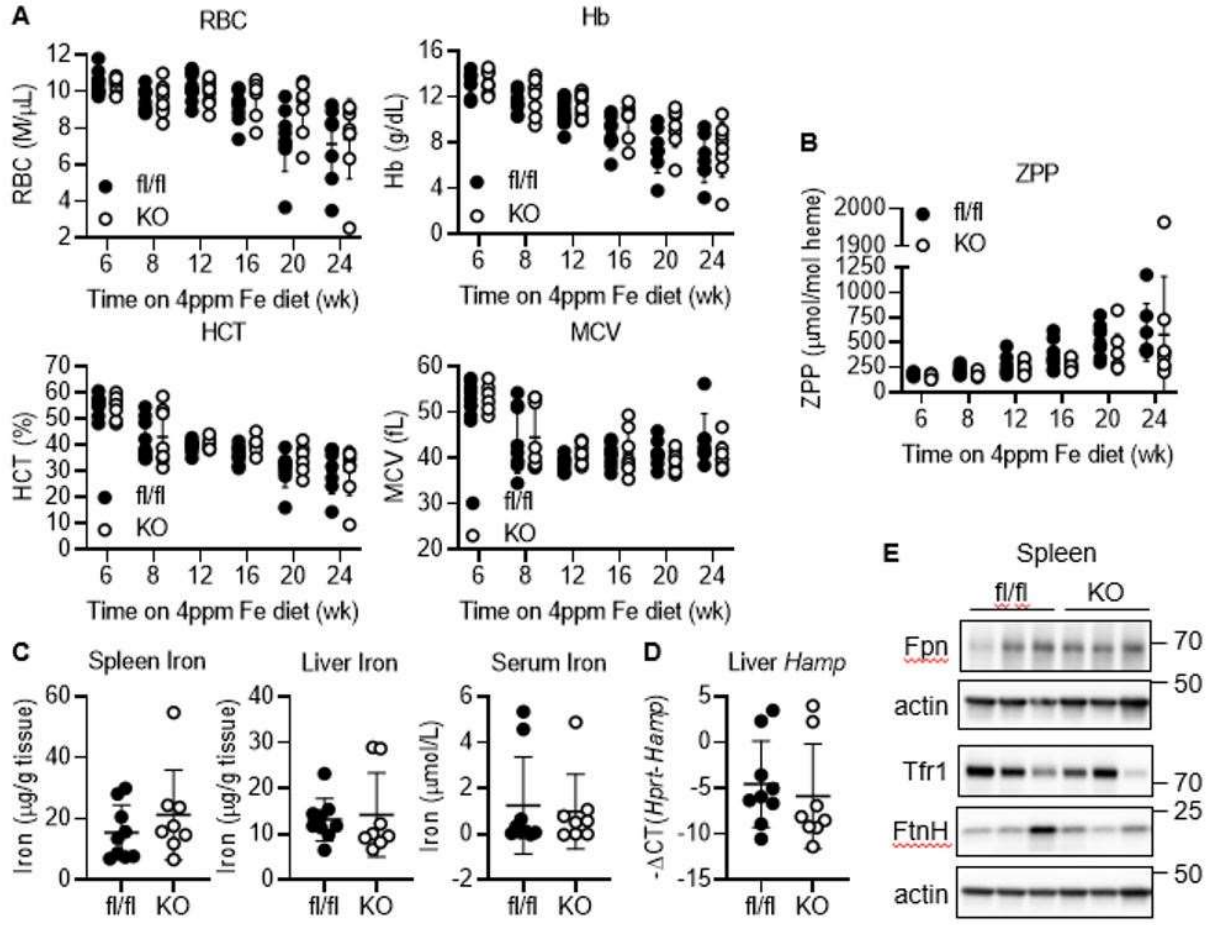

Figure 4: Loss of ZIP8 has no effect on response to iron deficiency in mice. ZIP8 KO mice and littermate controls (fl/fl) were placed on 4ppm Fe diet and complete blood counts (CBCs) were measured at 6, 8, 12, 16, 20 and 24 weeks on the diet. Tissues and serum were harvested at the end of the treatment. **(a)** CBCs from ZIP8 KO and fl/fl mice. Hb: hemoglobin, HCT: hematocrit, MCV: mean corpuscular volume. **(b)** Blood zinc protoporphyrin (ZPP) levels. **(c)** Spleen, liver and serum non-heme iron levels from iron-deficient ZIP8 KO mice and fl/fl mice. **(d)** Representative Western blot for splenic Fpn, Tfr1, and FtnH protein. **(e)** Liver *Hamp1* mRNA.

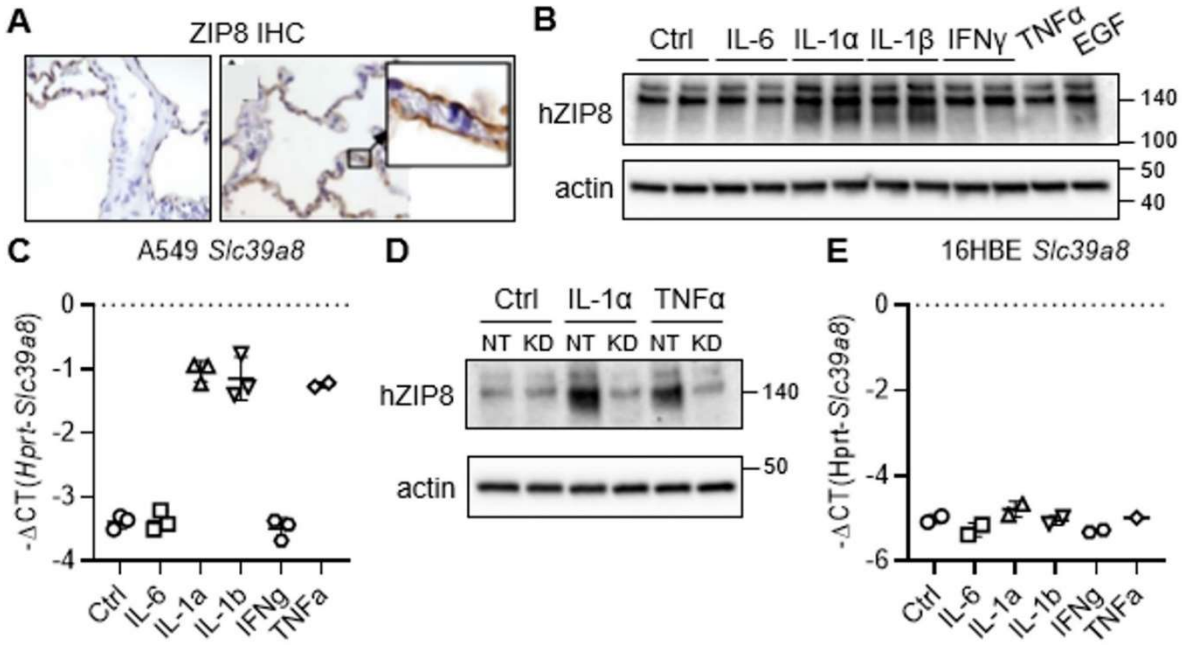

Figure 5: ZIP8 is induced by inflammation in human alveolar epithelial cells. (a) Representative images for immunohistochemistry (IHC) for ZIP8 in normal human lung tissue (n=3 biological replicates). Images are 10x magnification; inset is 40x. **(b-d)** A549 cells (human alveolar epithelial cell line) were serum starved for 24 hrs, then treated with 50 ng/ml recombinant human IL6, IFNγ, IL1α, IL1β, TNFα or EGF for 16 hrs. **(b)** Representative Western blot for ZIP8 protein expression. **(c)** *SLC39A8* mRNA levels. **(d)** ZIP8 siRNA knockdown. NT: non-targeting siRNA, KD: ZIP8 siRNA **(e)** 16HBE cells (human bronchiolar epithelial cell line) *SLC39A8* mRNA levels after treatment for 16 hours.

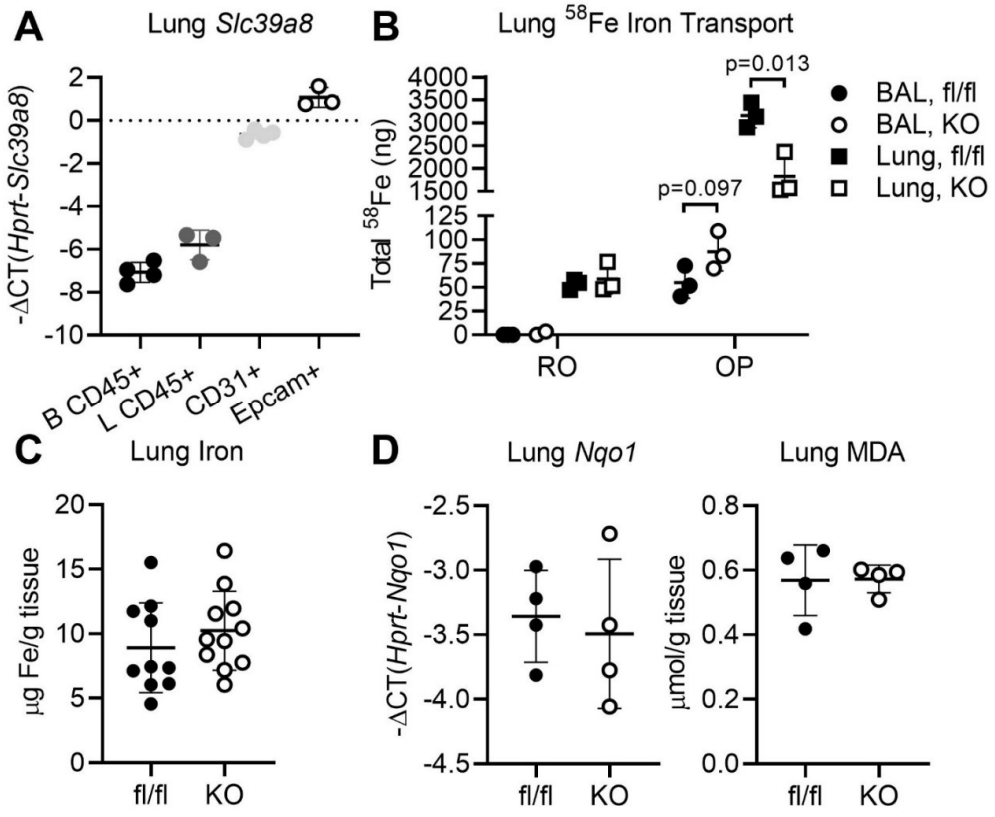

Figure 6: ZIP8 transports iron from the airspace into the lung. (a) *Slc39a8* mRNA levels of C57BL/6 mouse lung subpopulation cell types. B CD45+: BAL macrophages. L CD45+: lung macrophages. CD31+: endothelial cells. Epcam+: epithelial cells. **(b)** ZIP8 KO mice and littermate controls (fl/fl) were treated with 5 µg of $^{58}Fe^{2+}$ via retroorbital injection (RO) or oropharyngeal aspiration (OP) and harvested after 4 hrs for ICP-MS analysis of ^{58}Fe levels. **(c-d)** 16-week-old ZIP8 KO and fl/fl mouse lung **(c)** non-heme iron levels and **(d)** *Nqo1* mRNA and malondialdehyde (MDA) levels. p values were determined by two-tailed t-test.

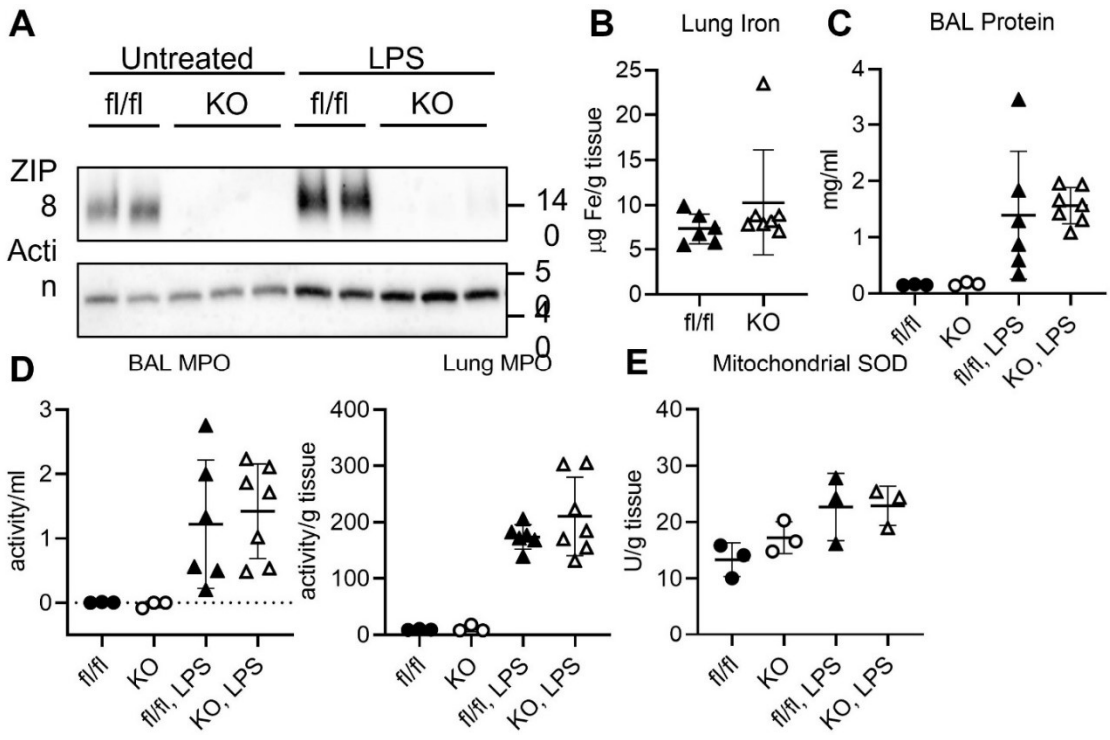

Figure 7: ZIP8 does not play a significant role in LPS-induced acute lung injury. 16-week-old ZIP8 KO mice and littermate controls (fl/fl) were treated with 15 mg/kg LPS through oropharyngeal (OP) aspiration to induce acute lung injury (ALI) and harvested after 3 days. A subset of mice in both groups were left untreated for comparison. n=3-7 mice per group **(a)** Representative Western blot for ZIP8 in lung lysate. **(b)** Lung non-heme iron levels. **(c)** BAL protein levels. **(d)** BAL and lung tissue myeloperoxidase (MPO) activity. **(e)** Lung mitochondrial superoxide dismutase (SOD).

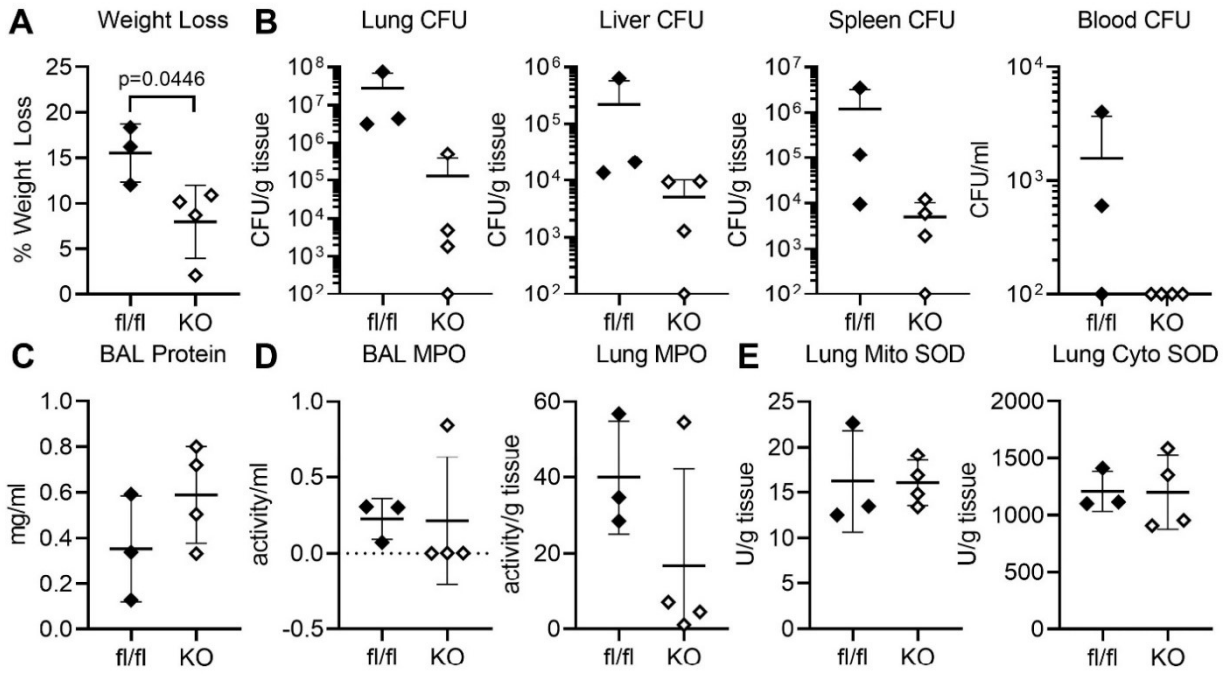

Figure 8: ZIP8 deletion is protective against *K. pneumoniae* infection. ZIP8 KO mice and littermate controls (fl/fl) were infected with 1500 colony forming units (CFU) of *K. pneumoniae* via oropharyngeal aspiration and weighed daily until harvest at 3 days **(a)** Percent weight loss in ZIP8 KO and fl/fl mice. **(b)** CFU counts in lung, liver, spleen and blood after infection. **(c)** BAL protein levels. **(d)** BAL and lung tissue myeloperoxidase (MPO) activity. **(e)** Lung mitochondrial and cytosolic superoxide dismutase (SOD). p values were determined by two-tailed t-test.

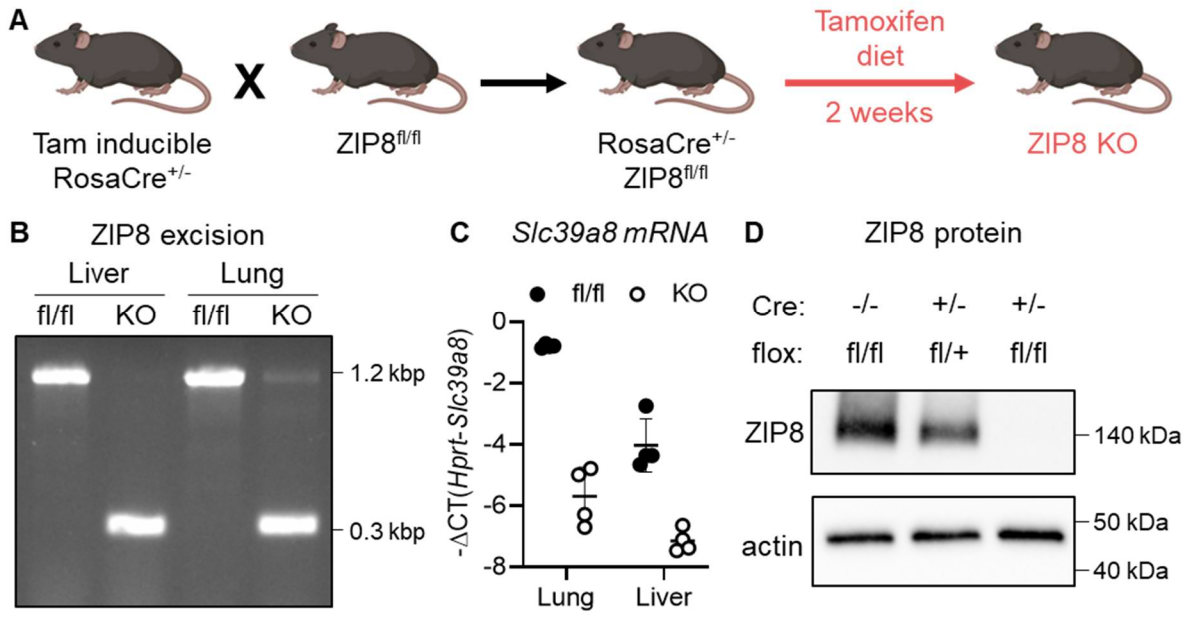

Supplemental Figure 1: Confirmation of ZIP8 deletion in ZIP8 KO mice. (a) Breeding and diet schematic to generate ZIP8 KO mice. **(b-d)** Knockout of ZIP8 (KO) was confirmed by **(b)** excision of ZIP8 exon 3, **(c)** Slc39a8 mRNA knockdown, and **(d)** loss of ZIP8 protein. fl/fl: littermate control.

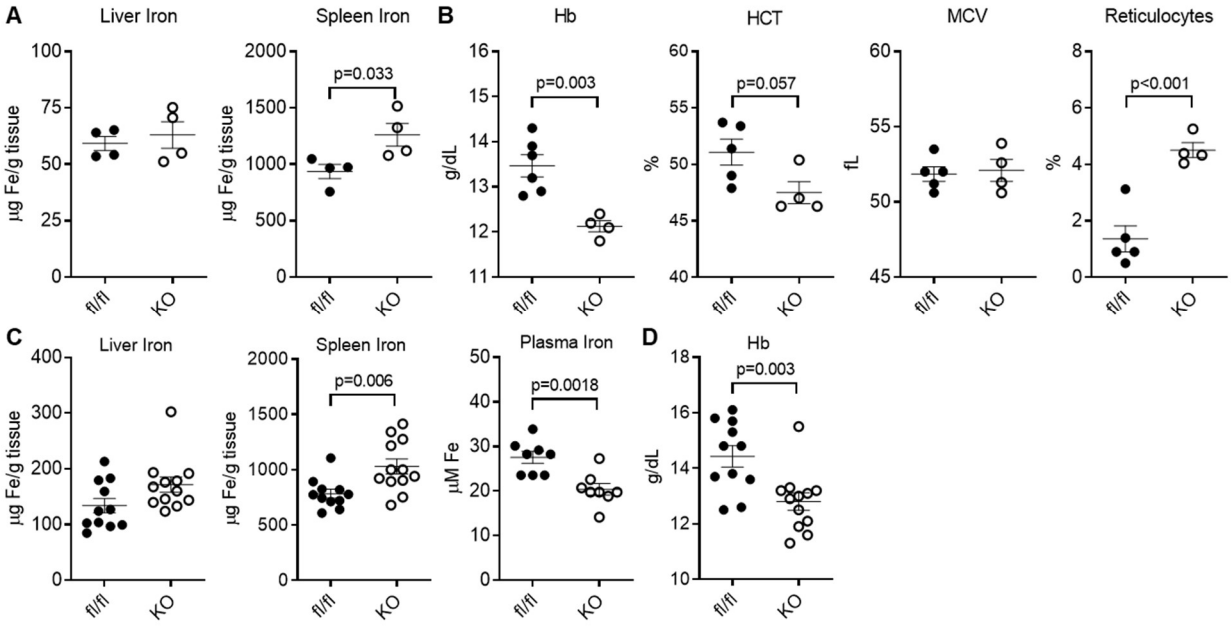

Supplemental Figure 2: Baseline ZIP8 KO mice have altered iron homeostasis. (a-b) Male RosaCre^{+}ZIP8$^{fl/fl}$ and RosaCre^{-}ZIP8$^{fl/fl}$ mice at 8 wk of age were injected with tamoxifen (100 mg/kg for 5 consecutive days) to generate ZIP8 KO mice and littermate controls (fl/fl), then analyzed at 16 wk of age. **(a)** Liver and spleen non-heme iron levels and **(b)** Hematological parameters for ZIP8 KO and fl/fl mice. Hb: hemoglobin, HCT: hematocrit, MCV: mean corpuscular volume. **(c-d)** Male and female RosaCre^{+}ZIP8$^{fl/fl}$ and RosaCre^{-}ZIP8$^{fl/fl}$ mice were put on tamoxifen diet (Teklad TD.130857) at 4 wk of age for 4 wk to generate ZIP8 KO mice and littermate controls, then switched to standard rodent diet (Teklad 7912) for 4 wk. Mice were analyzed at 12 weeks of age. **(c)** Liver, spleen and plasma non-heme iron levels of ZIP8 KO and fl/fl mice. **(d)** Hemoglobin levels for ZIP8 KO and fl/fl mice. p-values determined by unpaired Student's t-test.

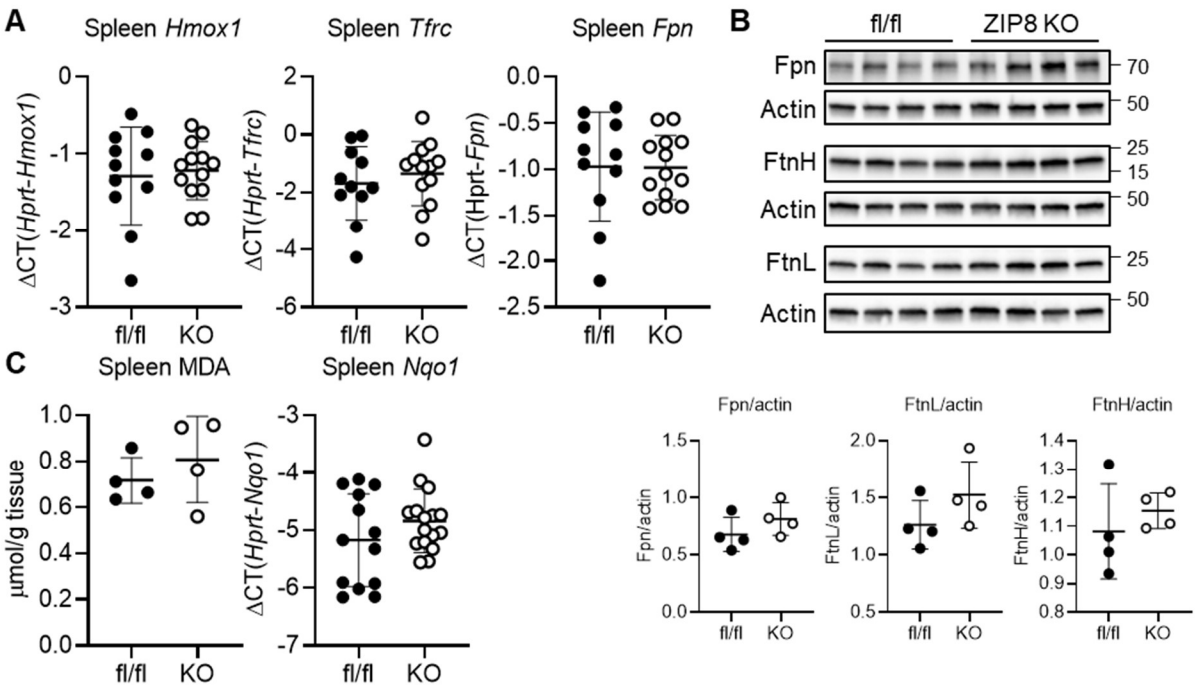

Supplemental Figure 3: Iron transport and storage protein levels in ZIP8 KO spleens are unchanged. 16-week-old ZIP8 KO mouse and littermate control (fl/fl) spleens were harvested. **(a)** Hmox1, Tfrc, Fpn mRNA levels, **(b)** representative Western blot of ferroportin (Fpn) and ferritin heavy and light chain (FtnH, FtnL) proteins (Graphs depict quantification of band intensity by densitometry with corresponding densitometry values), **(c)** malondialdehyde (MDA) levels, and Nqo1 mRNA levels.

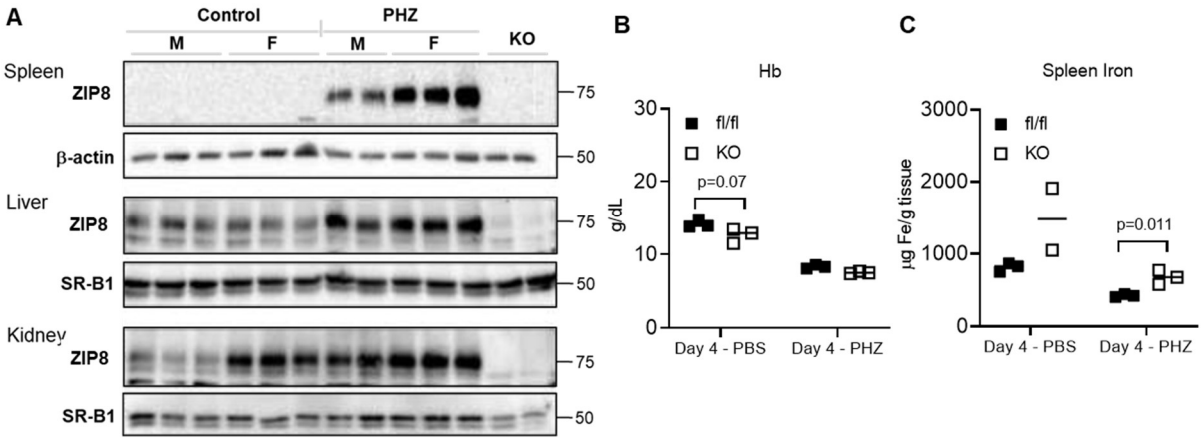

Supplemental Figure 4: ZIP8 KO and WT mice have similar responses to phenylhydrazine. 6-month-old ZIP8 KO mice and littermate controls (fl/fl) were treated with two consecutive daily i.p. injections of 60 mg/kg phenylhydrazine (PHZ) or vehicle control to induce hemolytic anemia, then harvested after 48 h. **(a)** Western blot for spleen, liver, and kidney ZIP8. M: male, F: female. Prior to Western analysis, tissue lysates were digested with PNGase F to cleave N-linked glycans (ref. 15). **(b)** Hemoglobin levels after PHZ injection. **(c)** Splenic non-heme iron. p-values determined by Student's unpaired t test.

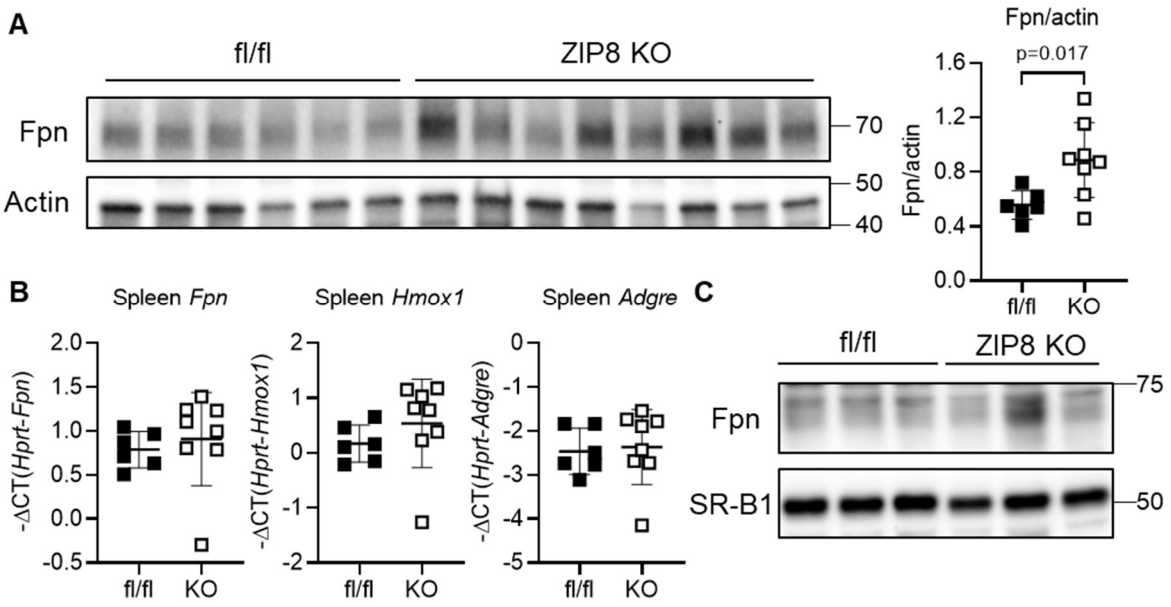

Supplemental Figure 5: Phenylhydrazine increases ferroportin in ZIP8 KO spleens compared to WT spleens. ZIP8 KO and littermate controls (fl/fl) were treated with PHZ and their spleens analyzed at **(a-b)** day 7 or (c) 48 hours. **(a)** Western blot of ferroportin (Fpn) protein in ZIP8 KO and fl/fl mouse, and **(b)** splenic Fpn, Hmox1, Adgre mRNA levels. **(c)** 48 hr Western blot for splenic Fpn protein. p-values determined by two-tailed t test.

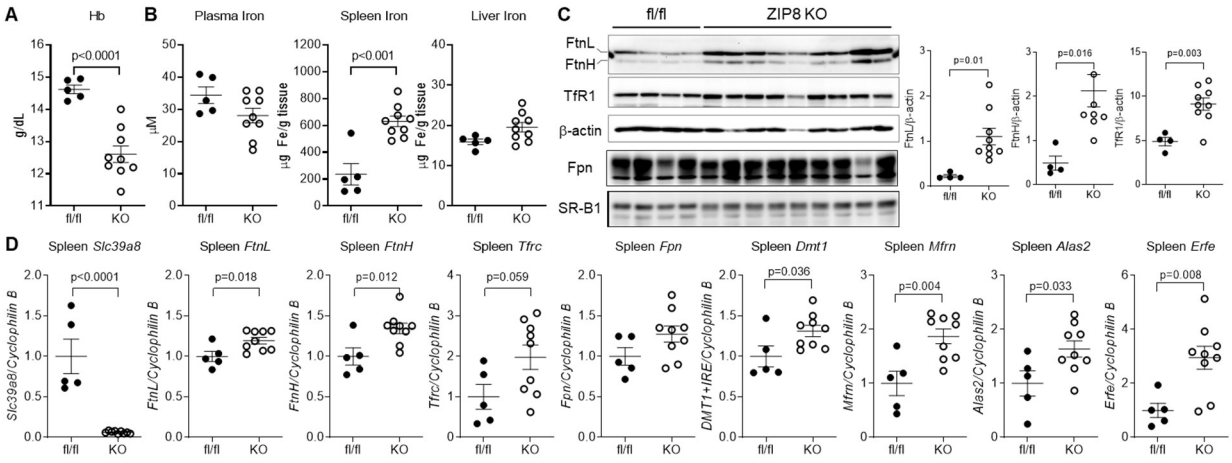

Supplemental Figure 6: Effect of iron-deficient diet on ZIP8 KO mice. 7-wk-old RosaCre^{+}ZIP8$^{fl/fl}$ and RosaCre^{-}ZIP8$^{fl/fl}$ mice were put on a tamoxifen diet (Teklad TD.130857) for 4 wk to generate ZIP8 KO mice and littermate controls (fl/fl), then placed on iron-deficient 4 ppm Fe diet (modified AIN-93G rodent diet) for 8 wk starting at 11 wk of age. **(a)** Hemoglobin levels in iron-deficient ZIP8 KO and fl/fl mice. **(b)** Plasma, spleen and liver non-heme bound iron in iron-deficient ZIP8 KO and fl/fl mice. **(C)** Western blot for splenic ferritin heavy and light chains (FtnH, FtnL), transferrin receptor (TfR1) and ferroportin (Fpn) in ZIP8 KO vs fl/fl mice. **(c)** Splenic mRNA levels of various iron-related proteins. p-values determined by Student's unpaired t test.

Supplemental Table 1: Primers for RT-PCR

Target Gene	Forward Primer (5' -> 3')	Reverse Primer (5' -> 3')
UCLA		
Mouse Hprt	CTG GTT AAG CAG TAC AGC CCC	CGA GAG GTC CTT TTC ACC AGC
Mouse Slc39a8	AAC TTC TCT GCC ATC TGC CC	GGC TTT GCG TTG TGC TTT CT
Mouse Hamp	CCT ATC TCC ATC AAC AGA TG	AAC AGA TAC CAC ACT GGG AA
Mouse Erfe	ATC GGG CTG GAG AAC AGC	TGG CAT TGT CCA AGA AGA CA
Mouse Hmox1	CCT CAC AGA TGG CGT CAC TT	TCT GCA GGG GCA GTA TCT TG
Mouse Tfrc	TCA TGA GGG AAA TCA ATG AT	GCC CCA GAA GAT ATG TCG GAA
Mouse Fpn	ATG GGA ACT GTG GCC TTC AC	TCC AGG CAT GAA TAC GGA GA
Mouse Nqo1	CAC GGG GAC ATG AAC GTC AT	GGA GTG TGG CCA ATG CTG TA
Mouse Saa-1	TGA CCA GGA AGC CAA CAG	GTA GGA AGA CCA GAC C
Mouse Adgre	CTT TGG CTA TGG GCT TCC AGT	GCA AGG AGG ACA GAG TTT ATC
Human HPRT	GCC CTG GCG TCG TGA TTA GT	AGC AAG ACG TTC AGT CCT GTC
Human SLC39A8	CAG TGT GGT ATC TCT ACA GGA TGG A	CAG TTT GGG CCC CTT CAA A
UF		
Mouse Cyclophilin B	GTCCACACCCTTTTCCGGT	GCACCTTCATATTGCGCTCC
Mouse Slc39a8	AACTTCTCTGCCATCTGCCC	GGCTTTGCGTTGTGCTTTCT
Mouse FtnL	GAGGTCCCGTGGATCTGTGT	GGAATCCCCGGGTCTGTT
Mouse FtnH	AAGATGGGTGCCCCTGAAG	CCAGGGTGTGCTTGTCAAAGA
Mouse Tfrc	CTCCATAGAGTTTGCTGACACCAT	TCCAGCCTCACGAGGAGTGTAT
Mouse Fpn	TCACCTGGCTACGTCGAAAAT	GCTGGGCTAGTCCTGAGAATAGAC
Mouse DMT1 + IRE	TGACGGCAGCAGAATTCCTT	CACCCCATCCCTGTACAAATG
Mouse Mfrn	CTAATGGGGTAGCTGGGAGT	AGCGCTGTTTCACCACTTCT
Mouse Alas2	GGGCTAAGAGCCATTGTCCT	ATGGCTTCGGGTGGTTGAAT
Mouse Erfe	ATGGGGCTGGAGAACAGC	TGGCATTGTCCAAGAAGACA

Supplemental Table 2: Antibodies

Target Protein	Primary Antibodies
UCLA	
Mouse and human beta-actin	Monoclonal antibody-peroxidase A3854, Sigma
Mouse Zip8	Monoclonal mouse antibody 9D4A9, Genscript; See Methods for generation of antibody
Mouse Ferroportin	Rat monoclonal IC7, Amgen
Mouse Ferritin Heavy Chain	Rabbit monoclonal antibody 4393, Cell Signaling Technology
Mouse Ferritin Light Chain	Goat polyclonal NBP1-06986, Novus Biologicals
Mouse Transferrin Receptor	Mouse monoclonal antibody H68.4, ThermoFisher
Human Zip8	Rabbit polyclonal antibody HPA038832, Sigma
Secondary Antibodies:	
Anti-mouse IgG HRP antibody 7076, Cell Signaling Technology	
Anti-rabbit IgG HRP antibody 7074, Cell Signaling Technology	
Anti-goat IgG HRP antibody 2354, Santa Cruz	
Anti-rat IgG HRP (AbCam, #ab102213	
ImmPRESS horse anti-rabbit IgG HRP detection kit MP-7401, Vector Laboratories	
UF	
Mouse beta-actin	Mouse monoclonal antibody AC-15, AM4302, Ambion
Mouse SR-B1	Rabbit polyclonal antibody NB400-104, Novus Biologicals
Mouse Zip8	Rabbit polyclonal antibody described in Wang et al., J Biol Chem.2012, 287:34032-43
Mouse Ferroportin	Rabbit polyclonal antibody described in Knutson et al., Proc Natl Acad Sci U S A.2005, 102:1324-8
Mouse Ferritin	Rabbit polyclonal, F5012, Sigma
Mouse Transferrin Receptor	Mouse monoclonal, 13-6890, Life Technologies
Secondary Antibodies:	
Anti-mouse IgG HRP antibody 32430, Invitrogen	
Anti-rabbit IgG HRP antibody NA9340V, GE Healthcare	

REFERENCES

1. Nemeth E, and Ganz T. Hepcidin-Ferroportin Interaction Controls Systemic Iron Homeostasis. *Int J Mol Sci.* 2021;22(12).
2. Kosman DJ. A holistic view of mammalian (vertebrate) cellular iron uptake. *Metallomics.* 2020;12(9):1323-34.
3. Vogt AS, Arsiwala T, Mohsen M, Vogel M, Manolova V, and Bachmann MF. On Iron Metabolism and Its Regulation. *Int J Mol Sci.* 2021;22(9).
4. Delaby C, Rondeau C, Pouzet C, Willemetz A, Pilard N, Desjardins M, et al. Subcellular localization of iron and heme metabolism related proteins at early stages of erythrophagocytosis. *PLoS One.* 2012;7(7):e42199.
5. Ganz T. Iron and infection. *Int J Hematol.* 2018;107(1):7-15.
6. Stefanova D, Raychev A, Deville J, Humphries R, Campeau S, Ruchala P, et al. Hepcidin Protects against Lethal Escherichia coli Sepsis in Mice Inoculated with Isolates from Septic Patients. *Infect Immun.* 2018;86(7).
7. Michels KR, Zhang Z, Bettina AM, Cagnina RE, Stefanova D, Burdick MD, et al. Hepcidin-mediated iron sequestration protects against bacterial dissemination during pneumonia. *JCI Insight.* 2017;2(6):e92002.
8. Stefanova D, Raychev A, Arezes J, Ruchala P, Gabayan V, Skurnik M, et al. Endogenous hepcidin and its agonist mediate resistance to selected infections by clearing non-transferrin-bound iron. *Blood.* 2017;130(3):245-57.
9. Goetz DH, Holmes MA, Borregaard N, Bluhm ME, Raymond KN, and Strong RK. The neutrophil lipocalin NGAL is a bacteriostatic agent that interferes with siderophore-mediated iron acquisition. *Mol Cell.* 2002;10(5):1033-43.

10. Drago-Serrano ME, Campos-Rodriguez R, Carrero JC, and de la Garza M. Lactoferrin: Balancing Ups and Downs of Inflammation Due to Microbial Infections. *Int J Mol Sci.* 2017;18(3).

11. Fritsche G, Nairz M, Libby SJ, Fang FC, and Weiss G. Slc11a1 (Nramp1) impairs growth of Salmonella enterica serovar typhimurium in macrophages via stimulation of lipocalin-2 expression. *J Leukoc Biol.* 2012;92(2):353-9.

12. Zhang V, Nemeth E, and Kim A. Iron in Lung Pathology. *Pharmaceuticals (Basel).* 2019;12(1).

13. Ghio AJ, Soukup JM, Dailey LA, and Madden MC. Air pollutants disrupt iron homeostasis to impact oxidant generation, biological effects, and tissue injury. *Free Radic Biol Med.* 2020;151:38-55.

14. Jenkitkasemwong S, Wang CY, Mackenzie B, and Knutson MD. Physiologic implications of metal-ion transport by ZIP14 and ZIP8. *Biometals.* 2012;25(4):643-55.

15. Wang CY, Jenkitkasemwong S, Duarte S, Sparkman BK, Shawki A, Mackenzie B, et al. ZIP8 is an iron and zinc transporter whose cell-surface expression is up-regulated by cellular iron loading. *J Biol Chem.* 2012;287(41):34032-43.

16. van Raaij SEG, Srai SKS, Swinkels DW, and van Swelm RPL. Iron uptake by ZIP8 and ZIP14 in human proximal tubular epithelial cells. *Biometals.* 2019;32(2):211-26.

17. Nebert DW, and Liu Z. SLC39A8 gene encoding a metal ion transporter: discovery and bench to bedside. *Hum Genomics.* 2019;13(Suppl 1):51.

18. Sunuwar L, Frkatovic A, Sharapov S, Wang Q, Neu HM, Wu X, et al. Pleiotropic ZIP8 A391T implicates abnormal manganese homeostasis in complex human disease. *JCI Insight.* 2020;5(20).

19. Costas J. The highly pleiotropic gene SLC39A8 as an opportunity to gain insight into the molecular pathogenesis of schizophrenia. *Am J Med Genet B Neuropsychiatr Genet.* 2018;177(2):274-83.

20. Galvez-Peralta M, Wang Z, Bao S, Knoell DL, and Nebert DW. Tissue-Specific Induction of Mouse ZIP8 and ZIP14 Divalent Cation/Bicarbonate Symporters by, and Cytokine Response to, Inflammatory Signals. *Int J Toxicol.* 2014;33(3):246-58.

21. Pyle CJ, Akhter S, Bao S, Dodd CE, Schlesinger LS, and Knoell DL. Zinc Modulates Endotoxin-Induced Human Macrophage Inflammation through ZIP8 Induction and C/EBPbeta Inhibition. *PLoS One.* 2017;12(1):e0169531.

22. Knoell DL, Smith D, Bao S, Sapkota M, Wyatt TA, Zweier JL, et al. Imbalance in zinc homeostasis enhances lung Tissue Loss following cigarette smoke exposure. *J Trace Elem Med Biol.* 2020;60:126483.

23. Wang B, He L, Dong H, Dalton TP, and Nebert DW. Generation of a Slc39a8 hypomorph mouse: markedly decreased ZIP8 Zn(2)(+)/(HCO(3)(-))(2) transporter expression. *Biochem Biophys Res Commun.* 2011;410(2):289-94.

24. Chen J, Galvez-Peralta M, Zhang X, Deng J, Liu Z, and Nebert DW. In utero gene expression in the Slc39a8(neo/neo) knockdown mouse. *Sci Rep.* 2018;8(1):10703.

25. Lin W, Vann DR, Doulias PT, Wang T, Landesberg G, Li X, et al. Hepatic metal ion transporter ZIP8 regulates manganese homeostasis and manganese-dependent enzyme activity. *J Clin Invest.* 2017;127(6):2407-17.

26. Kovtunovych G, Eckhaus MA, Ghosh MC, Ollivierre-Wilson H, and Rouault TA. Dysfunction of the heme recycling system in heme oxygenase 1-deficient mice: effects on macrophage viability and tissue iron distribution. *Blood.* 2010;116(26):6054-62.

27. White C, Yuan X, Schmidt PJ, Bresciani E, Samuel TK, Campagna D, et al. HRG1 is essential for heme transport from the phagolysosome of macrophages during erythrophagocytosis. *Cell Metab.* 2013;17(2):261-70.

28. Bellelli R, Federico G, Matte A, Colecchia D, Iolascon A, Chiariello M, et al. NCOA4 Deficiency Impairs Systemic Iron Homeostasis. *Cell Rep.* 2016;14(3):411-21.

29. Soe-Lin S, Apte SS, Andriopoulos B, Jr., Andrews MC, Schranzhofer M, Kahawita T, et al. Nramp1 promotes efficient macrophage recycling of iron following erythrophagocytosis in vivo. *Proc Natl Acad Sci U S A.* 2009;106(14):5960-5.

30. Forbes JR, and Gros P. Divalent-metal transport by NRAMP proteins at the interface of host-pathogen interactions. *Trends Microbiol.* 2001;9(8):397-403.

31. Giorgi G, D'Anna MC, and Roque ME. Iron homeostasis and its disruption in mouse lung in iron deficiency and overload. *Exp Physiol.* 2015;100(10):1199-216.

32. Zhang Z, Zhang F, An P, Guo X, Shen Y, Tao Y, et al. Ferroportin1 deficiency in mouse macrophages impairs iron homeostasis and inflammatory responses. *Blood.* 2011;118(7):1912-22.

33. Agoro R, Taleb M, Quesniaux VFJ, and Mura C. Cell iron status influences macrophage polarization. *PLoS One.* 2018;13(5):e0196921.

34. Hall SC, Smith DR, Dyavar SR, Wyatt TA, Samuelson DR, Bailey KL, et al. Critical Role of Zinc Transporter (ZIP8) in Myeloid Innate Immune Cell Function and the Host Response against Bacterial Pneumonia. *J Immunol.* 2021;207(5):1357-70.

35. Liu MJ, Bao S, Galvez-Peralta M, Pyle CJ, Rudawsky AC, Pavlovicz RE, et al. ZIP8 regulates host defense through zinc-mediated inhibition of NF-kappaB. *Cell Rep.* 2013;3(2):386-400.

36. Pyle CJ, Azad AK, Papp AC, Sadee W, Knoell DL, and Schlesinger LS. Elemental Ingredients in the Macrophage Cocktail: Role of ZIP8 in Host Response to Mycobacterium tuberculosis. *Int J Mol Sci.* 2017;18(11).

37. Sangkhae V, Fisher AL, Wong S, Koenig MD, Tussing-Humphreys L, Chu A, et al. Effects of maternal iron status on placental and fetal iron homeostasis. *J Clin Invest.* 2020;130(2):625-40.

38. Fisher AL, Sangkhae V, Presicce P, Chougnet CA, Jobe AH, Kallapur SG, et al. Fetal and amniotic fluid iron homeostasis in healthy and complicated murine, macaque, and human pregnancy. *JCI Insight.* 2020;5(4).

39. De Vooght V, Vanoirbeek JA, Haenen S, Verbeken E, Nemery B, and Hoet PH. Oropharyngeal aspiration: an alternative route for challenging in a mouse model of chemical-induced asthma. *Toxicology.* 2009;259(1-2):84-9.

CHAPTER 4: EVALUATING BMPR2 MUTANT MICE AS A MODEL FOR STUDYING IRON DEFICIENCY IN PULMONARY HYPERTENSION

Manuscript submitted:

EVALUATING BMPR2 MUTANT MICE AS A MODEL FOR STUDYING IRON DEFICIENCY IN PULMONARY HYPERTENSION

Vida Zhang[1,2], Tomas Ganz[1], Elizabeta Nemeth[1], Soban Umar[3†], Airie Kim [1†*]

[1]Department of Medicine, David Geffen School of Medicine, UCLA, Los Angeles, CA, USA

[2]Department of Molecular and Medical Pharmacology, UCLA, Los Angeles, CA, USA

[3]Department of Anesthesiology, UCLA, Los Angeles, CA, USA

[†]These two authors contributed equally to this work.

*AirieKim@mednet.ucla.edu; David Geffen School of Medicine, 10833 Le Conte Ave 43-229 CHS, Box 951690, Los Angeles, CA 90095; (310) 825-7499

Mutations in bone morphogenetic protein receptor type II (Bmpr2) are the most common genetic causes of pulmonary arterial hypertension (PAH), with Bmpr2 mutations found in 82% of patients with a family history of PAH. In addition, patients with Bmpr2 mutations develop PAH at a younger age (1). However, the low penetrance of Bmpr2 mutations (20-30%) (1) indicates that a "second hit" is often necessary for a patient to develop PAH. One potential second hit is iron deficiency, which is commonly associated with PAH. Iron deficiency occurs in a reported 63% of PAH patients, and its severity correlates with decreased exercise tolerance and worse survival (2). A molecular link between iron deficiency and PAH is that BMP signaling also plays a large role in iron homeostasis by inducing hepcidin, the master systemic iron regulator produced by the liver (3). Our goal was to establish a mouse model of iron deficiency in BMPR2-associated PAH.

We generated Bmpr2 heterozygous (Het) and littermate control (Ctrl) mice by crossing Bmpr2 floxed mice (4) (kindly provided by Dr. Paul Yu from Harvard University) with CMV-Cre mice. Heterozygous deletion of Bmpr2 was confirmed by qPCR (-ΔCT(*Hprt-Bmpr2*): Ctrl -3.49±0.06 vs Het -4.27±0.36, **Fig 1a**). Male and female Bmpr2 Het and Ctrl mice were weaned onto a regular diet or a 4ppm Fe low-iron diet for 2 or 5 months. While mice on the low iron diet had a significant decrease in liver iron stores after 2 and 5 months on the diet, confirming decreased iron stores, there was no significant difference between the Bmpr2 Het and Ctrl mice (**Fig 1b**). We also measured the expression of hepcidin via *Hamp* mRNA. We expected hepcidin to be lower in iron-deficient mice and that partial loss of Bmpr2 would decrease it further, as hepcidin is induced in response to BMP signaling (3). We found that while liver *Hamp* mRNA decreases overall in response to iron deficiency, partial loss of Bmpr2 had no significant effect on hepcidin expression at any time point (**Fig 1c**).

The complete blood counts (CBCs) also showed no significant effect of Bmpr2 loss on the iron-deficient phenotype. As expected, mice on the low iron diet had decreased hemoglobin as

compared to mice on regular diet, which is consistent with iron-deficiency anemia (**Fig 1d**). Also unsurprising was the increased red cell distribution width (RDW) that occurred due to concurrent microcytosis from iron deficiency and relative macrocytosis from compensatory reticulocytosis (**Fig 1e**). Mean corpuscular volume (MCV) was also decreased at the 2-month timepoint, as expected due to iron-deficiency anemia, but then recovered back to normal values by 5 months, most likely due to the compensatory increase in circulating reticulocytes (**Fig 1f**). Thus, the hematological parameters showed no significant difference between Bmpr2 Het and Ctrl mice at any time point.

PAH severity was assessed via transthoracic echocardiography measurements of pulmonary acceleration time (PAT) and the ratio of PAT to pulmonary ejection time (PAT/PET) (5). A baseline PAT value of 30±1 ms for baseline normal mice was used as reference as reported previously (5). Prior reports in the literature have described the development of PH in murine models of iron deficiency (6), and our study also demonstrated increased right ventricular systolic pressures in both control and mutant iron-deficient mice, as demonstrated by higher PATs. Surprisingly, iron-deficient Bmpr2 Het mice had the same or mildly higher PATs than their littermate controls at both the 2-month (Ctrl 17.29 ms vs Het 19.88; difference -2.59, 95% CI [-5.34, 0.15]) and 5-month timepoints (Ctrl 16.46 ms vs Het 20.56; difference -4.10, 95% CI [-7.52, -0.68]) (**Fig 1g**). PAT/PET ratios for both genotypes were significantly lower after 5 months of diet compared to 2 months of diet, and the subtle improvement in pulmonary pressures in Bmpr2 Het mice at 5 months was no longer statistically significant (**Fig 1h**). The decrease in PAT/PET for both genotypes at 5 months could be secondary to the prolonged duration of iron deficiency contributing to the PAH phenotype.

Our initial expectation was that iron deficiency could provide the “second hit” for Bmpr2-related PAH development and worsen PAH outcomes. However, our Bmpr2 Het mice had similar or improved PAH parameters as measured by echocardiography compared to Ctrl mice when on low iron diet, which is counter to the correlation between iron deficiency and worse PAH parameters shown in clinical literature. Our contrary results could be due to several reasons. The loss of Bmpr2 could be compensated by an increase in other BMP type II receptors, such as ACTR2A (3), potentially causing a net overall increase in BMP signaling in the lungs. Another potential explanation is the mouse model itself. The mutation in the Bmpr2 allele in the mouse model used for these experiments is a loss of function, with exons 4 and 5 deleted (4). This could potentially produce a truncated Bmpr2 that binds to BMP ligands and downregulates other BMP signaling with unexpected downstream effects. Though there have been multiple links and associations between iron deficiency and PAH potentially through Bmpr2, the Bmpr2 mutant mouse model is not the appropriate model for elucidating this relationship.

AUTHOR CONTRIBUTIONS

T.G., E.N., and A.K. conceived and designed the experiments; V.Z., A.K., and S.U. performed experiments and prepared figures and manuscript; V.Z., T.G., E.N., A.K., and S.U. analyzed the data and approved final version of manuscript.

FIGURES

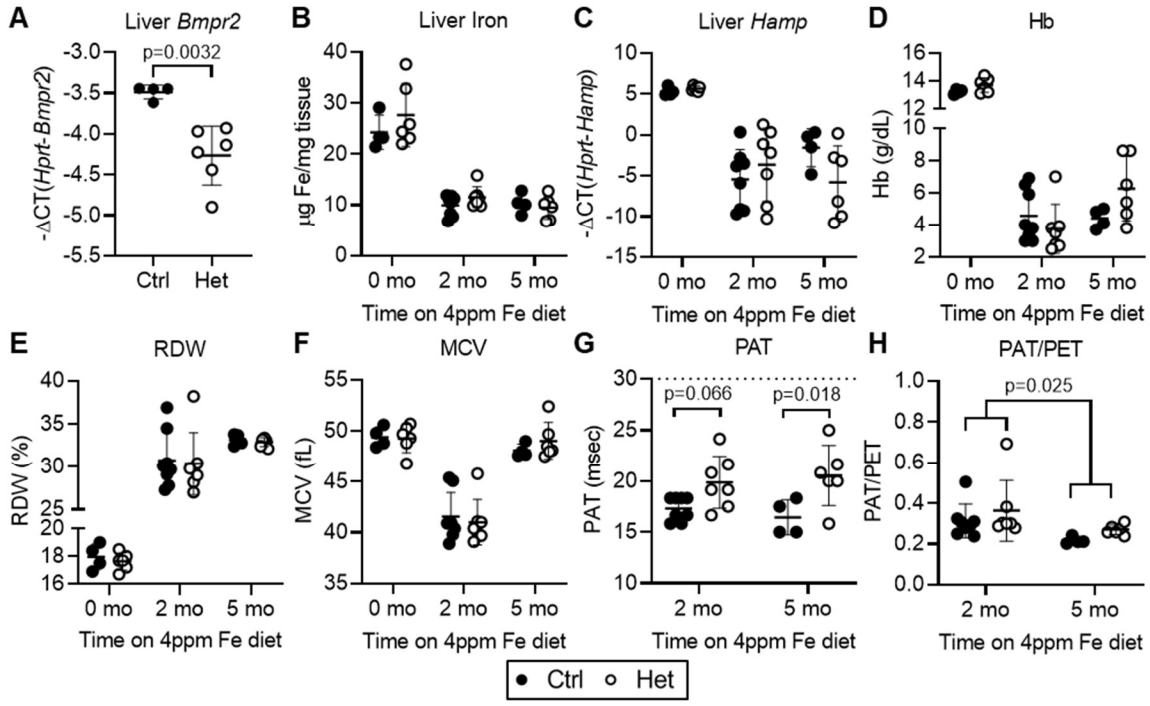

Figure 1: Iron-deficient Bmpr2 heterozygous (Het) mice have unexpectedly improved pulmonary hypertension compared to littermate controls (Ctrl). Bmpr2 Het and Ctrl mice were placed on 4ppm Fe low iron diet for 0, 2 or 5 months. Echocardiography was performed, then blood and livers were harvested for analysis. **(a)** Confirmation of Bmpr2 reduction via liver Bmpr2 mRNA levels in untreated mice. **(b-c)** Iron homeostasis as assessed by **(b)** non-heme liver iron levels and **(c)** liver Hamp mRNA levels. **(d-f)** Complete blood counts. **(d)** Hemoglobin (Hb). **(e)** Red cell distribution width (RDW). **(f)** Mean corpuscular volume (MCV). **(g-h)** Pulmonary hypertension as assessed by **(g)** pulmonary acceleration time (PAT) and **(h)** the ratio of PAT to pulmonary ejection time (PAT/PET). p values as determined by **(a)** two-tailed t-test or **(b-h)** two-way ANOVA with multiple comparisons.

REFERENCES

1. Evans, J.D., et al., BMPR2 mutations and survival in pulmonary arterial hypertension: an individual participant data meta-analysis. Lancet Respir Med, 2016. **4**(2): p. 129-37.
2. Rhodes, C.J., et al., Iron deficiency and raised hepcidin in idiopathic pulmonary arterial hypertension: clinical prevalence, outcomes, and mechanistic insights. J Am Coll Cardiol, 2011. **58**(3): p. 300-9.
3. Sangkhae, V. and E. Nemeth, Regulation of the Iron Homeostatic Hormone Hepcidin. Adv Nutr, 2017. **8**(1): p. 126-136.
4. Beppu, H., et al., Generation of a floxed allele of the mouse BMP type II receptor gene. Genesis, 2005. **41**(3): p. 133-7.
5. Thibault, H.B., et al., Noninvasive assessment of murine pulmonary arterial pressure: validation and application to models of pulmonary hypertension. Circ Cardiovasc Imaging, 2010. **3**(2): p. 157-63.
6. Cotroneo, E., et al., Iron homeostasis and pulmonary hypertension: iron deficiency leads to pulmonary vascular remodeling in the rat. Circ Res, 2015. **116**(10): p. 1680-90.

CHAPTER 5: OVEREXPRESSION OF ERYTHROFERRONE IMPAIRS SURVIVAL IN β-THALASSEMIA MOUSE MODELS

ABSTRACT

β-thalassemia, caused by mutations in the β-globin gene, is a genetic disease characterized by ineffective erythropoiesis, anemia and iron-overload associated with multi-organ dysfunction. In anemias with ineffective erythropoiesis, the erythroid hormone erythroferrone (ERFE) is pathologically overproduced. ERFE functions by suppressing the iron regulatory hormone hepcidin, and the chronic suppression of hepcidin in β-thalassemia results in excessive iron absorption and iron overload, even in the absence of blood transfusions. A major obstacle in studying the role of ERFE in β-thalassemia has been the lack of a mouse model that expresses elevated ERFE akin to human patients. Our lab generated ERFE overexpressing transgenic mice with varying levels of ERFE and showed that they developed dose-dependent iron overload and relative hepcidin deficiency. Two ERFE overexpressing mouse lines (high: E(H) and moderate: E(M)) were crossed with *Hbb*$^{Th3/+}$ mice, a widely used model of β-thalassemia, to generate double mutants (T-E(H) and T-E(M)) to analyze the effect of ERFE on the pathophysiology of ineffective erythropoiesis. We observed that there was a noticeably skewed genotypic ratio of the offspring from these pairing, with almost no T-E(H) pups surviving to adulthood and T-E(M) pups making up only ~9% of surviving pups from their respective breedings compared to the 25% expected. At embryonic day 18.5 (close to term ~19.25d), however, there was the expected distribution of all genotypes in both breedings, indicating that Th3/ERFE pups are conceived but do not survive perinatally. In the T-E(M) mice that did survive to adulthood, we observed significantly higher liver iron levels compared to Th3 littermates, indicating that excessive ERFE increases liver iron loading in a mouse model of β-thalassemia. Our data thus far show that elevated ERFE levels have a negative effect on perinatal survival in β-thalassemia and cause increased iron loading. These results support the role of ERFE as a cause of iron overload in human patients and suggest that neutralizing excessive ERFE has potential therapeutic applications for facilitating healthy growth and development and preventing iron overload in β-thalassemia.

INTRODUCTION

Systemic iron homeostasis is tightly regulated by the hepatic peptide hormone hepcidin. Hepcidin is induced in response to increased iron levels and inhibits both intestinal iron absorption and the mobilization of stored iron (1). Erythropoietic activity, which is highly dependent on adequate iron supply, is a strong regulator of iron homeostasis. The hormone erythroferrone (ERFE) is produced by erythroid cells in response to hemorrhage, hypoxia or other erythropoietic stimuli, and suppresses the production of hepcidin in order to increase iron availability for erythropoiesis (2,3). Recent evidence indicates that ERFE suppresses hepcidin expression by binding to select members of the bone morphogenetic protein (BMP) family (4-6) and inhibiting the BMP signaling that stimulates hepcidin production (7).

The goal of this study was to determine in mouse models the effect of ERFE levels approximating those measured in humans in the context of β-thalassemia. In patients with β-thalassemia and other anemias associated with ineffective erythropoiesis, ERFE levels are pathologically elevated, resulting in the chronic suppression of hepcidin, excessive iron absorption and eventual iron overload (8,9). The severity of ERFE increase in human patients is not, however, modeled in the commonly used mouse model of β -thalassemia intermedia, the Th3/+ mice (10,11). To determine the impact of serum ERFE levels more closely approximating those reported in patients with β -thalassemia on the thalassemic phenotype, we created a mouse model of β-thalassemia that overexpresses ERFE.

Our lab recently generated and characterized three lines of transgenic mice with varying levels of erythroid ERFE overexpression. These mice developed dose-dependent iron overload, impaired hepatic BMP signaling and relative hepcidin deficiency (7). To determine the effect of high ERFE in murine β-thalassemia, mice that carried the erythroid ERFE-overexpressing transgene were

interbred with Th3/+ thalassemic mice **(Supplemental Figure 1)**. As we showed that ERFE overproduction by itself reproduced the hyperabsorption of iron leading to hepatic iron overload, a key phenotypic feature of β-thalassemia, we expected to see an increase in iron loading in thalassemic mice with elevated ERFE levels compared to those with low ERFE levels.

METHODS

Transgenic mice

All experiments involving mice were conducted with the approval of the University of California, Los Angeles Animal Research Committee. ERFE-overexpressing transgenic mice were generated and ERFE expression levels confirmed as stated in (7), with one line having high-expression of ERFE (E(H)) and another having moderately highly expression of ERFE (E(M)). Th3/+ mice ($Hbb^{th3/+}$; JAX #003253) (10) were provided by Dr. Stefano Rivella (University of Pennsylvania). Th3/+ mice were crossed with E(H) mice to generate offspring with both the Th3 deletion and high ERFE levels (T-E(H)) as well as Th3/+, E(H) and WT littermates. Th3/+ mice were crossed with E(M) mice to generate offspring with both the Th3 deletion and moderately high ERFE levels (T-E(M)) as well as Th3/+, E(M) and WT littermates. At embryonic day 18.5 (E18.5) and at 16 weeks of age, mice were euthanized by isoflurane inhalation, and blood and tissues were harvested for analysis.

Measurement of iron-related and hematological parameters

Liver non-heme iron were measured by using a colorimetric assay according to the manufacturer's protocol (Sekisui Diagnostics). Prior to sampling, livers were homogenized in liquid nitrogen to reduce variation resulting from regional differences in hepatic iron deposition. Complete blood counts (CBCs) were measured by using a HemaVet blood analyzed (Drew Scientific).

RNA isolation and measurement of gene expression

Total RNA isolation was performed by using TRIzol (ThermoFisher Scientfic). cDNA was synthesized using the iScript cDNA Sythesis Kit (Bio-Rad) following the manufacturer's protocol. Relative mRNA expression for genes of interest were determined by quantitative RT-PCR using

SsoAdvanced Universal SYBR Green Supermix (Bio-Rad) and measured on a CFX-96 RT-PCR Detection System (Bio-Rad). Primer sequences for mouse Hprt (Fwd: 5' CTG GTT AAG CAG TAC AGC CCC 3'; Rev: 5' CGAGAGGTCCTTTTCACCAGC 3') and mouse Hamp (Fwd: 5' CCTATCTCCATCAACAGATG 3'; Rev: 5' AACAGATACCACACTGGGAA 3').

Statistical analysis

Statistical analysis was performed by using the statistical package included in Prism version 9 (GraphPad). $P<0.05$ was considered statistically significant. Means of experimental groups, defined by genotype, were compared with others by one-way ANOVA with Tukey's multiple comparisons test. Analysis of observed vs expected ratios when analyzing transgene inheritance was performed by using binomial testing and an expected transgene incidence of 50%. Fisher's exact test was used to analyze differences in phenotypic incidence between groups.

RESULTS

To generate a mouse model of β-thalassemia with elevated ERFE levels, we crossed two different ERFE-overexpressing mouse lines (high line, E(H), and moderate line, E(M)) with Th3/+ mice. From these breedings, we expected to generate wildtype (WT), Th3/+, E(H)/E(M) and T-E(H)/T-E(M) littermate mice to use for analyses **(Supp. Figure 1)**. We found a striking decrease in post-natal survival of T-E(H) pups produced by breeding Th3/+ mice with E(H) mice, with only 1 pup surviving to adulthood (**Table 1**). This lethality in the T-E(H) pups appeared to be attributable to post or perrinatal issues rather than embryo developmental complications as the ratio of pup genotypes at embryonic day E18.5 was in line with the expected Mendelian ratios. A similar, but less extreme, pattern of impaired survival was observed in T-E(M) pups produced by breeding Th3/+ mice with E(M) mice, with 8.8% of T-E(M) pups surviving to weaning age compared to the expected 25% (**Table 1**). While, in our hands, Th3 heterozygosity alone resulted in impaired survival prior to weaning, the diminished survival of T-E(H) and T-E(M) pups was greater than would be expected due to the observed independent effects of either ERFE-overexpression or Th3 heterozygosity on pup survival, suggesting a synergistic loss of viability of Th3/+ mice in the presence of elevated ERFE. This pattern was observed regardless of the genotype of the dam, suggesting it is due to ERFE expression by the pup alone rather than synergy between maternal and pup ERFE expression.

Despite impaired survival to weaning, we did not detect a significant decrease in complete blood count values (CBCs) between Th3/+ mice and T-E(H) or T-E(M) mice at E18.5 (**Figure 1**), indicating that impaired survival was not attributable to worse anemia. Surprisingly, there was slight but significant increase in hemoglobin (Hb) in near birth T-E(H) embryos compared with Th3/+ littermates (Th3 4.875 g/dL vs T-E(H) 6.125 g/dL) (**Figure 1**). This increase is possibly attributable to increased mobilization of fetal liver iron stores for erythropoiesis as T-E(H) mice

had lower levels of both hepcidin (fetal liver *Hamp* mRNA, -ΔCT(*Hprt-Hamp*) Th3/+ 4.014 vs T-E(H) -2.948) and fetal liver iron (Th3/+ 88.1 μg/g tissue vs T-E(H) 72.12 μg/g tissue) relative to Th3/+ mice (**Figure 2**). This slight increase in Hb was not observed in the T-E(M) mice (**Figure 1**), suggesting that this may be due to the lower circulating levels of ERFE in T-E(M), as the decrease in fetal liver *Hamp* mRNA in T-E(M) mice compared to Th3/+ mice (-ΔCT(*Hprt-Hamp*) T-E(M) 0.064 vs Th3/+ 3.877) was less than that observed between T-E(H) and Th3/+ mice, and there was no significant difference in fetal liver iron between the Th3/+ mice and T-E(M) mice (**Figure 2**).

In the surviving adult T-E(M) mice, we did not detect a substantial effect of ERFE overexpression on CBCs (**Figure 3**). Hb levels were not different between WT and E(M) mice, differing from our previous observation of a mild increase in hemoglobin levels with moderate ERFE overexpression at 16 weeks of age (7). Th3/+ mice demonstrated moderate anemia, attributable to ineffective erythropoiesis, as previously reported(10,11). We did not detect exacerbation of anemia by ERFE overexpression, as T-E(M) mice maintained hematological parameters similar to those of Th3/+ mice. In terms of iron levels, at 16 weeks of age both E(M) and Th3/+ mice accumulated excess liver iron compared with WT littermates as expected (**Figure 4**) (7,10,11). However, ERFE overexpression greatly increased liver iron loading in thalassemic mice as T-E(M) mice had liver non-heme iron levels much greater than either Th3/+ or E(M) mice. This observation supports the hypothesis (12) that variation in ERFE concentrations in human β-thalassemia and other iron-loading anemias contributes to the observed variation in iron overload in patients with non-transfusion dependent iron-loading anemias.

DISCUSSION

We found that elevated ERFE levels have a negative effect on post-natal survival in a mouse model of β-thalassemia, despite the Th3/+ and T-E(H)/T-E(M) littermates having similar hematological parameters and liver iron levels. In the T-E(M) mice that did survive to adulthood, however, T-E(M) mice had substantially increased liver iron compared to Th3 mice. Ongoing experiments are currently exploring potential mechanisms behind the increased mortality in T-E(M) mice and the increase in liver iron stores. The findings that elevated ERFE levels impair pup survival in a mouse model of β-thalassemia during early life and greatly increase iron loading in the context of ineffective erythropoiesis further supports the concept that ERFE is pathogenic in β-thalassemia and is a potential therapeutic target to reduce disease-associated complications.

AUTHOR CONTRIBUTIONS

T.G. and E.N. conceived and designed the experiments; V.Z., A.K., J.O., and R.C. performed experiments, V.Z., J.O., R.C., A.K., E.N., and T.G. analyzed the data and prepared figures and manuscript.

FIGURES

	Th3/+ x Erfe-Tg (H) N=38		Th3/+ x Erfe-Tg (M) N=57		Th3/+ x WT N=109	
3 weeks	**Expected**	**Observed ******	**Expected**	**Observed *** **	**Expected**	**Observed *** **
WT	25%	**55.3% (21)**	25%	**43.9% (25)**	50%	**67.9% (74)**
Th3	25%	**15.8% (6)**	25%	**15.8% (9)**	50%	**32.1% (35)**
ERFE	25%	**26.3% (10)**	25%	**31.6% (18)**	-	-
Th3-ERFE	25%	**2.6% (1)**	25%	**8.8% (5)**	-	-

	N=31		N=13		N=30	
E18.5	**Expected**	**Observed** NS	**Expected**	**Observed** NS	**Expected**	**Observed** NS
WT	25%	29% (9)	25%	23.1% (3)	50%	60% (18)
Th3	25%	19.4% (6)	25%	30.8% (4)	50%	40% (12)
ERFE	25%	22.6% (7)	25%	23.1% (3)	-	-
Th3-ERFE	25%	29% (9)	25%	23.1% (3)	-	-

Table 1. Impaired postnatal survival of Th3/+;ERFE-Tg (Th3-ERFE) mice. Th3/+ (Th3) mice were bred with either ERFE-overexpressing Line-H (Erfe-Tg (H)), Line-M (Erfe-Tg (M)), or wildtype (WT) mice. Expected and observed percentages of generated offspring with specified genotypes at either 3 weeks post birth (top table) or in utero at embryonic day E18.5 (bottom table). Total numbers are in parenthesis next to the percentages. Statistically significant differences from expected proportions were assessed by Chi-square testing (***=P<0.001, ****=P<0.0001).

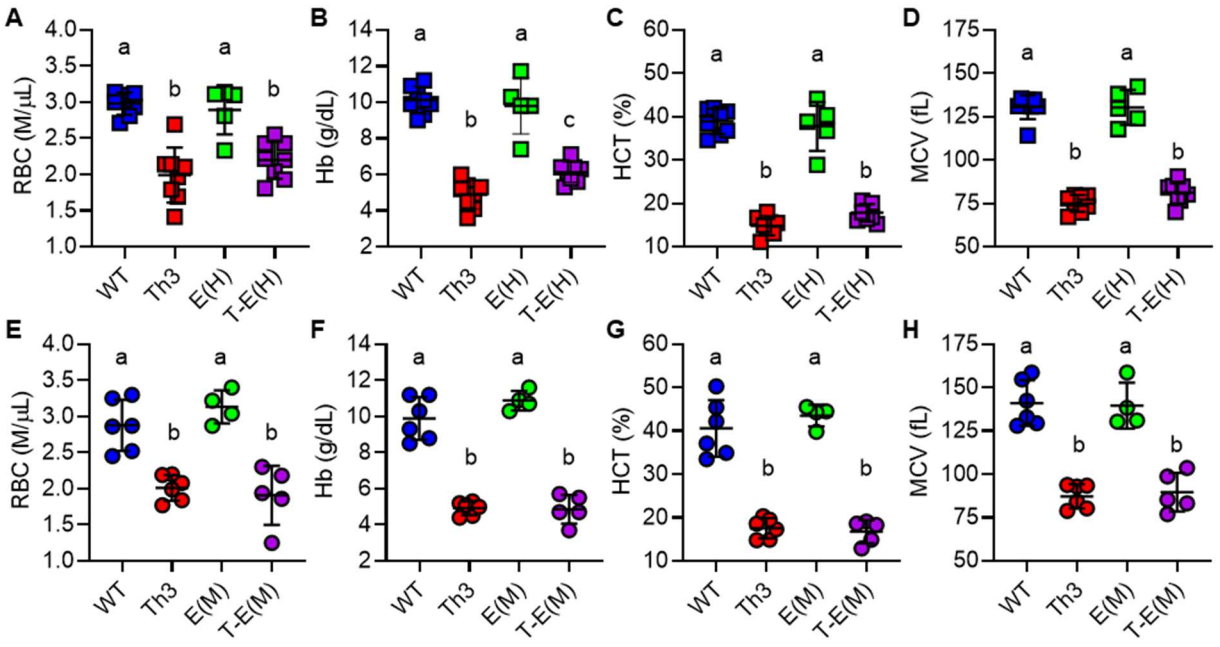

Figure 1. Complete blood count values (CBCs) in pups from Th3/+ (Th3) x ERFE-Tg(H) (E(H)) and Th3 x ERFE-Tg(M) (E(M)) breeding. Th3 mice were bred with either E(H) **(a-d)** or E(M) **(e-h)** mice to generate WT, Th3, E(H)/E(M) and T-E(H)/T-E(M) littermates. Pups were harvested at embryonic day 18.5 and blood was collected for CBCs. **(a,e)** Red blood cell (RBC) counts. **(b,f)** hemoglobin (Hb) levels. **(c,g)** hematocrit (HCT) percentages. **(d,h)** mean corpuscular volume (MCV) levels. p-values were assessed by one-way ANOVA with Tukey's multiple comparisons test; groups not sharing a common alphabetical superscript are significantly different ($p<0.05$).

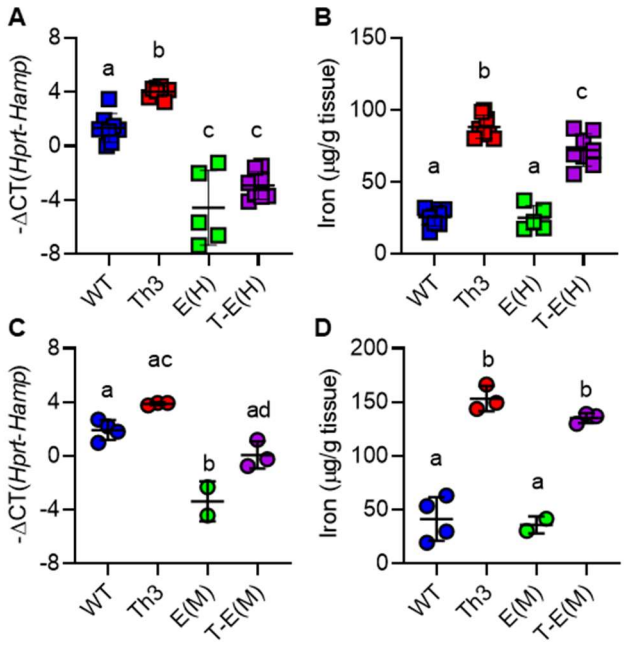

Figure 2. Fetal liver hepcidin expression and non-heme iron levels in pups from Th3/+ (Th3) x E(H) and Th3 x E(M) breeding. Th3/+ mice were bred with either **(a-b)** E(H) or **(c-d)** E(M) mice to generate WT, Th3, E(H)/E(M) and T-E(H)/T-E(M) littermates. Pups were harvested at embryonic day 18.5 and fetal livers were collected for analysis. Fetal liver **(a,c)** *Hamp* mRNA and **(b,d)** non-heme iron concentrations. p-values were assessed by one-way ANOVA with Tukey's multiple comparisons test; groups not sharing a common alphabetical superscript are significantly different ($p<0.05$).

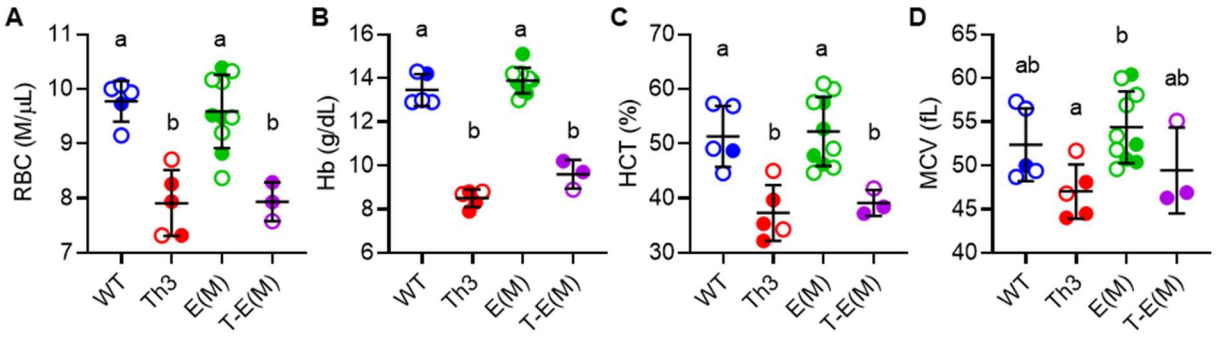

Figure 3. CBCs in adult mice generated by Th3/+ (Th3) x E(M) breeding. Th3 mice were bred with E(M) mice to generate WT, Th3, E(M) and T-E(M) littermates. Mice were harvested at 16 weeks of age and blood was collected for CBCs. **(a)** Red blood cell (RBC) counts, **(b)** hemoglobin (Hb) levels, **(c)** hematocrit (HCT) percentages, and **(d)** mean corpuscular volume (MCV) levels. Males are indicated by filled circles and females by open circles. p-values were assessed by one-way ANOVA with Tukey's multiple comparisons test; groups not sharing a common alphabetical superscript are significantly different ($p<0.05$).

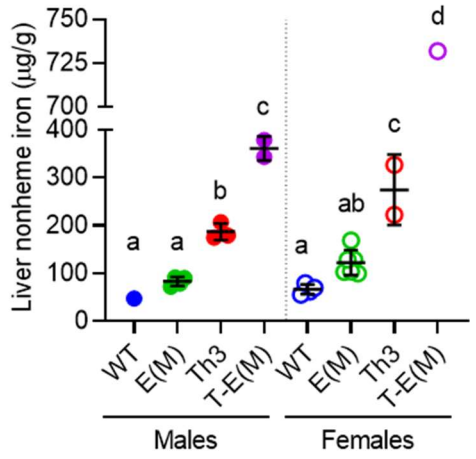

Figure 4. ERFE overexpression exacerbates liver iron overload in thalassemic mice. Th3/+ (Th3) mice were bred with E(M) mice to generate WT, Th3, E(M) and T-E(M) littermates. Mice were harvested at 16 weeks of age and livers were collected to measure liver non-heme iron levels. Males are indicated by filled circles and females by open circles. p-values were assessed by one-way ANOVA with Tukey's multiple comparisons test; groups not sharing a common alphabetical superscript are significantly different ($p<0.05$).

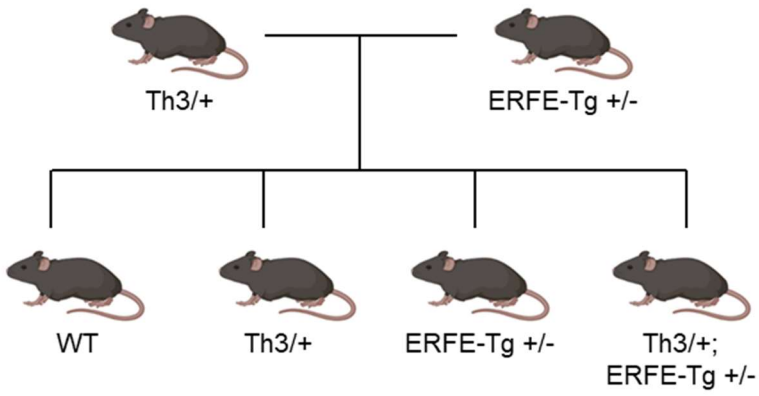

Supplemental Figure 1. Breeding scheme for Th3/+;ERFE-Tg (Th3-ERFE) mice and littermate controls.

REFERENCES

1 Nemeth, E. *et al.* Hepcidin regulates cellular iron efflux by binding to ferroportin and inducing its internalization. *Science* **306**, 2090-2093, doi:10.1126/science.1104742 (2004).

2 Pak, M., Lopez, M. A., Gabayan, V., Ganz, T. & Rivera, S. Suppression of hepcidin during anemia requires erythropoietic activity. *Blood* **108**, 3730-3735, doi:10.1182/blood-2006-06-028787 (2006).

3 Kautz, L. *et al.* Identification of erythroferrone as an erythroid regulator of iron metabolism. *Nat Genet* **46**, 678-684, doi:10.1038/ng.2996 (2014).

4 Arezes, J. *et al.* Erythroferrone inhibits the induction of hepcidin by BMP6. *Blood* **132**, 1473-1477, doi:10.1182/blood-2018-06-857995 (2018).

5 Arezes, J. *et al.* Antibodies against the erythroferrone N-terminal domain prevent hepcidin suppression and ameliorate murine thalassemia. *Blood*, doi:10.1182/blood.2019003140 (2020).

6 Wang, C. Y. *et al.* Erythroferrone lowers hepcidin by sequestering BMP2/6 heterodimer from binding to the BMP type I receptor ALK3. *Blood*, doi:10.1182/blood.2019002620 (2019).

7 Coffey, R. *et al.* Erythroid overproduction of erythroferrone causes iron overload and developmental abnormalities in mice. *Blood* **139**, 439-451, doi:10.1182/blood.2021014054 (2022).

8 Jones, E. *et al.* Hepcidin is suppressed by erythropoiesis in hemoglobin E beta-thalassemia and beta-thalassemia trait. *Blood* **125**, 873-880, doi:10.1182/blood-2014-10-606491 (2015).

9 Kearney, S. L. *et al.* Urinary hepcidin in congenital chronic anemias. *Pediatr Blood Cancer* **48**, 57-63, doi:10.1002/pbc.20616 (2007).

10 Yang, B. *et al.* A mouse model for beta 0-thalassemia. *Proc Natl Acad Sci U S A* **92**, 11608-11612, doi:10.1073/pnas.92.25.11608 (1995).

11 Kautz, L. *et al.* Erythroferrone contributes to hepcidin suppression and iron overload in a mouse model of beta-thalassemia. *Blood* **126**, 2031-2037, doi:10.1182/blood-2015-07-658419 (2015).

12 Andolfo, I. *et al.* The BMP-SMAD pathway mediates the impaired hepatic iron metabolism associated with the ERFE-A260S variant. *Am. J. Hematol.* **94**, 1227-1235, doi:10.1002/ajh.25613 (2019).

CONCLUDING REMARKS

The goal of this work was to examine the relationship between iron dysregulation and various lung pathologies and to clarify the role of the iron transporter Zip8 in the lung.

In Chapters One and Two, we utilized hepcidin knockout mice as a mouse model of severe iron overload to examine the effects of iron overload specifically on acute lung injury (ALI) and idiopathic pulmonary fibrosis (IPF). Our goal in Chapter One was to determine the effect of iron overload on ALI development, and it was necessary to use a model of sterile ALI to isolate the direct contributions of iron excess versus the effects of bacterial virulence. We found that iron overload by itself had a mild and transient effect on ALI severity, potentially via increased apoptosis in the lung, with no impact on recovery in mice. This suggests that severe systemic iron overload itself may not appreciably affect the clinical course and outcome of acute lung injury. In the IPF model described in Chapter Two, we also observed no effect of iron overload itself on whole-lung collagen or any noticeable differences in overall disease severity. While there have been clinical and translational studies linking iron overload and IPF, potential reasons for our observed results could be the inherent differences in the various genetic and dietary models of iron overload.

In Chapter Three, we examined the role of ZIP8, a transmembrane divalent metal ion importer that is most highly expressed in the lung and inducible by inflammatory stimuli. Our study has shown that while ZIP8 may play a role in systemic iron recycling, as indicated by increased splenic iron in ZIP8 KO mice, it does not appear to have a significant role in pulmonary iron regulation or host defense despite its high level of expression in the lung. This study resulted in the development of several tools to further study ZIP8, including a novel global inducible ZIP8 KO

mouse and a novel anti-mouse ZIP8 antibody. These tools will serve to enable future studies of ZIP8 function *in vivo*, as there remains more to be learned about ZIP8 and iron regulation.

In Chapter Four, our goal was to establish a mouse model of iron deficiency in BMPR2-associated PAH. Our initial expectation was that iron deficiency could provide the "second hit" for Bmpr2-related PAH development and worsen PAH outcomes. Our Bmpr2 Het mice, however, had similar or improved PAH parameters compared to control mice, which is counter to what is observed in clinical literature. Thus, though there have been multiple links and associations between iron deficiency and PAH potentially through Bmpr2, the Bmpr2 mutant mouse model is not the appropriate model for elucidating this relationship.

In Chapter Five, we explored the effect of excessive erythroferrone (ERFE) in a mouse model of β-thalassemia. We found that elevated ERFE levels impair pup survival in a mouse model of β-thalassemia during early life and greatly increase iron loading in the context of ineffective erythropoiesis during adulthood. These findings suggest that ERFE is a potential therapeutic target in β-thalassemia patients.

Overall, this work has provided a better understanding of the effects of iron dysregulation on the lung. While we have found that inappropriate levels of iron have mild effects on lung pathologies in our mouse models, these studies will provide the foundation for future investigations into the relationship between iron and lung pathologies. In addition, this work has established that while ZIP8 does not play a clinically significant iron-related role in the lung, it is potentially involved in iron recycling in the spleen. Finally, this work also demonstrates the effect of excessive ERFE in worsening the iron-related complications in a mouse model of β-thalassemia.